

**BOND AND SERVICEABILITY CHARACTERIZATION OF CONCRETE
REINFORCED WITH HIGH STRENGTH STEEL**

by

Amir Soltani

BS in Civil Engineering, University of Tehran, 1999

Earthquake Engineering, MS, IIEES, 2002

Submitted to the Graduate Faculty of
Swanson School of Engineering in partial fulfillment
of the requirements for the degree of
Doctor of Philosophy

University of Pittsburgh

2010

UNIVERSITY OF PITTSBURGH
SWANSON SCHOOL OF ENGINEERING

This dissertation was presented

by

Amir Soltani

It was defended on

July 28, 2010

and approved by

Dr. Bahram Shahrooz, Professor, Civil and Environmental Engineering
University of Cincinnati

Dr. John Brigham, Assistant Professor, Civil and Environmental Engineering

Dr. Julie Vandebossche, Assistant Professor, Civil and Environmental Engineering

Dissertation Director:

Dr. Kent A. Harries, Associate Professor, Civil and Environmental Engineering

Copyright © by Amir Soltani

2010

BOND AND SERVICEABILITY CHARACTERIZATION OF CONCRETE REINFORCED WITH HIGH STRENGTH STEEL

Amir Soltani, PhD.

University of Pittsburgh, 2010

Recent revisions to the *AASHTO Construction Specifications* permit the specification of ASTM A1035 reinforcing steel. A1035 reinforcing bars are low carbon, chromium steel bars characterized by a high tensile strength (100 or 120 ksi) and a stress-strain relationship having no yield plateau. Because of their high chromium content, A1035 bars are reported to have superior corrosion resistance when compared to conventional reinforcing steel grades. For this reason, designers have specified A1035 as a direct, one-to-one, replacement for conventional reinforcing steel as an alternative to stainless steel or epoxy-coated bars. The *AASHTO LRFD Design Specifications*, however, limit the yield strength of reinforcing steel to 75 ksi for most applications. Therefore, although A1035 steel is being specified for its corrosion resistance, its higher yield strength cannot be utilized.

The objective of this research is to evaluate existing *AASHTO LRFD Design Specifications* to determine their applicability when using high strength ASTM A1035 reinforcing bars in reinforced concrete structures. The study encompasses material testing and characterization, detailed analytical studies, component tests, and full-scale member testing. The analytical and experimental research program investigates ultimate strength and service behavior and detailing of members designed with high-strength reinforcement. Specifically, the topics addressed are: a) experimental evaluation of hooked bar development length of high-strength reinforcement; b) experimental evaluation of the fatigue performance of members reinforced

with high-strength reinforcement; and c) parametric evaluation of serviceability and crack opening in flexural members, comparing the results with available experimental results.

The applicability of current *Specification* requirements for hooked bar development lengths was confirmed through a series of pull-out tests having development lengths that were shorter than those required by present *Specifications* equations. Tests resulted in bar rupture outside of the anchorage region with very little slip clearly indicating the efficacy of the hooked bar development requirements in *Specifications*. It is recommended that such anchorage regions be provided with cover and confining reinforcement – based on current design requirements – when high-strength bars are used. The presence of confining reinforcement effectively mitigates potential splitting failures and results in suitably conservative anchorage capacities.

Two large-scale proof tests conducted as part of this study and a review of available published data demonstrate that presently accepted values for the fatigue or ‘endurance’ limit for reinforcing steel are applicable and likely conservative, when applied to higher strength bars. Additionally, it is shown that fatigue considerations will rarely affect the design of typical reinforced concrete members having $f_y \leq 100$ ksi.

The extension of present *AASHTO LRFD Bridge Design Specifications* for hooked bar anchorage and fatigue to permit reinforcing bar yield strengths not exceeding 100 ksi was validated for concrete strengths up to 10 ksi.

A fundamental issue in using A1035 or any other high-strength reinforcing steel is that the stress at service load is expected to be greater than when conventional steel is used. Consequently, the service-load reinforcing strains are greater, affecting deflection and crack widths. Based on the results of available flexural test, deflections and crack widths at service load levels were evaluated. Both metrics of serviceability were found to be within presently

accepted limits, and were predictable using current *Specifications* provisions. A limitation on service-level stresses of $f_s \leq 60$ ksi is recommended.

TABLE OF CONTENTS

1.0	INTRODUCTION.....	1
1.1	MOTIVATION, HISTORY AND CONTEXT	1
2.0	MECHANICAL PROPERTIES.....	4
2.1	MATERIAL STRUCTURE	4
2.1.1	Stress-Strain relationship.....	4
2.1.2	Modulus of elasticity, E	6
2.2	EXPERIMENTALLY DETERMINED MECHANICAL PROPERTIES RESULTS.....	6
2.3	STRUCTURAL BEHAVIOR.....	7
2.4	CONCRETE MATERIAL PROPERTIES.....	7
3.0	BOND CHARACTERISTICS OF HIGH STRENGTH REINFORCING BAR IN CONCRETE.....	13
3.1	PARAMETERS AFFECTING BOND STRESS.....	15
3.1.1	Transverse ribs and local bond stress.....	15
3.1.2	Confinement	16
3.1.3	Yield stress.....	17
3.1.4	Embedment length.....	17
3.1.5	Concrete properties	18
3.2	EXPERIMENTAL TESTING OF BOND BEHAVIOR.....	18

3.2.1	Pullout specimens	19
3.2.2	Beam end specimens.....	19
3.2.3	Beam anchorage and splice specimens	20
3.2.4	Hook anchorage specimens.....	22
3.3	BOND EXPRESSIONS IN CODE PROVISIONS.....	23
3.3.1	Anchorage of standard hooks.....	24
3.4	ANCHORAGE OF HIGH-STRENGTH STEEL REINFORCING BARS HAVING STANDARD HOOKS IN CONCRETE.....	29
3.4.1	Hook anchorage results.....	32
4.0	FATIGUE PERFORMANCE OF HIGH STRENGTH REINFORCING STEEL	42
4.1	S-N RELATIONSHIPS.....	43
4.2	FACTORS AFFECTING FATIGUE PERFORMANCE.....	44
4.3	ACCOUNTING FOR FATIGUE IN DESIGN.....	47
4.4	CURRENT RESEARCH ON FATIGUE PERFORMANCE OF REINFORCING STEEL	48
4.5	FATIGUE BEHAVIOR OF CONCRETE BEAMS HAVING HIGH- STRENGTH REINFORCEMENT.....	50
4.5.1	Fatigue proof tests	51
4.5.2	Specimen details.....	54
4.5.3	Fatigue test protocol	54
4.5.4	Results of fatigue test 1.....	55
4.5.5	Results of fatigue test 2.....	55
4.5.5.1	SEM of fatigue test 2 failure.....	56
4.5.6	Summary of fatigue tests.....	57

4.5.7	Effect of fatigue provisions of AASHTO 5.5.3.2	57
4.5.7.1	Slabs.....	60
5.0	SERVICEABILITY: DEFLECTION AND CRACK CONTROL.....	69
5.1	DEFLECTION CONTROL FOR SERVICEABILITY OF REINFORCED CONCRETE	69
5.1.1	Deflection of reinforced concrete members.....	70
5.1.2	Evaluation of effective moment of inertia	72
5.1.2.1	Branson’s equation	72
5.1.2.2	Tension stiffening	76
5.1.2.3	Bischoff’s equation.....	77
5.1.2.4	Evaluation of Branson and Bischoff equations	79
5.1.3	Deflection in concrete members reinforced with high strength steel	80
	bars	80
5.1.3.1	Analytical study of deflection.....	80
5.1.3.2	Deflections of flexural members	81
5.2	CRACK CONTROL IN REINFORCED CONCRETE MEMBERS	83
5.2.1	Crack formation	85
5.2.2	Crack control	86
5.2.3	Early investigations of flexural and axial tension cracking.....	87
5.2.3.1	Flexural members	87
5.2.3.2	Tension cracking	89
5.2.4	Methods of effective crack control.....	91
5.2.4.1	Reinforcement stress.....	91
5.2.4.2	Bond characteristics.....	92

5.2.4.3	Distribution of reinforcement	92
5.2.4.4	Diameter of reinforcement	92
5.2.4.5	Reinforcing ratio	93
5.2.4.6	Concrete cover	93
5.2.4.7	Material properties of concrete	94
5.2.5	Code provisions and expressions for cracking and crack control.....	94
5.2.5.1	ACI 318	96
5.2.5.2	AASHTO LRFD.....	100
5.2.5.3	Permissible crack widths	101
5.2.6	Crack control in concrete members reinforced with high strength steel bars.....	102
5.2.6.1	Crack widths.....	102
5.2.6.2	Crack spacing	103
5.2.6.3	Effect of repeated load.....	104
5.2.6.4	Analytical study of crack characterization.....	105
5.2.6.5	Direct tension model to investigate the crack development	105
5.2.6.6	Observed crack widths	113
6.0	CONCLUSIONS, RECOMMENDATIONS AND FUTURE RESEARCH	129
6.1	CONCLUSIONS AND RECOMMENDATIONS	129
6.1.1	Anchorage of high-strength steel reinforcing bars having standard hooks in concrete	130
6.1.2	Fatigue behavior of concrete beams having high-strength reinforcement...	131
6.1.3	Serviceability consideration of concrete members reinforced with high strength steel bars.....	132

6.1.3.1	Parametric study of deflection.....	132
6.1.3.2	Crack control.....	133
6.2	FUTURE RESEARCH	134
6.2.1	Bond characteristics	134
6.2.2	Fatigue characteristics	135
6.2.3	Serviceability consideration.....	135
APPENDIX	136
	AN ANALYTICAL APPROACH TO CALCULATE THE CRACK FORMATION IN A REINFORCED CONCRETE PRISM	136
REFERENCES	140

LIST OF TABLES

Table 2.1 Chemical composition of reinforcing steel.....	8
Table 2.2 Representative stress-strain curves for high strength reinforcing steel.	8
Table 2.3 Measured material properties for A1035 and A615 reinforcing steel used in experimental program.....	8
Table 2.4 Concrete mix designs and material properties.....	9
Table 3.1 Hook specimen details and test results.	36
Table 4.1 Fatigue stress ranges (f_r) corresponding to a fatigue life of 2 million cycles.	62
Table 4.2 Fatigue limit predictions	62
Table 5.1 Details of flexural beam specimens F1-F6 (Shahrooz et al. 2010).....	115
Table 5.2 Comparison of experimental and calculated deflections at service load levels.....	116
Table 5.3 Required AASHTO bar spacing, s (in).....	117
Table 5.4 Direct tension analysis results.....	117

LIST OF FIGURES

Figure 2.1 Stress-strain curves for A615 and A1035 #5 reinforcing bars (Ward 2008). A clearly defined yield plateau is evident in the A615 curve and absent in the A1035 curve... 10	10
Figure 2.2 Graphical representation of the Ramberg-Osgood function..... 10	10
Figure 2.3 Measured and predicted values of A1035 stress-strain behavior. 11	11
Figure 2.4 Stress – strain curves for reinforcing steel used in this experimental program. 12	12
Figure 3.1 Development test geometries. 37	37
Figure 3.2 Hook test setup and specimen details..... 38	38
Figure 3.3 Typical Concrete Shear Failure (Specimen H8-2). 38	38
Figure 3.4 Strains along hook embedment at selected bar stresses. 39	39
Figure 3.5 Slip versus bar stress. 40	40
Figure 3.6 Slip of embedded hooks. 41	41
Figure 4.1 Observed 2 million cycle stress limits as a function of minimum stress level, f_{min} 63	63
Figure 4.2 Fatigue specimen test 1. 64	64
Figure 4.3 Cumulative damage curves for Fatigue test 1. 65	65
Figure 4.4 Cumulative damage curves for Fatigue test 2. 65	65
Figure 4.5 Fatigue failure of single bar in Fatigue Test 2..... 66	66
Figure 4.6 SEM images of failure surface. 67	67
Figure 4.7 Predicted and experimental S-N data. 68	68

Figure 4.8 Fatigue stress as proportion of AASHTO 5.5.3.2 fatigue limit.....	68
Figure 5.1 Tension stiffening (Bischoff 2007)	118
Figure 5.2 Branson’s and Bischoff’s equations as a function of M_a/M_{cr}	119
Figure 5.3 Steel stress versus crack width (Thomas 1936).....	119
Figure 5.4 Stress distribution and configuration in a concrete member between two cracks (Reis et al 1965).	120
Figure 5.5 Strain profile.....	120
Figure 5.6 Dimensions used in crack control equations.	121
Figure 5.7 Allowable Stress vs. Bar Spacing; assumes 2 in. concrete cover and #8 bar (Destefano et al. 2003).	121
Figure 5.8 Crack development in direct tension test.....	122
Figure 5.9 The adopted model of bond stress distribution.....	123
Figure 5.10 Free body diagram of reinforcing steel in segment to one side of crack.....	123
Figure 5.11 Bond stress and resulting steel and concrete strain distribution between adjacent cracks in a reinforced concrete member.	124
Figure 5.12 Direct tension test in the parametric study.	125
Figure 5.13 Corresponding bar stresses causing the last crack formation. (Based on Table 5.4)	125
Figure 5.14 The extension of crack opening vs. reinforcing bar stresses.	127
Figure 5.15 Measured crack widths with longitudinal reinforcing bar stress for flexural beams.	128

NOMENCLATURE

a	length of shear span, 102 in. in all cases;
A	A_e/n , is the area of concrete in tension surrounding each bar;
A_b	the area of the bar;
A_e	the area of concrete having the same centroid as the n reinforcing bar;
A_s	A_e/n , is the effective area of concrete surrounding each bar;
c_c	clear concrete cover for reinforcement nearest the tension face;
d	effective depth of beam;
d^*	controlling cover distance (shown in Figure 5.6);
d_b	diameter of the bar;
d_c	distance from tension face to centroid of nearest reinforcing bar;
E	elastic modulus;
f_c'	the concrete compressive strength;
f_{cr}	the cracking stress of concrete usually expressed as a scalar multiple of $\sqrt{f_c'}$;
f_h	the bar stress which cannot be greater than the yield strength of the bar f_y ;
f_{min}, f_f	algebraic minimum and maximum stress level (compression negative);
f_s	steel stress calculated by elastic cracked section analysis;
f_{ss}	service level stress in the steel reinforcement;
f_u	Ultimate steel stress;
f_y	yield strength of steel;
h	overall depth of beam;
h_l	$(1-k)d$;

h_2	$h-kd$;
I	moment of inertia of the section;
I_g	moment of inertia of gross concrete section;
K	a factor depending on the degree of fixity of the supports (page 89);
K	constant (page 62);
K	distance from neutral axis to compression face divided by effective depth of beam (page 113);
L	clear span length;
l'	the greater of $4d_b$ or 4 in.;
l_{dh}	the development length for a hooked bar;
m	an empirically derived exponent;
m	stress exponent;
M	the applied moment;
M_a	is the applied moment at which deflections are calculated ($M_a > M_{cr}$);
M_{cr}	cracking moment;
N	E_s/E_c modular ratio (page 92);
n	number of bars in concrete area effectively subjected to uniform tension, A_e (page 107);
N	number of cycles to cause fatigue failure;
p	the bar circumference, assumed constant along the bar length;
P	total applied load in four point bending (sum of two point loads);
R	h_2/h_1 (also known as β);
r/h	ratio of base radius to height of rolled-on transverse deformations;
S	applied stress range;

S	Minimum Crack spacing (From Table 5.4);
s_I	0.024 in. for unconfined concrete and 0.039 in. for confined concrete,
$T(x)$	the force in the bar;
t_b	bottom cover measured from the center of lowest bar;
t_s	side cover measured from the center of outer bar (also known as d_c);
w	self weight of beam, taken as 16.7 lb/in. in all cases;
w_c	0.016 in. limiting crack width;
w_c	unit weight of concrete;
y	the distance from the uncracked neutral axis to the extreme tension face of the member;
y_t	neutral axis of gross concrete section, nominally 8 in.
α and β	constants depending on the value of $n\rho$ (page 94).
β	$1 + 0.08d_c$;
ϵ_s	Steel Strain;
λ	a factor accounting for the use of lightweight concrete (also unity for this study);
ρ	the reinforcement ratio;
$\tau(x)$	the bond stress distribution along the length of the bar;
ϕ	the resistance factor for anchorage;
ψ	coefficient which depends on the size of the bar, the length of the lead straight embedment, side concrete cover and cover extension of the tail;
ψ_s	crack spacing factor;
Ψ_t and Ψ_e	factors to account for 'top cast' bars and the use of epoxy coated reinforcing steel;
τ_{max}	the maximum bond stress capacity; for good bond conditions: $\tau_{max} = 2.0\sqrt{f'_c}$;

ACKNOWLEDGEMENTS

I would like to express my deepest gratitude to my advisor, Dr. Kent A. Harries, for his advisement, caring and patience. He provided an excellent atmosphere and wise guidance during my research and education. This project had extensive experimental tests and required complex analytical studies; I would not be able to finish my dissertation without his support.

I would like to recognize the National Cooperative Highway Research Program for providing the funding which made this project possible and especial thanks to all committee members for their contributions and assistance. Further I wish to acknowledge Dr. Baharam Sharooz for his kind encouragement and advice.

In recognition of all your help and support I would like to mention all the staff of the School of Engineering in particular the library staff at University of Pittsburgh.

Finally yet importantly, I also extend my heartfelt thanks to my beloved family for their blessing, my friends/classmates for their help and wishes for the successful completion of this project.

“I dedicate this dissertation to my mother and brother, Mahnaz and Soheil and to memory of my father”

Amir Soltani

1.0 INTRODUCTION

This research is based on activities associated with Tasks 8.1, 8.2, 8.6 and 8.7 of National Cooperative Highway Research Program (NCHRP) Project 12-77 *Structural Concrete Design with High-Strength Steel Reinforcement*. With the integration of innovative materials into the nation's infrastructure, the validity of using such materials must be considered. This study considers the use of high-strength steel reinforcing bars as an alternative to conventional ASTM A615¹ (2006) Grade 60 reinforcing bars in concrete structures.

1.1 MOTIVATION, HISTORY AND CONTEXT

For many years the design of reinforced concrete structures was dominated by the use of steel reinforcement with yield strength, f_y , equal to 40 ksi. In the late 1960's, the typical yield strength increased to $f_y = 60$ ksi. Design with steel having higher yield strength values has been permitted; the 1971 edition of ACI 318 (1971), for instance, limited the yield strength to $f_y \leq 80$ ksi (Lepage et al. 2008). Currently ACI 318-08 permits the use of reinforcement having a design yield strength, defined as the stress corresponding to a strain of 0.0035, not exceeding 80 ksi. The exception is transverse reinforcement where the use of yield strength up to 100 ksi is permitted,

¹ For convenience, steel grades will only be referred by their ASTM designation (A615, A1035, etc.) and the citation only provided at the first occurrence in the text.

but may only be applied to the requirements for confinement in compression members. AASHTO LRFD *Specifications* (AASHTO 2007) similarly limit the use of reinforcing yield strength in design to at least 60 ksi and no greater than 75 ksi (exceptions are permitted with owner approval). Thus, AASHTO technically prohibits the use of 40 ksi reinforcing steel whereas ACI continues to allow its use. Both ACI and AASHTO limits have been written and interpreted not to exclude the use of higher strength grades of steel, but only limit the value of f_y that may be used in design calculations.

The limits on yield strength are primarily related to the prescribed limit on concrete compressive strain of 0.003 and to the control of crack widths at service loads. Crack width is a function of steel strain and consequently steel stress (Nawy 1968). Therefore, the stress in the steel reinforcement needs to be limited to some extent to prevent cracking from affecting serviceability of the structure. However, with recent improvements in the properties of concrete, such as the development of higher capacity concretes, the ACI 318-08 limit of 80 ksi and AASHTO limit of 75 ksi on the steel reinforcement yield strength is believed to be unnecessarily conservative for new designs. Additionally, an argument can be made that if a higher strength reinforcing steel is used but not fully accounted for in design, there may be an inherent over-strength in the member that has not been properly accounted for. This concern is most critical in seismic applications or when considering progressive collapse states. Neither are generally significant concerns for bridge structures and are beyond the scope of the present work. The argument most often made for adopting higher reinforcing bar design stress limits is simply that it permits a more efficient use of the available high strength steel material.

The ASTM A1035 (2007) reinforcing steel used in this study (commercially referred to as MMFX steel) has a yield capacity on the order of 120 ksi and is reported to be between 2 and

10 times more corrosion resistant than conventional A615 'black' steel. In some applications, A1035 reinforcing steel has been used to replace A615 steel on a one-to-one basis on the premise that it is more resistant to corrosion but not as costly as stainless steel grades. Clearly, if the enhanced strength of A1035 could be used in design calculations, less steel would be required resulting in a more efficient and economical structural system. In this case, reduction of the reinforcement ratio also helps to reduce reinforcement congestion and improve concrete placement.

This study encompasses material testing and characterizations, detailed analytical studies, component tests, and full-scale member testing. The analytical and experimental research program investigates ultimate strength and service behavior and detailing of members designed with high-strength reinforcement. Specifically, the topics covered are:

- a) Bond characteristics of high strength reinforcing bar in concrete;
- b) Fatigue performance of high strength reinforcing steel
- c) Serviceability: deflection and crack control;

The experimental portion of the research focuses only on reinforcing bars meeting the A1035 specification. This kind of steel reinforcement has been selected for testing because it is the highest strength non-prestressed reinforcement that is commercially available and, therefore, represents an upper bound. Since all other reinforcement has ultimate strengths between those of A1035 and A615, it should be possible to bracket the effects of using higher strength reinforcing steel and compare it with conventional practice.

2.0 MECHANICAL PROPERTIES

2.1 MATERIAL STRUCTURE

Typical carbon steel used for reinforcing steel (A615, A706, etc) has a ferritic-pearlitic microstructure, in which carbides form in the iron carbide phase (Elagroudy 2003). Microcomposite alloy steel, such as A1035, is a Fe-C-Cr-Mn alloy that has an average chromium content of approximately 9% - too low to be referred to as “stainless steel” (Cr > 10.5%) but sufficiently high to impart a degree of corrosion resistance when compared to “black steel” (A615 or A706). The basic differences between the microcomposite A1035 and A615 carbon steels are in their a) chemical composition and proportioning, b) the distribution of elements in the microstructure, and c) the production method used (Elagroudy 2003). Table 2.1 summarizes the prescribed chemical proportioning of A1035, A992 (stainless steel) and A615 grades of reinforcing steel.

2.1.1 Stress-Strain relationship

Conventional grades of reinforcing steel (represented by A615) have a well-defined yield plateau whereas high-strength grades (A1035) do not; representative curves are shown in Figure 2.1. Nonetheless, the value of the reinforcing bar yield strength, f_y , is a critical design parameter. Particularly where there is no well-defined yield plateau, characterization of the entire stress

strain relationship often may be required for analysis. The following methods may be utilized to characterize the stress-strain (f_s - ϵ_s) relationship of reinforcing bars that do not have exhibit a well-defined yield point:

- (a) An elastic-perfectly plastic model with f_y taken as the minimum specified yield strength.
- (b) An elastic-perfectly plastic model with f_y taken as that established based on stress at a given strain or using the 0.2% offset method.
- (c) Empirical material-specific equations such as those given in Table 2.2.
- (d) A Ramberg-Osgood (R-O) relationship. The modified R-O relationship given in Equation 2.1 is commonly used to model the stress-strain behavior of prestressing strand (Mattock and Hawkins 1972) and is appropriate for other high strength steel such as A1035.

$$f_s = E \epsilon_s \left\{ A + \frac{1-A}{[1+(B\epsilon_s)^C]^{1/C}} \right\} \leq f_u \quad (2.1)$$

Where;

f_u = Ultimate steel stress;

ϵ_s = Steel Strain;

The values of A and B in Equation 2.1, which are defined graphically in Figure 2.2, are calibrated to match the experimentally obtained stress-strain curve.

2.1.2 Modulus of elasticity, E

Regardless of yield or ultimate strength, all steel reinforcing bar grades have a reported modulus of elasticity, $E = 29,000$ ksi. There is no evidence that the modulus varies significantly from steel grade to steel grade. High strength steel does, however, exhibit an “elastic limit” where the modulus begins to decrease as evident in Figure 2.3. While this limit is partially a function of the steel capacity, it has been observed that A1035 steel behaves in an essentially linear manner to 70 ksi (Mast 2006) regardless of the ultimate capacity. It is noted that the form of equation used to capture the behavior of high strength reinforcing steel proposed by Vijay et al. (2002) and El-Hacha et al. (2006) (Table 2.2) captures the behavior at large strains and at ultimate capacity reasonably well (Figure 2.3), but it does not capture initial behavior well – as the modulus begins to degrade immediately in these equations (Figure 2.3 inset). The behavior proposed by Mast et al. (2008), on the other hand, captures the initially linear behavior and large strain behavior quite well (Table 2.2 and Figure 2.3). An R-O function is also able to capture the elastic limit behavior by manipulation of the factor c in Equation 2.1.

2.2 EXPERIMENTALLY DETERMINED MECHANICAL PROPERTIES RESULTS

As an indication of the mechanical properties of A1035 steel, Table 2.3 reports the experimentally determined properties for all reinforcing steel reported in this study and Figure 2.4 presents representative stress-strain curves obtained. All properties were obtained from tests compliant with ASTM test method E8 (2008).

2.3 STRUCTURAL BEHAVIOR

Despite the lack of a well-defined yield plateau, most high-strength reinforcing steel is capable of achieving ultimate strain values of 0.05 or higher (Mast et al. 2008 and Table 2.3). Thus, such steel is capable of deformations similar to those of mild steel, and can provide adequate member ductility. Therefore, high-strength reinforcing steel grades are appropriate for the design and construction of reinforced concrete flexural members.

Desirable structural behavior implies that at service load, the member should display small deflections and minimal cracking while at higher loads the member should display larger but controlled deflections and sufficient cracking to provide warning before reaching its ultimate strength. Both deflection and cracking are primarily a function of steel strain near the tension face of the member and therefore related to the elastic modulus of the reinforcing steel. Desirable ultimate behavior of a member is related to ductility, which relates to yielding or inelastic deformation of the steel reinforcement. For lower strength reinforcing materials, the only way to obtain high strains near the tension face at ultimate strength is to ensure yielding of the tension steel, however, for high-strength materials, this may no longer be necessary (Mast et al. 2008).

2.4 CONCRETE MATERIAL PROPERTIES

Two concrete mixes, having nominal design compressive strengths of 5 ksi and 10 ksi were used in this study. The concrete mix designs and material properties are presented in Table 2.4.

Table 2.1 Chemical composition of reinforcing steel.

designation	%Cr	%Ni	%C	%Mn	%Si	%P	%S	%N	%Mo	%Fe
A1035	8-10.9	-	0.15	< 1.5	< 0.5	< 0.035	< 0.045	< 0.05	-	balance
A615	-	-	< 0.50		-	< 0.060		-	-	balance
A992 - 316LN	16-18	10-14	0.03	< 2	< 1	< 0.045	< 0.030	0.10-0.16	2-3	balance
A992-2205	21-23	4.5-6.5	0.03	< 2	< 1	< 0.030	< 0.020	0.08-0.20	2.5-3.5	balance
A992-N32	16.5-19	0.5-2.5	0.15	11-14	<1	< 0.060	< 0.030	0.20-0.45	-	balance

Table 2.2 Representative stress-strain curves for high strength reinforcing steel.

Citation	Equation (all ksi units)
Vijay et al. 2002	$\sigma = 164(1 - e^{-182\varepsilon})$ for #4 bars
	$\sigma = 173(1 - e^{-168\varepsilon})$ for #8 bars
El-Hacha et al. 2006	$\sigma = 177(1 - e^{-185\varepsilon})$
Mast et al. 2008	$\sigma = 29000\varepsilon; \varepsilon \leq 0.00241$
	$\sigma = 170 - 0.43/(\varepsilon + 0.00188); \varepsilon > 0.00241$

Table 2.3 Measured material properties for A1035 and A615 reinforcing steel used in experimental program.

Steel		A 1035	A 1035	A 1035	A 1035	A 615 ¹	A 615 ²
Bar size		#8	#6	#5	#4	#3	#3
fu	ksi	154.6	161.3	164.1	174	103	107.8
eu		0.115	0.103	0.103	0.075	0.153	0.1331
Ecalc	ksi	27378	29001	26074	27850	29124	26178
fy based on ...							
$\varepsilon = 0.0035$	ksi	89.6	91.1	89.2	94.0	67.3	69.1
$\varepsilon = 0.0050$	ksi	108.8	111.7	112.5	117.0	68.4	73.0
$\varepsilon = 0.0070$	ksi	125.6	129.7	132.1	137.0	69.3	73.7
$\varepsilon = 0.0100$	ksi	134.4	138.6	143.2	156.0	70.6	75.1
2% offset	ksi	118.6	121.8	130.2	140.0	67.3	69.1
R-O parameters							
A		0.0554	0.0203	0.0145	0.004	-	-
B		225	198	186	172	-	-
C		2.9	2.4	2.3	2.8	-	-
Ecalc = secant modulus measured at 60 ksi for A1035 and 30 ksi for A615							
¹ Batch 1: all vertical ties in pull-out specimens							
² Batch 1B: all horizontal ties in pull-out specimens and all A615 in fatigue specimens							

Table 2.4 Concrete mix designs and material properties.

Mix		nominally 5 ksi		nominally 10 ksi	
Provider		Frank Bryan, Pittsburgh		Frank Bryan, Pittsburgh	
design f_c'	psi	4000		10000	
cast date		10/10/2008		10/16/2008	
		Qty	source	Qty	source
cement	lbs/cy	400	Essroc Cement Type I	825	Lehigh Cement Type I/II
fine agg	lbs/cy	1346	TriState Type A Sand	1105	TriState Type A Sand
coarse agg	lbs/cy	1450	TriState #57 Gravel; Tristate	1454	Georgetown S&G #8 Gravel
coarse agg	lbs/cy	300	TriState #8 Gravel; Tristate	430	TriState shot gravel
water	lbs/cy	254	Pittsburgh	24	Pittsburgh
SF	lbs/cy	175	Type C Essroc	67	Elkem
HRWR	oz/cy	4	Axim 800N	125	AXIM Allegro 122
stabilizer	oz/cy	-	-	38	MB Delvo
w/c		0.44		0.27	
unit weight	lbs/cf	146		151	
slump	in.	6		6	
air content	%	not tested		not tested	
		strength	age (days)	strength	age (days)
f_c	psi	6020	28	6620	7
		7120	104 ¹	7820	28
				9710	56

¹ midpoint of test schedule

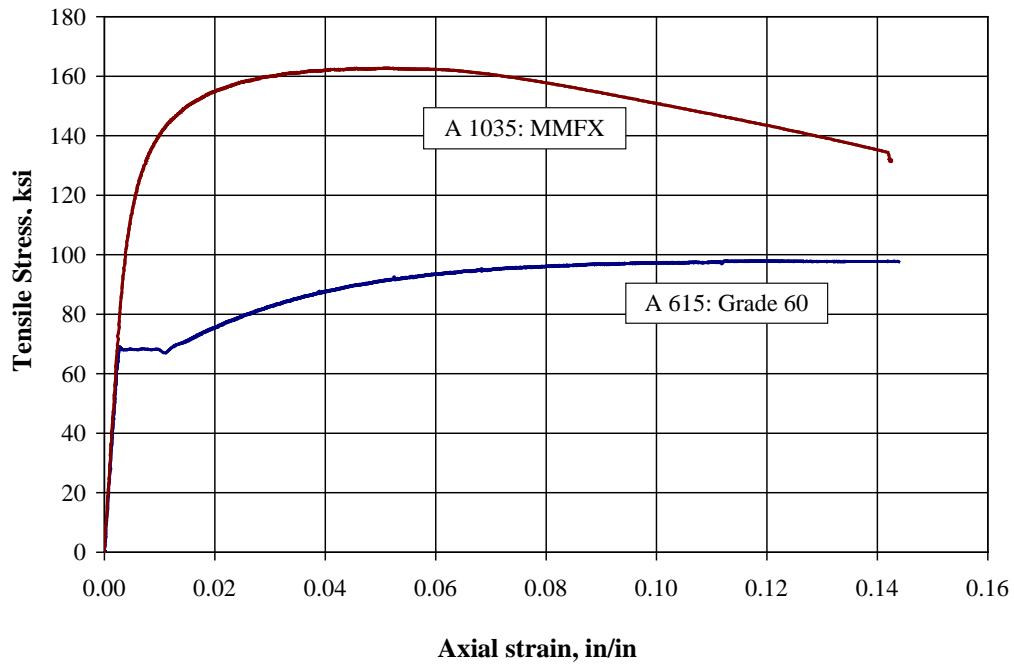


Figure 2.1 Stress-strain curves for A615 and A1035 #5 reinforcing bars (Ward 2008). A clearly defined yield plateau is evident in the A615 curve and absent in the A1035 curve.

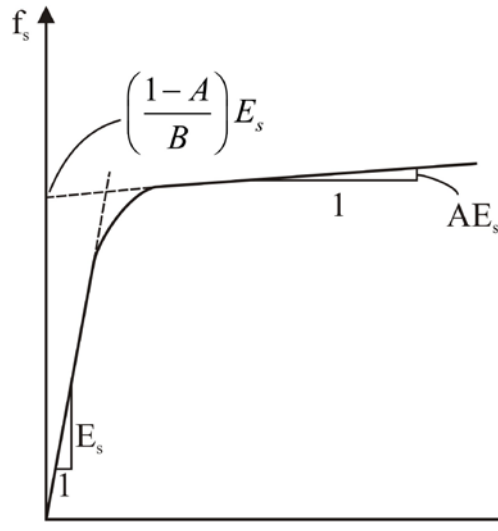


Figure 2.2 Graphical representation of the Ramberg-Osgood function.

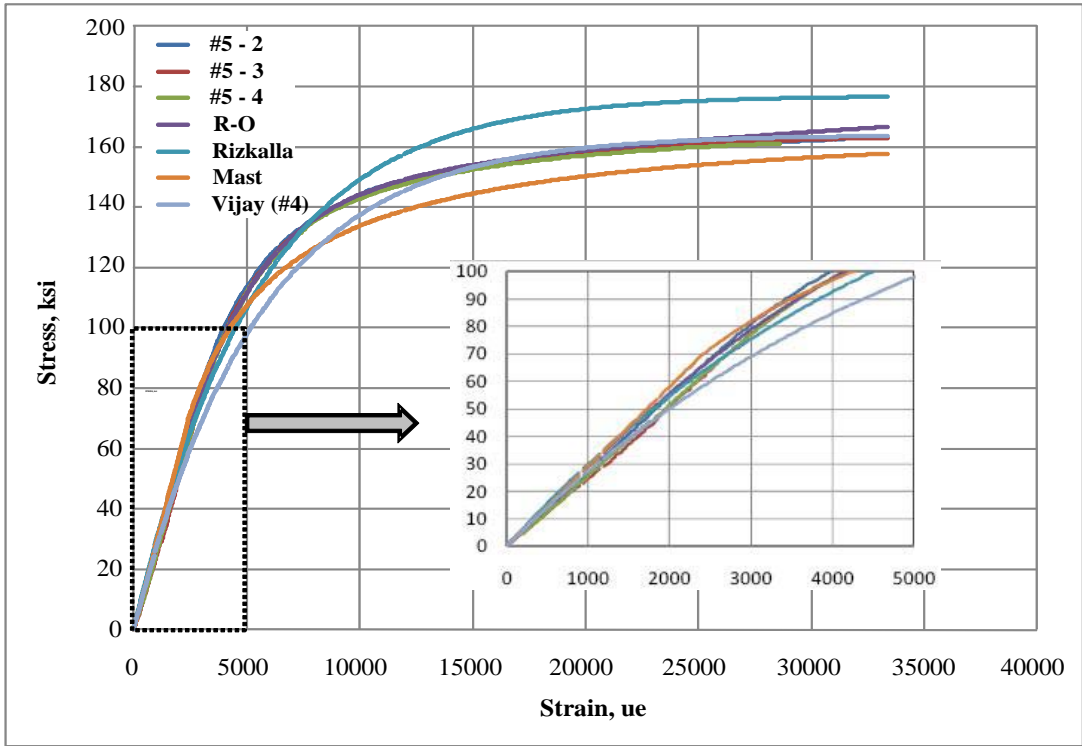
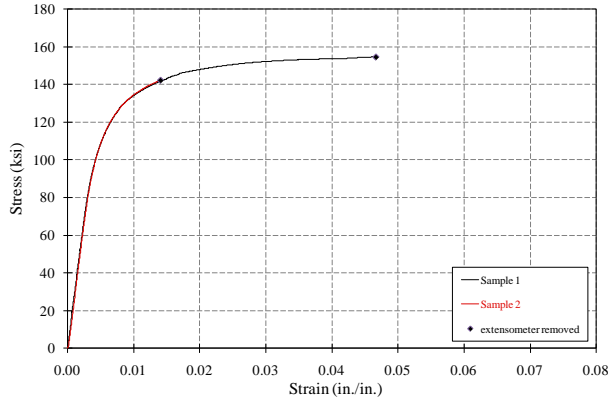
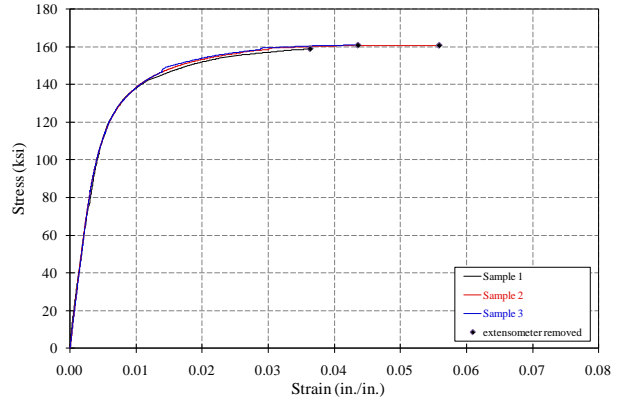


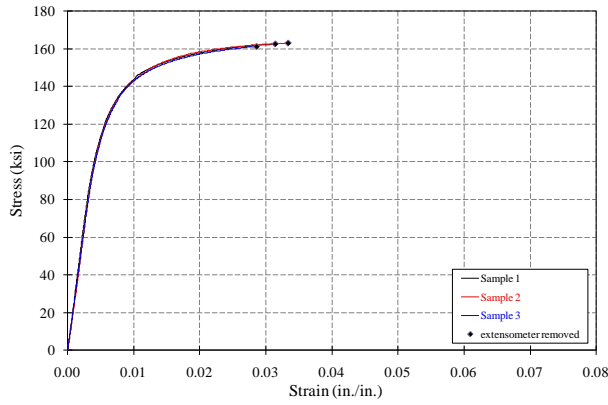
Figure 2.3 Measured and predicted values of A1035 stress-strain behavior.



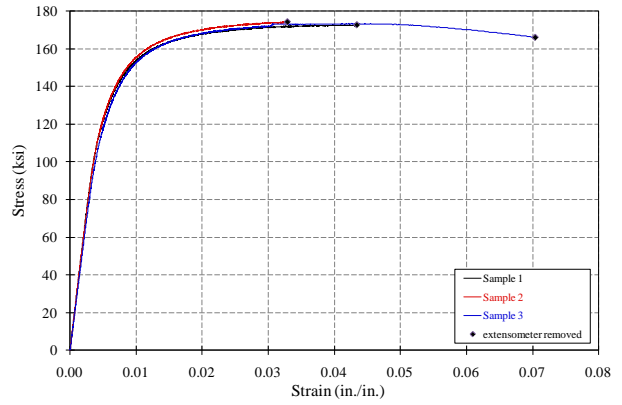
a) A1035 #8



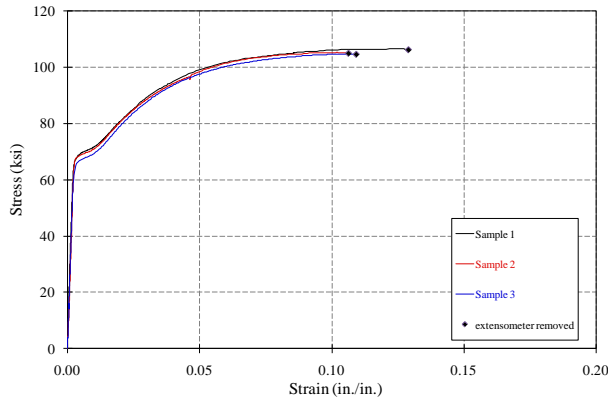
b) A1035 #6



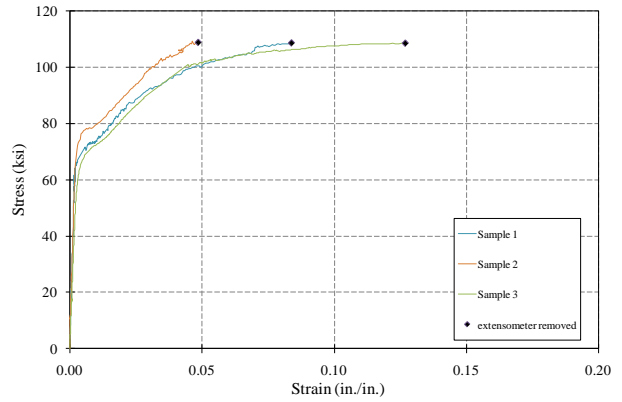
c) A1035 #5



d) A1035 #4



e) A615 #3 batch 1



f) A615 #3 batch 1B

Figure 2.4 Stress – strain curves for reinforcing steel used in this experimental program.

3.0 BOND CHARACTERISTICS OF HIGH STRENGTH REINFORCING BAR IN CONCRETE

Bond is an important factor in reinforced concrete design, as the bond between the concrete and the reinforcing steel transfers tensile forces from the concrete to the reinforcing steel. To transfer force adequately, there must be a sufficient length of reinforcing bar, known as the development length, over which the bar force is transferred from the concrete to the reinforcing steel. Similarly, the splice length between two bars must be adequate to transfer the bar force from one bar to the other through the surrounding concrete. The development/splice length required to adequately transfer force depends on many factors, including the geometry of the bar deformations, especially the height and spacing of 'ribs' or 'lugs', concrete cover, concrete strength, bar size, and the presence of confinement by transverse reinforcement.

Bond force is developed by friction, chemical adhesion, and mechanical interlock between bar deformations and the surrounding concrete. When adhesion is small and neglected, the remaining components form a resultant stress that can be further broken into longitudinal and radial components. For deformed bars, mechanical interlock is the primary method of bond force transfer. Inadequate bond force transfer can cause failure of the concrete by radial splitting emanating from the reinforcing steel or by shear along the tops of the ribs resulting in the reinforcing steel pulling out of the concrete.

Bond behavior can be described in four phases corresponding to a monotonically increasing load (Bond of Reinforcement in Concrete 2000):

- a) Low bond stresses, in which all three bond components are present (adhesion, mechanical interlock, and friction). No displacement of the bar relative to the concrete is observed. The only deformation is the compatible elastic deformation of the concrete and reinforcing bar.
- b) The bar starts to move (slip) with respect to the concrete. Transverse micro cracks form behind the bar deformations. Two bond components remain: interlock and friction.
- c) Microcracks spread radially outward from the bar. Confinement produced by either the surrounding concrete or transverse reinforcing steel can control the spreading of these cracks. Local concrete crushing at the bar deformations accelerates slip and softens the bond stress-slip curve.
- d) Bond failure occurs by either bar pullout (shear failure of concrete along ribs) or concrete splitting (uncontrolled radial cracking). Pullout will occur if the confinement is greater than the transverse-oriented component of the bond force; otherwise, splitting occurs.

Theoretical understanding of bond between the reinforcing steel and the concrete into which it is embedded provides a framework for design methodologies, but data are needed to calibrate theoretical derivations into design equations. Such data can only be obtained through experimental studies. Because the experimental data for bond stress have been critical for the empirical calibration of design equations, it is important to understand the ways in which bond has been traditionally measured when considering extending these design methodologies to

higher strength reinforcing steel. The following sections describe parameters affecting bond stress, experimental testing of bond behavior and resulting code based provisions.

3.1 PARAMETERS AFFECTING BOND STRESS

To reflect the actual bond phenomenon properly, bond strength needs to be expressed in terms of all contributing parameters. However, it is impractical to include in a design routine every variable that affects bond strength. Standardization of bar deformation patterns allows a degree of simplification in this regard. Nonetheless, the following sections provide a brief description of factors affecting reinforcing bar development (i.e., bond).

3.1.1 Transverse ribs and local bond stress

As tensile forces develop in a reinforcing bar, transverse cracks propagate from the edges of the ribs (Goto 1971). Mains (1951) showed experimentally that local bond stress can be more than twice the average bond stress. Lutz (1966) performed experimental studies of single rib specimens. He observed that at failure, the angle of the concrete wedge was between 30° and 45° and that ribs with face angles less than 30° showed poor bond-slip performance in tests. While rib face angle does not significantly affect bond strength within certain limits, rib bearing area has been shown to be important. Rib bearing area can be increased by manipulating one or both of two geometric parameters: the height of the ribs or the spacing of the ribs. Abrams (1913) was the first to recognize that bond was enhanced by increases in relative rib area. Studies by Darwin et al. (1996) show the same results. No study has been found on the affect of transverse ribs and

local stress on high-strength steel bars. In the present study, the transverse ribs for high-strength steel bars are essentially the same geometry as those of A615 reinforcing bars.

3.1.2 Confinement

The presence of transverse reinforcement as confinement surrounding developed/spliced bars will increase the ultimate bond force that may be developed by delaying the progression of radially-oriented splitting cracks. At the same time, the magnitude of the bond force needed to cause pullout bond failure remains unaltered as it is mostly unaffected by the transverse confinement. Accordingly, an increase in transverse reinforcement will eventually change the mode of bond failure from splitting to pullout failure. Any additional confinement, more than that needed to restrain the radial cracking sufficiently to cause the change from a splitting to a pullout failure, provides no additional increase in bond strength (Orangun et al. 1977). This behavior is the basis for limiting the confinement term $(c_b + K_{tr})/d_b < 2.5$ in Equation 3.2.

Conclusions from Seliem et al. (2009) on tests of A1035 high-strength steel reinforcing bars indicate that both ACI 318 and ACI 408 development length equations underestimate the effects of confinement although this underestimation is diminished as the splice length increases. The latter observation likely reflects the fact that the code relationships are based on an assumption of uniform bond stress while, in reality, bond stresses are known to have nonlinear distributions (Orangun et al. 1977). Seliem et al. demonstrate that the limit on the confinement factor $(c_b + K_{tr})/d_b$ may be increased from 2.5 to 3.0 in the ACI 318 equation (Equation 3.2) and from 4.0 to 5.0 in the ACI 408 equation. Significantly, both equations are shown to be non-conservative where no confinement is provided, particularly as the concrete strength increases. In Seliem's study, unconfined A1035 lap splices attained capacities of only 70 ksi to 90 ksi while

confined splices achieved capacities greater than 120 ksi. Results reported by Harries et al. (2010), demonstrate that with appropriate confinement, the full bar strength, exceeding 120 ksi, may be developed in lap splice tests.

3.1.3 Yield stress

Orangun et al. (1977) reported that yielding of developed/spliced bars will cause a reduction in bond strength. Darwin et al. (1996a and 1996b) and Zuo and Darwin (2000) reached an opposite conclusion: that the bond strength for bars that yield before bond failure is generally higher than that of higher strength bars having the same bonded length and confinement but that do not yield before failure. Darwin et al. observed that, in the case of bars not confined by transverse reinforcement, the yielding of the spliced bars has no effect on the bond strength. It is possible, in this case, that the larger deformations associated with yield are able to mechanically engage the transverse confining steel, thus making the bond capacity appear greater. This hypothesis however is untested.

3.1.4 Embedment length

As the embedment length of the bar increases, the cracked surface at failure also increases but in a less than proportional manner. Thus, the total energy needed to form the crack and, in turn, the total bond force required to fail the member, increases at a rate that is less than proportional to the increase in bonded length. Therefore, the common design practice (ACI, AASHTO, etc.) of establishing a proportional relationship between bond and development/splice length is highly conservative for very short bonded lengths, but becomes progressively less conservative, and

eventually unconservative, as the bonded length and stress in the developed/spliced bar increases (Darwin et al. 1996). This effect is accounted for in the ACI 318 ψ_s factor for small diameter bars.

3.1.5 Concrete properties

DeVries (1996) showed the ultimate bond capacity improved with increasing concrete compressive strength, and was roughly proportional to $(f'_c)^{0.67}$ although with much scatter. The splitting failure mode of bond is dependent on the tensile strength of concrete. Thus, the mechanical properties of concrete are important for good deformed bar development. Two other concrete related parameters can also have significant effects on bond capacity: lightweight concrete and top cast bars. Both of these issues are beyond the scope of the present work and are presently accounted for by factors applied to development length equations (see Section 3.3).

3.2 EXPERIMENTAL TESTING OF BOND BEHAVIOR

Five categories of bond specimens have been categorized from the literature: single bar pullout specimens, beam anchorage specimens, beam-end specimens, lap splice tensile, and beam specimens and hook anchorage specimens. Although several experimental studies may be said to use the same type of specimen, the particular details of specimens used in different studies vary.

3.2.1 Pullout specimens

In pullout specimens, generally, the bars are pulled from the surrounding concrete in such a way that the concrete surrounding the bar is subjected to compression (Figure 3.1a). This does not reflect the critical anchorage condition of a bar anchored in a tension zone. In such a test arrangement, compression struts form between the bar surface and the loading points on the concrete surface. Such transverse compression struts cause the effect of increasing the apparent bond strength and are not simulating typical situations encountered in structures and bridges. Typical *in situ* conditions have both the bar and the surrounding concrete placed in tension. This type of bond specimen is not recommended by ACI Committee 408 to determine the development length since it represents the least realistic conditions (ACI 2003). A variation of the pullout test often used to test hook anchorages (e.g.: El Hacha et al. 2006) is shown in Figure 3.1b; this specimen suffers from many of the same drawbacks of the single bar pullout specimen.

3.2.2 Beam end specimens

Beam-end specimens represent a more realistic type of specimen that can give better and more accurate results for bond behavior. In the beam end specimen, both the reinforcing and the surrounding concrete are subjected to tensile stresses (Figure 3.1c). To achieve such a state of stress, the compressive forces must be located away from the reinforcing bar a distance not less than the bonded length of the tested bar. Also a short length of the tested bar near the concrete free surface has to be unbonded from surrounding concrete to avoid a conical pullout failure of the concrete. ASTM Standard A944-99 adopts this type of bond specimen. Experimental studies indicate that the bond obtained using beam end specimens closely match those obtained using

full-scale reinforced concrete members (Elagroudy 2003). Ahlborn and DenHartigh (2003) presented a large study on establishing bond properties using beam-end specimens. No beam-end tests are known using high strength reinforcing steel.

3.2.3 Beam anchorage and splice specimens

The beam anchorage and splice specimens represent full scale specimens, designed to directly measure the bond strength of developed or spliced bars. These specimens replicate a flexural member with a defined bond length. Splice specimens are normally designed and tested under four point loading having the splice length lying within the constant moment region (Figure 3.1f). Their ease of fabrication and the close similarity between the stress profile, in both the concrete and reinforcing steel, with the actual stress profile in real flexural members result in splice specimens being the primary source of experimental data used to establish the current design provisions for development length.

Previous studies show that compared with Grade 60 steel, Grade 100 steel allows beam-splice specimens to reach higher loads and deflections before failure (Ansley 2002). Tests also indicate that for bars not confined by transverse reinforcement, longer splices will increase the load at failure and may provide additional ductility, although beyond a certain point increasing the splice length will not increase the load or deformation capacity (Peterfreund 2003).

Shebly (2008) tested full scale beam-splice test specimens in four-point bending having A1035 reinforcement. The results indicate that the development length equation prescribed in ACI 318-05 is not suitable for the design of unconfined or confined splices of this higher grade steel without the use of an additional modification factor. The development length equation recommended in ACI 408R-03 was, however, found to be suitable for both unconfined and

confined splices. Based on this study, both ACI 408 and ACI 318-05 code equations for bond underestimate the bond force capacity at low stress levels in the bar (within the linear portion of the stress-strain curve) and progressively overestimate the bond capacity of A1035 bars when the tensile stress levels exceed the proportional limit. This observation should not be surprising as existing bond recommendations are largely empirical and have been calibrated for steel exhibiting a linear behavior and a having a yield stress less than 75 ksi.

Elagroudy et al. (2006) also tested beam-splice specimens using high-strength steel bars. They concluded that there is no reason to believe that the bond behavior of the A1035 reinforcing bars is different from that of conventional carbon steel for stress levels below the proportional limit of the A1035 steel (approximately 70 ksi). The nonlinear behavior of the A1035 bars at high stress levels is considered to be the reason behind the observed change in the mode of failure from sudden to gradual. Elagroudy et al. indicate that the nonlinear ductile response of A1035 bars at stress levels beyond the proportional limit, has a strong influence in reducing the bond strength of A1035 bars compared to the bond strength that can be obtained when using other types of steel bars with the same splice length and level of confinement, but with linear stress-strain behavior at high stress levels.

Harries et al. (2010) present research on bond characterization of high-strength steel bars in beam splice specimens. This study clearly demonstrated that the present AASHTO (2007) and ACI 318 (2008) requirements for straight bar tension development length may be extended to develop bar stresses of at least 125 ksi (860 MPa) for concrete strengths up to 10 ksi (69 MPa). For higher strength steel, greater bar strain and slip will occur prior to development of the bar. The associated displacement of the bar ribs drives a longitudinal splitting failure beyond that where yielding of conventional bars would occur; thus, confining reinforcement is critical in

developing higher strength bars. The results presented by Harries et al. (2010) and previous work of Seliem et al. (2009) clearly indicate that confining reinforcement should always be used when developing, splicing or anchoring ASTM A1035 reinforcing steel.

3.2.4 Hook anchorage specimens

Figures 3.1d and e represent full scale hook anchorage specimens designed to directly measure the pull-out capacity of hooked bar anchorages. A number of variations of these specimens exist but most mimic the embedment of a beam or girder longitudinal reinforcing bar into a column joint region and are modeled on a study conducted by Marques and Jirsa (1975). This setup allows the developed bar to be located in a concrete tension field and the concrete compressive strut developed by the hook tail to be anchored by an appropriately located reaction mimicking the compressive zone of the beam whose steel is being developed. A variation of this test set-up is adopted in the present study and described in Section 3.4.

Ciancone (2008) evaluated the behavior of standard hook anchorage specimens made using #5 and #7 A1035 steel. No confinement reinforcement was provided in the specimens. While the #5 hooks were able to develop their yield capacity of 100 ksi, the #7 hooks were not. This result suggests an effect of bar size and reinforces the need for confining reinforcement when developing A1035 bars.

3.3 BOND EXPRESSIONS IN CODE PROVISIONS

AASHTO LRFD *Design Specification* §5.11.2.1.1 prescribes the basic tension development length of #11 bars and smaller, l_{db} , as (AASHTO 2007):

$$l_{db} = \frac{1.25A_b f_y}{\sqrt{f'_c}} > 0.4d_b f_y \quad (\text{ksi units}) \quad (3.1)$$

Where

A_b = the area of the bar being developed;

d_b = the diameter of the bar being developed;

f'_c = the concrete strength;

f_y = the bar yield stress; i.e., the stress to be developed by the splice.

Recommendations of NCHRP Project 12-60 (Ramirez and Russell 2008) being considered for adoption by AASHTO are based on the ACI 318 (2008) requirements for basic tension development length with an additional factor, $\Psi_c = 1.2$, applied when f'_c exceeds 10 ksi:

$$l_{db} = \left(\frac{3f_y \Psi_c \Psi_t \Psi_s \lambda}{40 \sqrt{f'_c \left(\frac{c_b + K_{tr}}{d_b} \right)}} \right) d_b \geq 12 \text{ in.} \quad (\text{psi units}) \quad (3.2)$$

Where

Ψ_t and Ψ_e = factors to account for ‘top cast’ bars and the use of epoxy coated reinforcing steel (in this study both are taken as unity);

λ = a factor accounting for the use of lightweight concrete (also unity for this study).

The $(c_b+K_{tr})/d_b$ term accounts for the beneficial effects of transverse confinement and has an upper limit of 2.5. For values of $(c_b+K_{tr})/d_b$ less than 2.5, splitting failures are likely; for values greater than 2.5, pullout failures, which cannot be affected by the addition of more confining reinforcement, are likely. The NCHRP 12-60 recommendations also differ from the ACI 318 formulation by removing the Ψ_s factor which reduces the development length ($\Psi_s = 0.8$) for #6 bars and smaller.

Although the current AASHTO requirement (Equation 3.1) does not address confinement, it can be shown to result in development lengths comparable to or slightly longer than those resulting from the more complex ACI 408 (2003) requirements and more conservative (i.e.: longer) than those resulting from the use of ACI 318 (2008) when typical levels of confinement are used (Harries et al. 2010). The AASHTO requirement, however, may underestimate the development required in cases where no confining reinforcement is provided (i.e.: $K_{tr} = 0$). It is recommended that confining reinforcement, designed in a manner consistent with current practice, should always be used when developing or splicing ASTM A1035 reinforcing steel in beams (NCHRP 12-77 and Seliem et al. 2009).

3.3.1 Anchorage of standard hooks

The AASHTO LRFD *Design Specifications* (AASHTO 2007) and ACI 318 (2008) flexural design equations are formulated to ensure that steel reinforcement will yield before the concrete crushes when the nominal strength of a reinforced concrete element is reached. Development of the yield strength of a reinforcing bar requires that a sufficient development length is available

on both sides of the critical section where this capacity is expected to be developed. In locations where space is limited, insufficient length may be available to ensure full development of straight bars. In these cases, it is common to bend the bar to form either a 90-degree or 180-degree hook. The required length to develop the hook is shorter due to the mechanical advantage provided by engaging the concrete located along the inside radius of the hook bend. The bar stress transferred to the concrete increases dramatically around the bend of the hook. The increase indicates that the bearing of the inside of the hook against the concrete provides a significant portion of the anchorage (MacGregor and Wight 2005). These bearing stresses cause transverse tensile stresses, which can result in a splitting failure when confinement reinforcement is not present.

Minor and Jirsa (1975) studied the factors that affect the anchorage capacity of bent deformed bars. Specimen geometry was varied to determine the effect of bond length, bar diameter, inside radius of bend, and angle included in the bend. Slip between the bar and the concrete was measured at several points along the bar as load was applied. Load-slip curves were used to compare different bar geometries. The results indicated that most of the slip occurred in the straight and curved portion of the hook, with little occurring in the tail.

Marques and Jirsa (1975) investigated the anchorage capacity of hooked bars in beam-column joints and the effect of confinement on development of such bars. The variables included bar size, hook geometry embedment length, confinement, and column axial load. They found that equations from ACI 318-71 underestimated the anchorage capacity of the hooks. They found that for their test specimens, the tensile stress in the hooked bar when the bond capacity was reached was:

$$f_h = 700 (1 - 0.3 d_b) \psi \sqrt{f'_c} \leq f_y \quad (\text{psi units}) \quad (3.3)$$

Where

f_h = the bar stress which cannot be greater than the yield strength of the bar f_y ;

d_b = diameter of the bar;

f'_c = the concrete compressive strength;

ψ = coefficient which depends on the size of the bar, the length of the lead straight embedment, side concrete cover and cover extension of the tail.

It was also found that the required straight lead embedment length between the critical section and hook could be expressed as follows:

$$l_l = \left[\frac{0.04A_b(f_y - f_h)}{\sqrt{f'_c}} \right] + l' \quad (\text{psi units}) \quad (3.4)$$

Where

l' = the greater of $4d_b$ or 4 in.,

A_b = the area of the bar;

Pinc et al. (1977) also studied beam-column joints to determine the effect of lead embedment length and lightweight aggregate concrete on the anchorage capacity of the hook. The first approach consisted of examining the hook and lead embedment separately. Variables $f_l/\sqrt{f'_c}$ and l_l/d_b were correlated to obtain the lead embedment ultimate stress (f_l):

$$f_l = 67\left(\frac{l}{d_b} - 3\right)\Psi\sqrt{f'_c} \quad (\text{psi units}) \quad (3.5)$$

The bar stress at failure (f_u) can be obtained by summing Equations 3.3 and 3.5 to obtain:

$$f_u = 550\left(1 - 0.4d_b + \frac{0.8l}{d_b}\right)\Psi\sqrt{f'_c} \quad (\text{psi units}) \quad (3.6)$$

In an alternative approach, the following equation was obtained when the hook and lead lengths were examined together using $f_u/\sqrt{f'_c}$ and l_{dh}/d_b :

$$f_u = \frac{50\Psi l_{dh}\sqrt{f'_c}}{d_b} \quad (\text{psi units}) \quad (3.7)$$

An equation was needed to provide a length necessary to develop the yield stress in the bar (not the ultimate stress). Consequently, f_y is substituted for f_u in Equation 3.7 and the equation is rearranged as follows:

$$l_{dh} = \frac{0.02d_b f_y}{\Psi\sqrt{f'_c}} \quad (\text{psi units}) \quad (3.8)$$

Where l_{dh} represents the development length for a hooked bar and is measured from the critical section to the back of the hook. Equation 3.8 is essentially that used by ACI 318 today.

The ACI 408.1R-79 document presented recommendations for standard hooks for deformed bars in tension based on the study reported by Pinc et al. (1977) and further discussion of these by Jirsa et al. (1979). Based on the research and discussion, ACI committee 408 recommended the following basic hook development length equation be adopted:

$$l_{dh} = \frac{960d_b}{\phi\sqrt{f'_c}} \quad (\text{psi units}) \quad (3.9)$$

Where ϕ represents the resistance factor for anchorage which was incorporated in the design equation. The basic development length (l_{dh}) is then modified by the following factors:

$f_y/60,000$ for reinforcement having yield strength over 60,000 psi;

0.7 for side cover

0.8 for use of confining reinforcement

1.25 for use of lightweight aggregate; and,

A_{sr}/A_{sp} for reinforcement in flexural members in excess of that required for strength.

In 1979 ACI 318 adopted the recommendations of ACI Committee 408, and the development length equation and factors have not changed since. The epoxy-coated factor of 1.2 which was proposed by Hamad et al. (1993) was added in ACI 318-95.

Currently the ACI hook development equation is:

$$l_{dh} = \frac{0.02\psi_e\lambda d_b f_y}{\sqrt{f'_c}} \geq 8d_b \quad (\text{psi units}) \quad (3.10)$$

And AASHTO requires the following hook development length:

$$l_{dh} = \frac{38d_b}{\sqrt{f'_c}} \quad (\text{ksi units}) \quad (3.11)$$

The addition of the factor to normalize for yield strength (i.e.: $f_y/60$) makes the AASHTO equation identical to the ACI equation with the difference in the coefficient being due to the differences in the units. Additional factors for cover, epoxy coating, and lightweight aggregate are also identical to the ACI factors and are listed above. The development length obtained from Equation 3.11 shall not be less than $8d_b$ or 6 in.

3.4 ANCHORAGE OF HIGH-STRENGTH STEEL REINFORCING BARS HAVING STANDARD HOOKS IN CONCRETE

Current ACI (2008) and AASHTO (2007) equations for the development length of standard hooks do not directly address the use of high-strength steel bars that do not have a well-defined yield plateau or a relatively flat post-yield stiffness. Equations used to calculate the development length of standard hooks were developed using test data from A615 bars. These equations need to be evaluated to determine their applicability when used to calculate hook development lengths for high-strength steel bars.

Eighteen A1035 hook anchorage specimens were tested. The specimen details, shown in Figure 3.2 and Table 3.1, include two concrete strengths, nominally 5 and 10 ksi; and three bar

sizes: #4, #5 and #8. The #4 bars were provided with standard (AASHTO §5.10.2.1) 180° hooks and are intended to represent a) the anchorage of stirrups in girder sections where the stirrups are also called upon to serve as interface reinforcement for a cast-in-place deck; or b) the anchorage of primary reinforcing in cantilever slabs. The #5 and #8 bars were provided with standard 90° (AASHTO §5.10.2.1) hooks and are intended to represent anchorage of these bars where insufficient length is provided to develop a straight bar. This condition may occur in a) starter bars for piers or abutments; b) wall piers; or c) in short or cantilever flexural members such as pier caps.

All hook development lengths tested were designed using Equation 3.11 with all appropriate modifications (AASHTO §5.11.2.1.3). In all the specimens, the calculated value of ℓ_{dh} was modified by the selected nominal values of f_y , 100 or 125 ksi (see Table 3.1), i.e., by using the factor $f_y/60$. All the specimens were provided with sufficient cover to permit the 0.7 reduction factor to be applied. For all the specimens having confining reinforcement (all but – N specimens in Table 3.1), the confinement was adequate to permit the 0.8 reduction factor to be applied. The objective of this limited test series was to serve as a series of ‘proof tests’ applying the existing AASHTO hooked bar development length requirements to the higher strength A1035 reinforcing steel. The measured material properties of the A1035 hooks and A615 confining steel are given in Table 2.3. The measured 28-day concrete strength for the specimens having nominal strengths of $f_c' = 5$ and 10 ksi were 6.03 and 9.67 ksi, respectively (Table 2.4). Strain gages were applied over the length of hooked embedment (Figure 3.4a) to determine bar stresses.

The test setup, shown in Figure 3.2, was designed to replicate as closely as possible (without a full-scale element test) the stresses in the vicinity of a hook anchorage in tension. The hollow core hydraulic ram placed over the bar directly places the bar in tension and the lever arm reaction to right of the bar (in Figure 3.2a) provides the equilibrating compression. In the setup used, the compression reaction is 1.2 times the bar tension, more than sufficient to provide the appropriate reaction force necessary to develop the hook. A short region of the hooked bar was left unbonded as it entered the concrete block (achieved by wrapping the bar in foam pipe insulation prior to casting concrete) resulting in the development length (l_{dh}) beginning 3 in. below the concrete surface. The debonded region was provided to a) mitigate the pullout of a cone of concrete at the concrete surface which affects the development behavior and slip results; and b) to provide additional concrete depth (h in Table 3.1) to mitigate the shear failure (that was nonetheless observed in Specimens H4-2 and H8-2, as will be discussed below) of a ‘cone’ of concrete anchored by the hook tail.

Each bar was anchored using a bolted in-line mechanical splice anchor (‘Zap Screwlock’ splice from BarSplice Products) with both sides of the splice anchor engaged. (The centering pin, intended to position the spliced bars, was removed to allow both sides of the splice anchor to be engaged on the same bar.) All anchor bolts were fully torqued (snap off bolts) except for the lower two, closer to the concrete surface, that were provided with only 1/3 and 2/3 of their recommended torque values, respectively. The reduced torque levels were intended to mitigate failure associated with the stress raisers that this anchorage produces (Coogler et al. 2008). This splice anchorage performed very well in this test series and is recommended for similar laboratory applications.

Each test was a simple monotonic pull-out test of the hooked bar. The test was conducted in load control and conducted such that failure occurred in approximately 15 minutes. Strain gage, slip and applied load data were automatically collected at a rate of 1 Hz.

3.4.1 Hook anchorage results

The results in terms of bar stress achieved and the failure mode observed for all eighteen specimens are shown in Table 3.1. All test specimens exceeded their design stresses of 100 or 125 ksi, denoted f_y in Table 3.1. Indeed, most specimens achieved their ultimate capacity (f_u in Table 2.3) as evidenced by a bar rupture failure in the exposed gage length – denoted ‘R’ in Table 3.1. All ruptured bars exhibited significant necking and elongation and were unaffected (except H5-1, see below) by the bar anchorage or loading mechanism. Observed rupture stresses agree well with the previously tested material properties (Table 2.3).

Specimen H5-1 (the first tested) exhibited a bar rupture that was affected by the installation of the splice anchor used to react the applied load (not actually part of the test). Nonetheless, this specimen still achieved a stress of 160 ksi. A change was made to the splice installation (see above) and this failure mode was mitigated for all subsequent tests.

Only two of the #8 specimens were tested to bar rupture; the remaining tests were stopped prior to failure at a stress of 140 ksi, which was greater than the required proof load. The tests were stopped in the interest of laboratory safety (a rupturing #8 A1035 is a significant projectile).

In two specimens having very short development lengths, the ultimate failure was a shear ‘cone’ in the concrete (denoted C in Table 3.1). This failure mode a) significantly exceeded the required proof loads; b) occurred at loads very close to those expected to cause bar rupture; and

c) is an artifact of the test specimen and would not be expected in ‘real world’ applications. Figure 3.3 shows an example of such a ‘C’ failure. Providing a longer debonded region (i.e.: larger value of h , see above) would have mitigated this failure mode.

Strain profiles demonstrate that the hooks are well developed and efficiently transfer stress to the concrete through bond. Figure 3.4 plots the experimentally observed bar strains along the length of the hooks (reported in units of bar diameters (d_b) for the sake of normalization). The uppermost data point on each curve ($d_b = 0$) is obtained from a mechanical clip gage mounted a few inches above the concrete specimen. This clip gage was the same instrument used in the bar tension tests reported in Table 2.3. The next data point ($d_b = 3$) is obtained from the strain gage located $3d_b$ into the concrete (see the right hand inset in Figure 3.4a). As would be expected, these first two strains are similar since little development has yet been engaged. The next data point down is obtained from the strain gage located $5d_b$ from the start of the hook bend and the final data point is $5d_b$ past the bend on the hook tail. The strains at this final location are all very small indicating that the hook itself is not being engaged in tension. The strain gages used were very small (0.25 in. overall length); their installation does not affect the bond stress development in any significant manner. The data in Figure 3.4 are given at stresses of 60 ksi (yield of mild steel), 100 ksi, 125 ksi (design values for this test), and 140 ksi (maximum value at which data are available for all specimens).

The ‘slip’ of the hook was measured using displacement transducers to measure the relative movement of the bar as it is ‘pulled out’ of the concrete. Slip versus bar stress curves are shown in Figure 3.5. Since the slip measurement is obtained over a distance of exposed bar (about 5 in. in most tests), the reported slip is greater than the ‘actual’ slip due to the strain over this unbonded length. Figure 3.6a shows the slip recorded at stress levels of 60, 100, 125, and

140 ksi. The ‘ultimate’ stress is the slip reported at the maximum stress obtained as given in Table 3.1. Figure 3.6b shows only the slip values reported at 125 ksi sorted against a) concrete strength (5 or 10 ksi); b) design bar stress (100 or 125 ksi); and c) the presence of confining reinforcement (N specimens had no confining reinforcement).

Observations drawn from Figure 3.6 include:

- a) Through the proof loads (100 and 125 ksi), slip is limited and rarely exceeds 0.06 in. Indeed, through stresses of 140 ksi, slip rarely exceeds 0.09 in. and is not affected by bar size, concrete strength, development length, or the presence of confining reinforcement.
- b) Slip is not significant until near the ultimate load (greater than 140 ksi). It is noted that in some cases, the large values of slip include the plastic deformation of the reinforcing bar within the gage length over which slip is measured.
- c) Slip at 125 ksi is marginally (<0.01 in.) more pronounced for the 10 ksi concrete. This slight increase is believed to result from the use of smaller aggregate and its effect on mechanical bond.
- d) Slip at 125 ksi is unaffected by the development length provided. Hence, there is reserve bond capacity beyond that implicitly assumed by the development length calculation.
- e) The specimens having confining steel exhibited marginally (<0.02 in.) greater slip at 125 ksi than those that did not. This observation is counterintuitive and may simply represent the natural scatter of the data.

This series of hook embedment tests was intended as proof tests of the present AASHTO hook development requirements given by Equation 3.11. These tests have shown that the present

requirement is adequate to develop up to 125 ksi in 10 ksi concrete in cases where adequate cover and confinement – based on current design requirements – are provided.

In using higher strength steel, greater bar strain and slip will occur prior to development of the bar. The associated displacement of the bar lugs drives a longitudinal splitting failure beyond that where yielding of conventional bars would occur; thus, confining reinforcement is critical in developing higher strength bars. The results of this study and previous work (Seliem et al. 2009) clearly indicate that confining reinforcement, designed in a manner consistent with current practice, should always be used when developing, splicing, or anchoring ASTM A1035 or other high strength reinforcing steel.

Table 3.1 Hook specimen details and test results.

ID	A ^a bar size – hook angle	f _c ' ksi	f _y ^b ksi	l _{hd} ^c in.	h ^a in.	D ^a in.	s ₁ ^a in.	B ^a bars	C ^a in.	ultimate ksi	failure ^d
Steel	A1035					A615		A615	A615		
H4-1N	#4 – 180°	5	100	10	16	none	n.a.	4 #4	#3 @ 6	179	R
H4-4N	#4 – 180°	5	125	12	18	none	n.a.	4 #4	#3 @ 6	177	R
H4-1	#4 – 180°	5	100	8	14	5 #3 @ 1.5	1	4 #4	#3 @ 6	177	R
H4-4	#4 – 180°	5	125	10	16	6 #3 @ 1.5	1	4 #4	#3 @ 6	177	R
H4-2	#4 – 180°	10	100	6 ^e	12	3 #3 @ 1.5	1	4 #4	#3 @ 6	173	C/R
H4-5	#4 – 180°	10	125	8	14	5 #3 @ 1.5	1	4 #4	#3 @ 6	176	R
H5-1N	#5 – 90°	5	100	13	19	none	n.a.	4 #5	#3 @ 6	168	R
H5-4N	#5 – 90°	5	125	16	22	none	n.a.	4 #5	#3 @ 6	168	R
H5-1	#5 – 90°	5	100	10	16	5 #3 @ 1.88	1.25	4 #5	#3 @ 6	160	RA
H5-4	#5 – 90°	5	125	13	19	6 #3 @ 1.88	1.25	4 #5	#3 @ 6	168	R
H5-2	#5 – 90°	10	100	8	14	4 #3 @ 1.88	1.25	4 #5	#3 @ 6	167	R
H5-5	#5 – 90°	10	125	9	15	4 #3 @ 1.88	1.25	4 #5	#3 @ 6	168	R
H8-1N	#8 – 90°	5	100	20	26	none	n.a.	4 #8	#3 @ 6	140	NA
H8-4N	#8 – 90°	5	125	25	31	none	n.a.	4 #8	#3 @ 6	140	NA
H8-1	#8 – 90°	5	100	16	22	5 #3 @ 3	2	4 #8	#3 @ 6	153	NA
H8-4	#8 – 90°	5	125	20	26	6#3 @ 3	2	4 #8	#3 @ 6	138	NA
H8-2	#8 – 90°	10	100	12	18	3 #3 @ 3	2	4 #8	#3 @ 6	162	C (no R)
H8-5	#8 – 90°	10	125	15	21	4#3 @ 3	2	4 #8	#3 @ 6	166	R

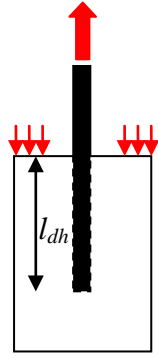
^a see Figure 3.2

^b design yield stress to be developed in Equation 3.11

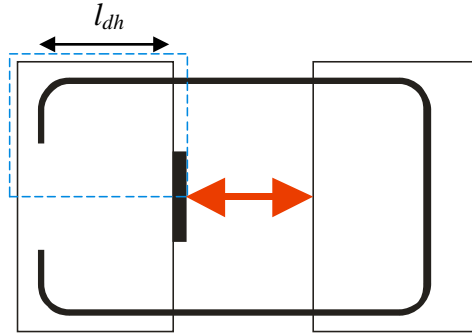
^c see Equation 3.11

^d failure mechanisms: R = bar rupture; RA = bar rupture affected by bar anchor; C = concrete shear failure; NA = test stopped prior to failure for safety considerations – in this case, the maximum obtained bar stress is reported.

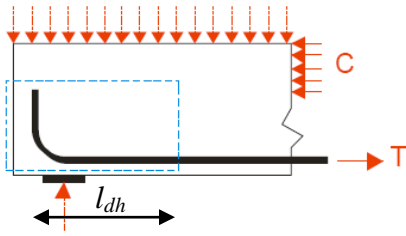
^e minimum development length



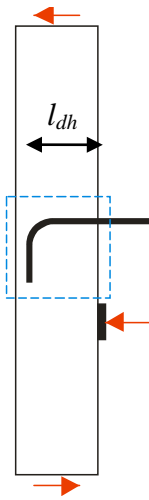
a) pull-out test



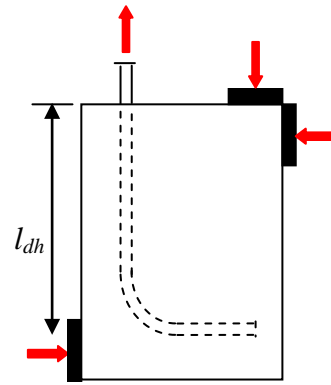
b) hook anchorage pull-out tests
(after El Hacha et al. 2006)



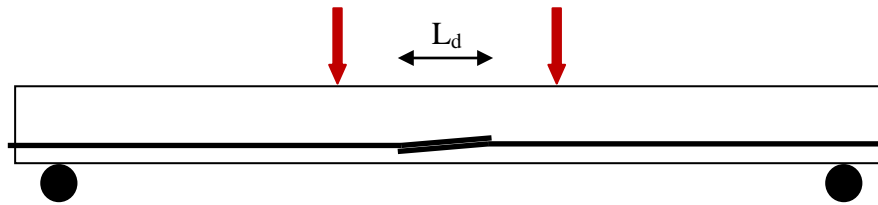
c) beam-end test



d) beam connection
test (after Marques and
Jirsa 1975)

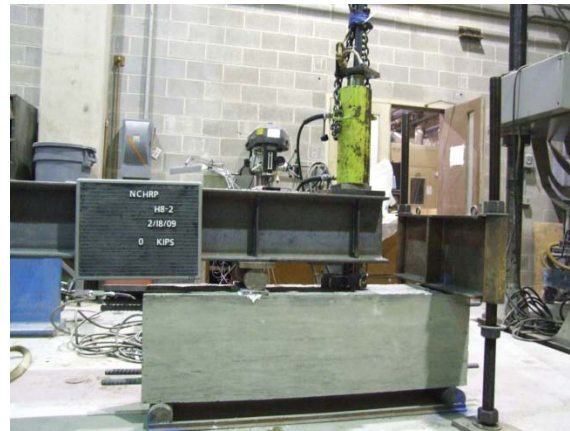
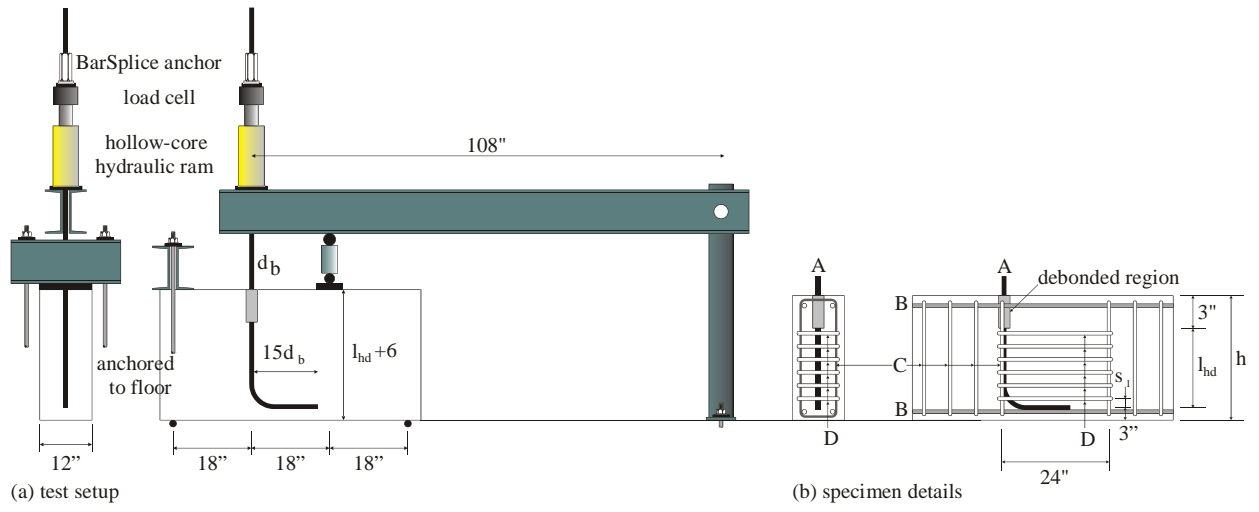


e) hook anchorage test



f) beam splice test

Figure 3.1 Development test geometries.



(c) Specimen H8-2 (image is reversed from figure a)

Figure 3.2 Hook test setup and specimen details.

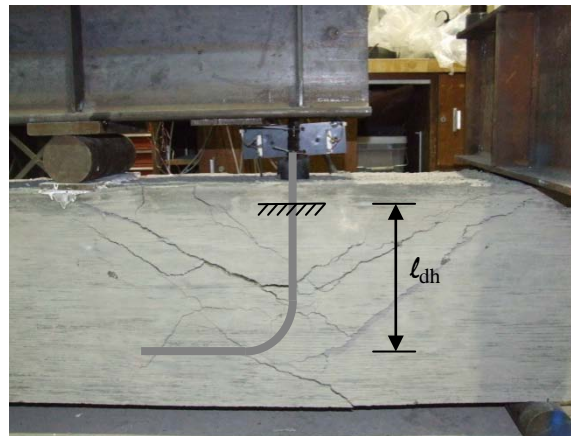
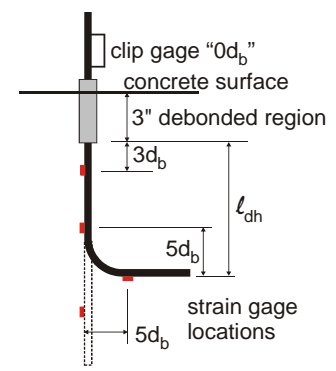
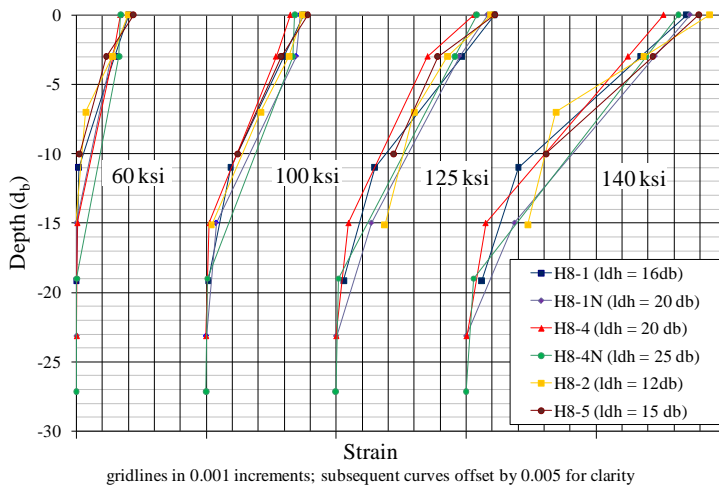
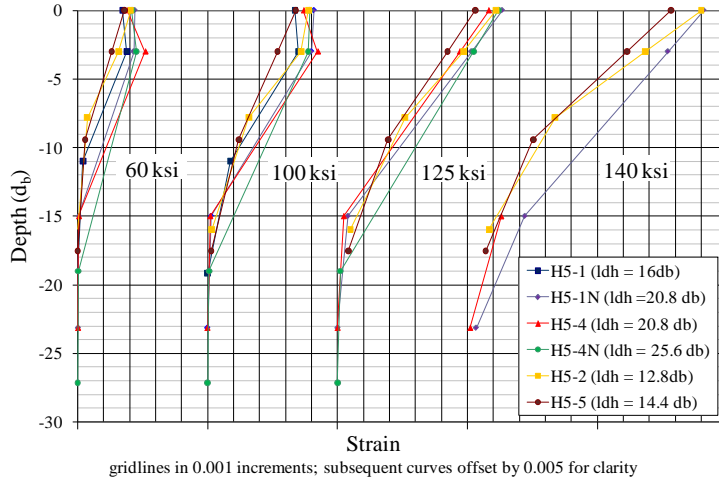


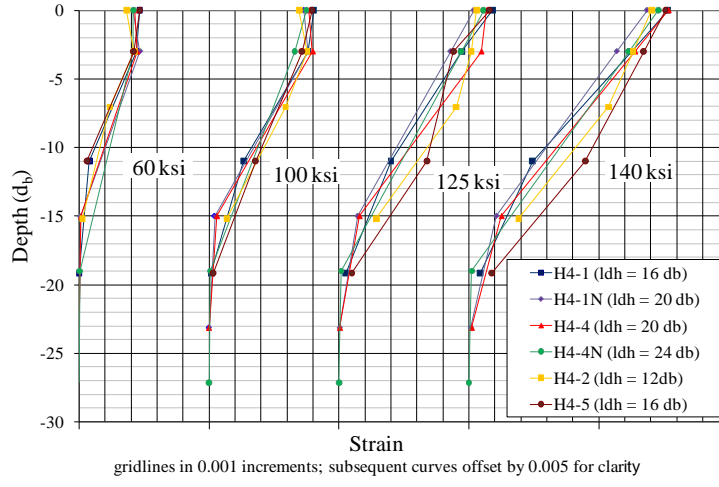
Figure 3.3 Typical Concrete Shear Failure (Specimen H8-2).



a) #8 90° hook specimens

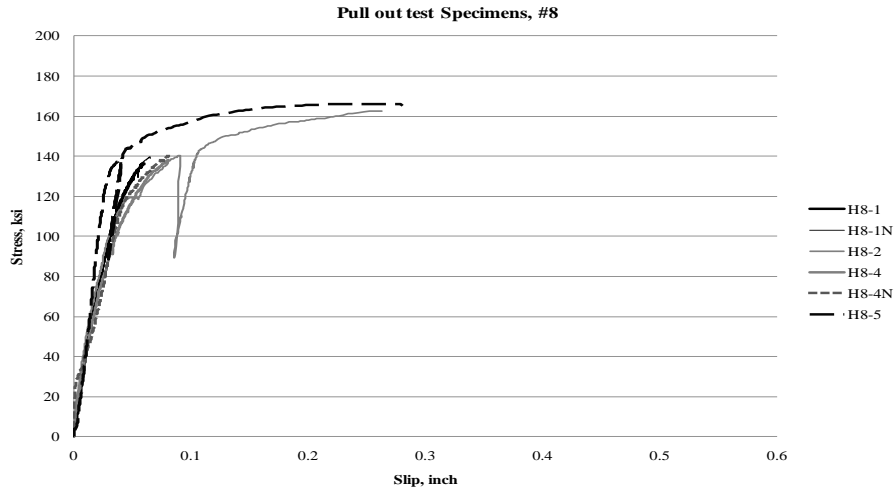


b) #5 90° hook specimens

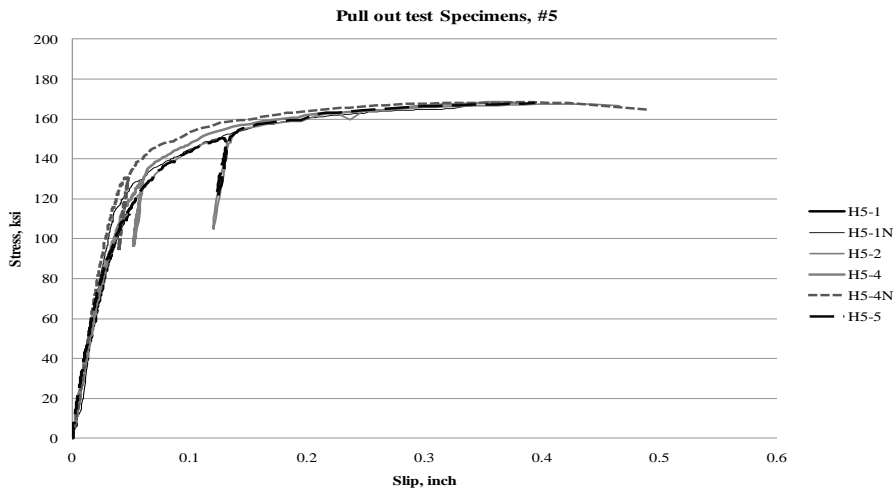


c) #4 180° hook specimens

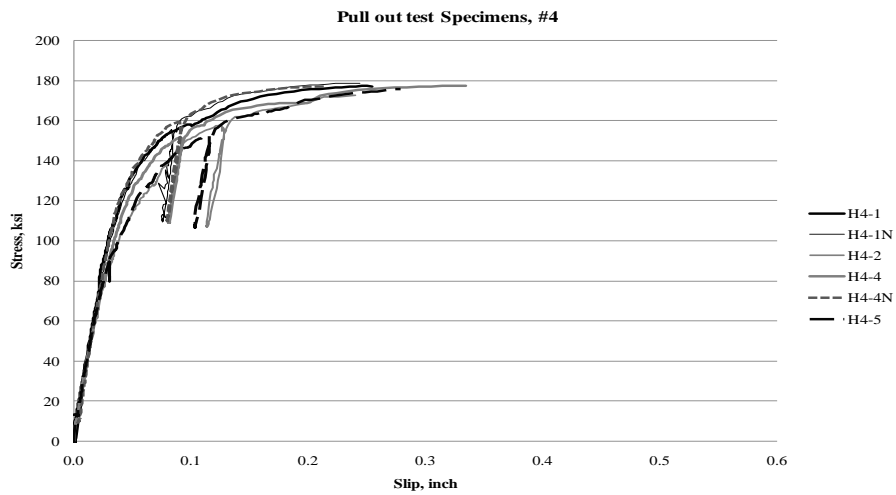
Figure 3.4 Strains along hook embedment at selected bar stresses.



a) #8 90° hook specimens

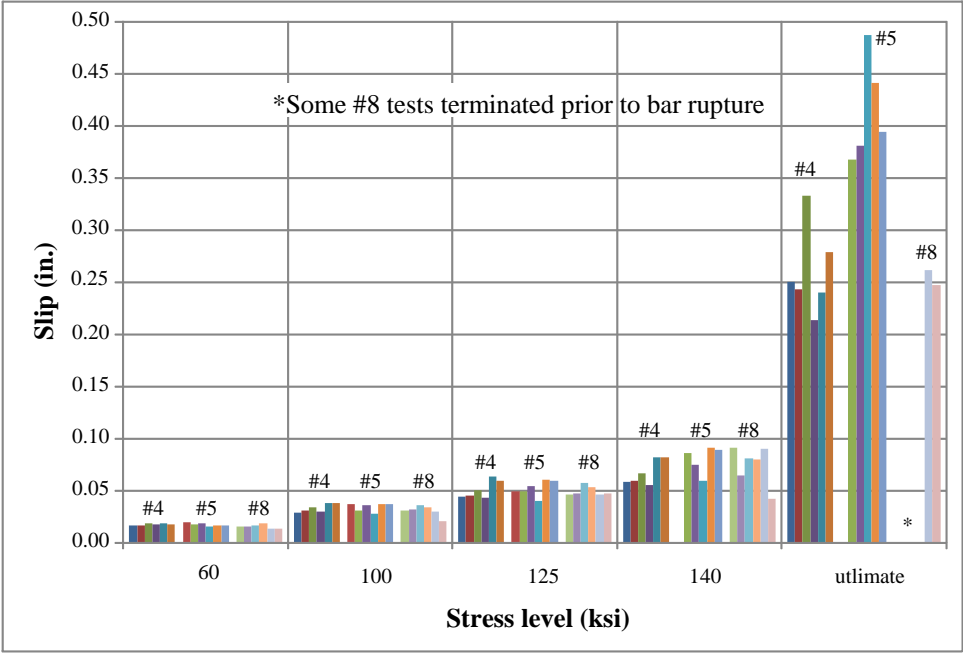


b) #5 90° hook specimens

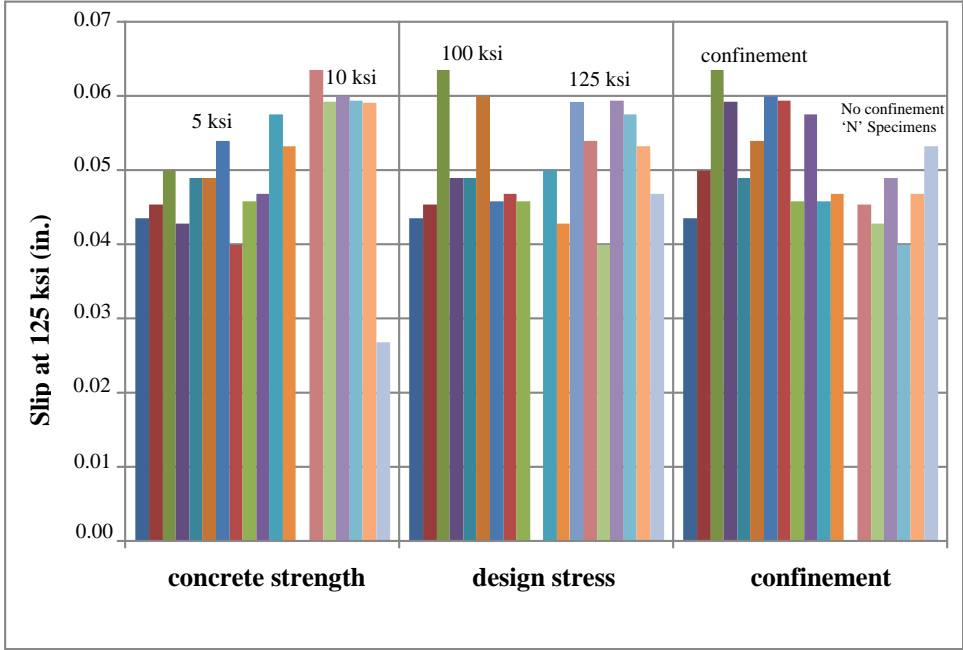


c) #4 180° hook specimens

Figure 3.5 Slip versus bar stress.



(a) slip at different stress levels.



(b) slip at 125 ksi.

Figure 3.6 Slip of embedded hooks.

4.0 FATIGUE PERFORMANCE OF HIGH STRENGTH REINFORCING STEEL

Fatigue is a process of progressive structural change in a material subjected to transient loads, stresses or strains. Such transient effects occur through repetition of all or part of the live load in structures such as bridges, gantry girders, and machine foundations. The transient loads may be random (wind-induced effects) or periodic. Periodic loads may have one frequency (machine vibrations) or may include multiple frequencies as occurs on bridge structures. The repeated application of live load (vehicle transits of a bridge, for instance) may result in fatigue damage to any susceptible element. The load spectrum for a particular structural member is required for the prediction of its fatigue behavior. Fatigue strength is defined as the maximum repeated stress range (S) that may be sustained without failure for a specified number of loading cycles (N). The stress range is defined as the algebraic difference between the maximum and the minimum stress in a stress cycle: $S = f_f - f_{min}$; that is: the transient stress. Most ferrous materials exhibit an 'endurance limit' or 'fatigue limit', a value of S below which failure does not occur for an unlimited number of cycles. The following sections focus on the fatigue behavior of steel reinforcing bars for reinforced concrete structures. In general, the concrete material fatigue performance exceeds that of the steel and is not considered in design (Neville 1975).

4.1 S-N RELATIONSHIPS

In order to predict fatigue behavior (in this case to establish appropriate experimental parameters), it is necessary to establish the S - N relationship for reinforcing bars in concrete tested under repeated flexure. The S - N approach requires numerous fatigue test data points to establish the relationship between the stress range, S , and the number of cycles to failure, N . Fatigue data exhibits considerable scatter and therefore numerous repeated tests are needed to develop the “best-fit” relationship that describes the fatigue behavior of the material with a reasonable confidence level. There has been a significant amount of research studying fatigue of reinforcing steel and multiple (necessarily empirical) equations have been developed to describe its behavior. Many correspond to the same general form of the equation:

$$S^m \times N = k \quad (4.1)$$

where

S = applied stress range;

m = stress exponent;

N = number of cycles to cause fatigue failure; and

k = constant.

Parameters m and k are dependent upon the units used to express S . Values of m and k are given based on bar size and, in some cases, the expected fatigue life, N . Available models are all based on reinforcing steel having nominal yield strength, f_y , between 40 and 75 ksi. No significant difference in steel reinforcing bar S - N behavior is observed over this range of yield values (MacGregor et al. 1971, Mallet 1991). Additionally, some models are based on axial tension tests

of bars in air, while others are based on bars in concrete beams tested in flexure. Moss (1982) demonstrated that the fatigue life of bars tested in concrete exceeds that of bars tested in air. This difference is believed to be a manifestation of the tension-stiffening phenomenon (see Section 5.1.2.2). Most of the relevant studies have been conducted in Europe (Moss 1980, Tilly and Moss 1982, Mallet 1991). Best practices based on these studies have been adopted by the CEB FIB Model Code (1990) and these $S-N$ relationships are adopted here². The relationships given are for #5 bars.

$$S^5 \times N = 2.621 \times 10^{17} \text{ (ksi)} \qquad N < 1,000,000 \qquad (4.2)$$

$$S^9 \times N = 2.115 \times 10^{26} \text{ (ksi)} \qquad 1,000,000 < N < 100,000,000 \qquad (4.3)$$

There are no $S-N$ relationships for reinforcing steel prescribed by ACI or AASHTO standards.

4.2 FACTORS AFFECTING FATIGUE PERFORMANCE

It has been shown by many researchers in a variety of contexts (new construction, retrofit applications, etc.) that the fatigue behavior of reinforced concrete members is governed by the behavior of the internal reinforcing steel. Plain concrete appears to have no endurance limit because high cycle-low stress loading does not contribute to fatigue damage (Mallet 1991). Neville (1975) observes that concrete softens with cycling, resulting in a redistribution of force in a reinforced concrete member. Thus, as a reinforced member is cycled at a constant applied

² the outcome of a number of fatigue studies conducted by Harries have all shown that Equations 4.2 and 4.3 are the most representative of the fatigue behavior of #5 bars in concrete beams in flexure (Harries et al. 2006),

load, the stress range applied to the steel ‘drifts’ upwards as additional force is distributed to the steel (Harries and Aidoo 2005). This effect is rarely accounted for in beam-type fatigue tests where the stress range reported is conventionally that at $N = 1$ (as will be done in the present study).

Factors that affect the fatigue strength of deformed reinforcing bars include:

- a) chemical composition, microstructure, inclusions, rolling defects etc.;
- b) grade of bar (yield and ultimate strength);
- c) size of bar;
- d) embedment in concrete;
- e) minimum stress level, f_{min} ;
- f) geometry of deformations (ribs); and,
- g) presence of bends or welding.

Of the factors noted, the first five have only a minor influence on the fatigue characteristics of deformed bars. Geometry of the ribs has a very significant influence on the fatigue strength. Ribs are provided to improve bond to concrete but they also cause stress concentrations. Ribs reduce fatigue strength due to the fact that the junctions of the longitudinal and transverse ribs with the body of the bar form regions of stress concentration inducing a "notch effect" that results in crack initiation and a brittle failure. Wascheidt (1965) found that the fatigue strength of 0.63 in. diameter ribbed bars was 18% lower than that of smooth round bars for axial tests in air. Snowden (1971) obtained a similar result for bending fatigue of 17 ft long beams. Helgason et al. (1969) found 1 in. ribbed bars in concrete beams had a fatigue strength of

27.5 ksi at 10 million cycles. For bars having ribs well-rounded at their root and making a small angle with the bar axis, higher fatigue strength values are obtained (of course, as discussed in Chapter 3, such ribs result in poorer bond performance). Both Bannister (1969) and Burton and Hognestad (1967) found that longitudinally oriented ribs resulted in fatigue strength as much as 40% lower than that for bars having only transverse ribs. This reduction is likely due to the additional notch effect resulting from the intersection of ribs and the stress raiser being oriented parallel to the principal stress. Most bar patterns available today, including those used for A1035 bars, have both transverse and longitudinal ribs.

Fatigue strength increases very slightly with an increase in the grade of bar and decreases with an increase in bar diameter. This effect is not peculiar to reinforcing bars and can be explained by there being a greater likelihood of flaws on the larger surface area of the larger bar. There is a similar 'size' effect on static strength. Frost et al. (1974) found that the effect of bar size on fatigue strength is no more than 5% for plain round bars from 0.5 to 1.4 in. diameter. The effect is much greater for deformed bars. Helgason et al. (1969) found 1.4 in. bars had about 10% lower fatigue strength than 0.63 in. bars when tested in concrete beams. However, bar size effects seem to be more pronounced in axial tests in air than in bending tests.

The effect of embedment in concrete is significant only for bars with poor bond characteristics (see Chapter 3). There is also a slight reduction in fatigue strength at high minimum stress levels. Fatigue strength falls rapidly at bends having a small radius of curvature. Welds act as significant stress raisers and when applied in the region of maximum stress in the bar can reduce the fatigue strength up to 50% (MacGregor 1971). Other stress raisers including manufacturer's identification (mill) marks, surface discontinuities from worn or chipped rollers at the steel mill and fretting can also adversely affect the fatigue life of reinforcing bars (Mallet

1991). For example, fatigue ruptures of bars tested in concrete having transverse reinforcement almost always fail at the location of a transverse bar. This failure pattern is due to the stress concentrating effect of fretting of the perpendicular bar on the bar subject to fatigue stresses (this behavior was observed in the present study).

4.3 ACCOUNTING FOR FATIGUE IN DESIGN

The AASHTO (2007) limit for fatigue-induced stress in mild steel reinforcement is based on the outcome of NCHRP Project 4-7 reported by Helgason et al. (1976). The maximum permitted stress range in straight reinforcement resulting from the fatigue load combination is given in AASHTO LRFD (2007) §5.5.3.2 as:

$$f_f \leq 21 - 0.33f_{min} + 8(r/h) \quad (\text{ksi units}) \quad (4.4)$$

Where

f_{min} = algebraic minimum stress level (compression negative);

r/h = ratio of base radius to height of rolled-on transverse deformations; 0.3 may be used in the absence of actual values.

Recent revisions to AASHTO LRFD §5.5.3.2 incorporate the default r/h ratio:

$$f_f \leq 24 - 0.33f_{min} \quad (\text{ksi units}) \quad (4.5)$$

The AASHTO-prescribed relationship is shown to represent the lower-bound results of many fatigue studies considering a range of bar sizes and is reported applicable for ASTM A615 Grades 40, 60, and 75 reinforcing bars (Corley et al. 1978). Significantly, bar size is not considered in the AASHTO-prescribed limit although it is well established that larger bar sizes typically have lower fatigue limits (Tilly and Moss 1982).

4.4 CURRENT RESEARCH ON FATIGUE PERFORMANCE OF REINFORCING STEEL

It is recognized that the use of high-strength reinforcement may permit a reduction of the total area of steel required for flexural resistance. The resulting larger stresses in the steel may adversely affect fatigue performance of the member. Specifically, if designed efficiently, both the minimum and maximum stresses will increase. However the maximum stress may be increased to a greater degree, resulting in a larger stress range under transient loads. Fatigue behavior of reinforcing bars is very sensitive to rib geometry but not appreciably sensitive to steel grade. Thus, the fatigue performance of high strength reinforcing steel is not likely to be proportional to the steel yield capacity or the stress levels inherent in an efficient design. Thus, in order to optimize design, an understanding of the fatigue behavior of high strength reinforcement is required.

DeJong et al. (2006) present a study of the fatigue behavior of high-strength reinforcing steel. DeJong conducted fatigue tests on ASTM A1035 steel having a reported (0.2% offset) yield value of 116 ksi and ultimate tensile strength of 176 ksi. Tests on #3, #4, and #5 bars demonstrated a fatigue strength (at $N = 1$ million cycles) of 45 ksi. Companion tests on Grade 60

reinforcing bars had a fatigue life of 24 ksi. Stress-life tests using polished machined coupons resulted in similar results, with $N = 5$ million cycle fatigue limits of 167 ksi and 91 ksi for the ASTM A1035 and Grade 60 steel, respectively. Such results are commonly observed: the stress range fatigue limit is approximately equal to the tensile strength of the material for smooth polished specimens. The results also clearly identify the detrimental effect of the presence of ribs on the bars – the fatigue lives were reduced significantly despite the greater number of cycles for the polished specimen tests. There are no other known studies of the fatigue performance of high strength reinforcing steel.

In order to establish the validity of AASHTO-established fatigue limits (Equation 4.5) and to assess the effects of yield strength on fatigue performance, a review of available fatigue data was conducted. Table 4.1 summarizes these studies. While few studies report on bars having $f_y > 75$ ksi, the fact that these studies report different steel grades (i.e. 40, 60 and 75 ksi) permit some trends to be established. Figure 4.1 shows the reported fatigue endurance limits as a function of yield strength. Although stress range is the critical parameter affecting fatigue, this data have been sorted by the value of f_{min} which is shown to have little effect on the results. Figure 4.1 shows no values of the endurance limit falling below 24 ksi. Thus, the present AASHTO recommendations for f_f are deemed to be conservative for tension-tension fatigue (i.e.: f_{min} positive). Additionally, a correlation between endurance limit and f_y is evident. Thus, the penalty paid by using Equation 4.5 with high strength steel is unjustified. While Equation 4.6 (below) does not recognize the correlation between f_f and f_{min} , it does remove this penalty in a justifiable manner.

4.5 FATIGUE BEHAVIOR OF CONCRETE BEAMS HAVING HIGH-STRENGTH REINFORCEMENT

Although there are data that suggest an improved fatigue limit for higher-strength bars (DeJong et al. 2006) may be permissible, conventional wisdom suggests that this should not be the case. Certainly there are insufficient data at this time to make any recommendation in the direction of increasing the AASHTO fatigue limit and/or making the fatigue limit a function of yield (or tensile) capacity. Nonetheless, the present AASHTO fatigue limit (Equation 4.5) is believed to be universally conservative for the reasons that follow:

- a) The f_{min} term is appropriate where f_{min} is positive but appears to be “calibrated” to result in the same stresses as those used for working stress design using Grade 40 steel.
- b) The equation itself represents an extreme lower bound. Corley et al. (1978) report: “A No. 11 Grade 60 bar fractured in fatigue after 1,250,000 cycles when subjected to a stress range of 21.3 ksi and a minimum stress of 17.5 ksi tension. *This is the lowest stress range at which a fatigue fracture has been obtained in an undisturbed North American produced reinforcing bar*” [emphasis added].

The impact of applying the AASHTO equation to higher-strength reinforcing steel is that f_{min} may be increased, taking advantage of the higher strength steel, resulting in an unwarranted reduction in the fatigue limit. It is therefore proposed to normalize f_{min} by the yield stress, f_y . Calibrating this equation so that there is no effect for Grade 60 reinforcement, one arrives at:

$$f_f \leq 24 - 20(f_{min}/f_y) \text{ (ksi units)} \quad (4.6)$$

While still felt to be conservative, this equation recognizes that fatigue behavior of ferrous metals is largely unaffected by the yield strength of the material itself; thus, the baseline endurance limit of 24 ksi is unchanged.

In practice, the value of f_{min} will generally be on the order of $0.10f_y$ to $0.30f_y$. For Grade 60 A615 steel, the present AASHTO requirement (Equation 4.5) results in fatigue limits of 22 to 18 ksi, respectively. Applying the same equation to steel having a yield strength of 120 ksi, for instance, results in the unwarranted reduction of the permitted fatigue stress to 20 to 12 ksi, respectively. The values imply that the higher strength material has reduced fatigue performance, which is contrary to all available data. The ironic outcome, in terms of design, is that *more* of the higher strength steel is required to carry the same transient loads. Equation 4.6, on the other hand, results in the fatigue limits for the 120 ksi steel being the same as those of the 60 ksi steel. This latter result, while still believed to be conservative for the reasons given above, is nonetheless more rational.

4.5.1 Fatigue proof tests

It should be noted that the limited scope of the fatigue testing program conducted herein served as a “proof test” to examine whether the existing AASHTO specifications for the fatigue limit state are applicable to members with high-strength reinforcement. Thus, it is necessary to select a stress range, S , appropriate to the number of cycles to be tested, N .

The AASHTO fatigue limits are derived largely from tests having $N=2,000,000$. However, as code-prescribed limits, they must be understood to be appropriate for the ‘life of the structure’. AASHTO LRFD (2007) §6.6.1.2.5 provides some guidance as to a) the definition of a fatigue cycle; and b) the expected number of cycles over the life of a structure. Based on

AASHTO-recommended values, a deck slab on an urban interstate may undergo approximately 1 million fatigue cycles per year:

$$N = 365 \times n \times ADTT_{SL} = 930,750 \text{ cycles} \quad (4.7)$$

where $ADTT_{SL} = 0.85(ADTT) = 0.85(0.15ADT)$ with $ADT = 20,000$ and $n = 1$.

The supporting girders (assuming the bridge exceeds 40 feet (12 m)) will undergo twice this number of cycles. Clearly, not all bridges see these many cycles: A lightly travelled two-lane rural highway bridge may undergo only about 100,000 cycles per year:

$$N = 365 \times n \times ADTT_{SL} = 109,500 \text{ cycles} \quad (4.8)$$

where $ADTT_{SL} = 1.0(ADTT) = 1.0(0.15ADT)$ with $ADT = 1,000$ and $n = 2$.

The selection of an appropriate fatigue proof test must consider at least the following:

1. Practical value of N . Two million cycle tests are most common and may be considered 'standard'. At 1.2Hz, a 2 million cycle test takes three weeks. Generally there is more scatter in results as N is taken less than 1 million cycles. Larger values of N are felt to be impractical for large-scale laboratory tests and few such tests are reported in the literature.
2. A minimum stress, f_{min} , must be used that is adequate to represent 'dead load' and to permit safe and efficient control of the test protocol. A value $f_{min} = 0.10f_y$ is commonly used.

3. The value of the stress range, S , is selected to ‘match’ the value of N selected. Considering the previous discussion:
 - i. Assume $f_{min} = 0.10f_y$; therefore, $f_r = S \leq 22$ ksi (using Equation 4.6).
 - ii. Based on the CEB (1990) S - N relationships given in Equations 4.2 and 4.3 (summarized in Table 4.2), $S = 22$ ksi corresponds to $N = 20,000,000$ which correlates reasonably well with the expected range of fatigue life anticipated by AASHTO. For example, a deck slab on an urban interstate will undergo approximately 20 million fatigue cycles over a 20-year life (Equation 4.7).
 - iii. Based on this correlation and Table 4.2, setting $S = 28$ ksi for a 2 million cycle test is an appropriate surrogate for a 20 million cycle test having $S = 22$ ksi. The latter is the AASHTO ‘proof protocol’ but would take upwards of 7 months to complete, while the former may be conducted in a practical time frame (3 weeks).
4. AASHTO limits are based on *in air* tests that are acknowledged to yield lower fatigue endurance limit values than *in concrete* flexural beam tests.
5. Limited available data (DeJong et al. 2006) suggest that A1035 microcomposite alloy steel has superior fatigue resistance to A615 ‘black steel’.

The specimen protocols described below were selected considering these factors.

4.5.2 Specimen details

Specimen details were selected to correspond to flexural tests conducted elsewhere within the NCHRP 12-77 project (Specimen F3 from the University of Cincinnati's tests of flexural behavior). Two beams 16 in. deep x 12 in. wide having 4 #5 A1035 longitudinal bars and #3 A615 stirrups spaced at 9 in. along the entire length of the beam were cast with 10 ksi concrete. The beams were 18.5 ft long and were tested in midpoint flexure over a span of 16.5 ft; 4 in. wide neoprene supports were used making the face-to-face dimension of the span 16'-2" (Figure 4.2). The measured material properties of the steel reinforcement are given in Table 2.3 and the measured concrete compressive strength was 9.67 ksi (Table 2.4). Cyclic testing was carried out at a frequency of 1.2 Hz. At regular intervals, the frequency was reduced to 0.003 Hz (1 cycle in 5 minutes) and a fully instrumented cycle was carried out.

4.5.3 Fatigue test protocol

The protocol adopted involved testing the first beam at a stress range (in the primary #5 A1035 reinforcing bars) of 32 ksi. The justification being that if the beam withstands 2 million cycles at stress greater than 28 ksi, it has *de facto* exceeded the current AASHTO requirements and thus represents a proof test with good confidence. Since the first beam successfully resisted 2 million cycles, the second beam was tested at a greater stress range (46 ksi). All test control is based on reinforcing bar stress measured using strain gages. There were four strain gages in each specimen: one mounted on each A1035 tension reinforcing bar and located in the midspan.

4.5.4 Results of fatigue test 1

Fatigue Test 1 was tested between 03/10/2009 and 03/31/2009. The applied load at midspan was cycled between 7 and 17 kips at a rate of 1.2Hz for 2 million cycles. The measured stress range in the A1035 longitudinal steel was 31.1 ksi in the initial test cycles. Strain gages were lost during the first 100,000 cycles (this is expected). Due to the nature of fatigue damage, however, the stress range will increase marginally throughout the test. It is noted that due to equipment malfunction, Fatigue Test 1 was unintentionally loaded to an applied load exceeding 30 kips during a few initial cycles. These few higher stress range cycles had little impact on the beam behavior beyond causing additional cracks.

During fatigue cycling, no notable degradation in beam stiffness was noted. There was a small drift in absolute displacements attributable to degradation of the neoprene pads and ‘settling’ of the test frame. Nonetheless, the differential displacement (that measured between 7 and 17 kips applied load) remained essentially constant. Figure 4.3 shows both the deflection (left axis) and secant stiffness measured between applied loads of 7 and 17 kips (right axis) cycle histories for Fatigue Test 1. Crack width measurements both during fatigue cycling and following the fatigue test during a monotonic load cycle to 46 kips were remarkably consistent and confirmed the measured bar’s stresses. Fatigue Test 1 behaved very well and indicated that the A1035 bars can maintain 2 million cycles at 31 ksi with little or no apparent damage.

4.5.5 Results of fatigue test 2

Fatigue Test 2 was tested between 04/14/2009 and 04/16/2009. The applied load at midspan was cycled between 7 and 25 kips at a rate of 1.2Hz. The measured stress range in the A1035

longitudinal steel was 45.5 ksi in the initial test cycles. One of the four reinforcing bars (a corner bar, bar 1) experienced a fatigue-induced fracture at $N = 155,005$. The final instrumented cycle was $N = 100,000$. As shown in Figure 4.4, the deflections were increasing with cycling although the differential displacement (between 7 and 25 kips) remained relatively constant. The secant stiffness (also measured between 7 and 25 kips) demonstrated some decay in the initial 100,000 cycles. The final data points at $N = 155,005$ in Figure 4.4 were obtained from a single cycle following fatigue failure and clearly indicate the effect of the loss of one of the four primary reinforcing bars. Figure 4.5a shows the ruptured bar following testing. The bar failed at the location a stirrup which is typical of such fatigue failures as they are often affected by fretting at the transverse bar locations. Figure 4.5c shows the fracture surface of the bar which is clearly indicative of a fatigue failure.

4.5.5.1 SEM of fatigue test 2 failure

The failure of a bar at $N = 155,005$ under S of 45.5 ksi is very close to the prediction which is thought to be conservative. Therefore an investigation of the fatigue failure surface using scanning electron microscopy (SEM) was conducted (Figure 4.6). The SEM revealed aluminum (Al) inclusions in the fracture surface (Figure 4.6b) and a significant silicon (Si) inclusion at the edge of the bar section thought to have served as a crack initiator (Figure 4.6c and Figure 4.6d). Figure 4.6 provides both the SEM image and backscatter spectral analysis for each image. The spectrum shown in Figure 4.6a is of the A1035 material and agrees well with the specified composition of this material (Table 2.1).

The spectrum shown in Figure 4.6b is taken from the dark inclusion shown in the image. This figure clearly indicates presence of pure aluminum. The aluminum cannot be accounted for. A1035 material contains no aluminum but the inclusion was apparently embedded in the section

and therefore unlikely to be contamination occurring following the fracture (there was also no aluminum used in the test frame or instrumentation). Figures 4.6c and 4.6d show the same location on opposite faces of the fracture. A 0.3 mm diameter inclusion at the edge of the bar is evident in these images. The spectrum indicates that this inclusion is silicon. A1035 steel is specified to have a maximum silicon content of 0.50% (Table 2.1). Therefore, the presence of silicon should not be a surprise. The size of the inclusion, however, and its location at the edge of the bar may have resulted in a stress concentration that initiated the fatigue failure of this bar.

4.5.6 Summary of fatigue tests

The CEB $S-N$ relationship for #5 bars (and smaller) given in Equations 4.2, 4.3 and the two $S-N$ pairs from the tests conducted are shown in Figure 4.7. Since both of the experimental data points fall above the $S-N$ curve, it may be concluded that the specimen performance exceeded that predicted by the curve; (i.e.: for a given stress range, S , the fatigue life, N , was higher than predicted), although not by a significant degree. It is believed, nonetheless, that these tests both serve as proof tests of the AASHTO LRFD recommendations (Equation 4.5) that presently limits the fatigue stress range to 24 ksi for the case of tension-tension fatigue (i.e.: $f_{min} > 0$).

4.5.7 Effect of fatigue provisions of AASHTO 5.5.3.2

In general, fatigue strength behavior of reinforced concrete members is governed by the behavior of the internal reinforcement. The geometry and deformation of reinforcement are the main factors affecting fatigue performance.

When using higher strength reinforcement, the minimum stress level (f_{min}) will increase although likely not in proportion to the increase in service level stress. Thus, the transient stress range increases. In order to understand the role that fatigue may play in the design of reinforced concrete flexural members, the following approach was taken.

The following nominal moments are determined at the midspan of a simply supported beam having length L :

DL = dead load (self weight). This value is determined for a range of values of DL/LL_{lane} from 0.5 to 4.0.

LL_{lane} = specified lane load = 0.64 k/ft (AASHTO LRFD 3.6.1.2.4)

LL_{truck} = greatest effect of design tandem (3.6.1.2.3) and design truck (3.6.1.2.2). For a truck on a simple span, the minimum 32-kip axle spacing of 14 feet is used.

$LL_{fatigue}$ = effect of single design truck having 32-kip axle spacing of 30 feet (3.6.1.4.1)

It is recognized that the maximum moment does not occur exactly at the midspan. However, the error in making this assumption is quite small and becomes proportionally smaller as the span length increases (Barker and Puckett 2007).

From these moments, the STRENGTH I and FATIGUE design moments are determined (AASHTO LRFD 3.4.1):

$$STRENGTH = 1.25DL + 1.75LL_{lane} + (1.75 \times 1.33)LL_{truck}$$

$$FATIGUE = (0.75 \times 1.15)LL_{fatigue}$$

Where the 1.33 and 1.15 factors are for impact loading (IM) (3.6.2.1).

In order to normalize for distribution, multiple lanes, etc, it is assumed that the STRENGTH design is optimized; therefore, the stress in the primary reinforcing steel under STRENGTH conditions is $\phi f_y = 0.9f_y$ regardless of bridge geometry. Hence, the reinforcing stress associated with the FATIGUE load is:

$$f_f = 0.9f_y \times (FATIGUE/STRENGTH)$$

Similarly, the minimum sustained load will result in a reinforcing stress of:

$$f_{min} = 0.9f_y \times (DL/STRENGTH)$$

The stress in the reinforcing steel under FATIGUE conditions is then normalized by the allowable stress determined from (Equation 4.6):

$$f_f \leq 24 - 20(f_{min}/f_y) \text{ (ksi)}$$

The results from this approach are shown in Figure 4.8 for simple spans $L = 10$ to 160 feet and $DL/LL_{lane} = 0.5, 1, 2$ and 4. In this plot, the vertical axis reports the stress range/fatigue limit ratio: $f_f/[24 - 20(f_{min}/f_y)]$

Based on this approach, it is not expected that the fatigue limits of 5.5.3.2 will affect design using $f_y = 60$ ksi over the range considered since the ratio of stress range/fatigue limit is less than unity for all cases. The effects of using $f_y = 100$ ksi in this simplified scenario include an expected increase in f_{min} and f_f equal to the ratio of yield strengths = $100/60 = 1.67$. As seen in Figure 4.8, however, the calculated stress range remains below the fatigue limit given by Equation 4.6 for all spans except those shorter than 20 feet having $f_y = 100$ ksi.

The effect of continuing to use the extant AASHTO equation: $f_r \leq 24 - 0.33f_{min}$ is relatively negligible, shifting the 100 ksi curves upwards by less than 5%, in the scenario presented.

Thus, despite the inherent conservativeness of the AASHTO LRFD fatigue provisions, it is not believed that these provisions will impact most rational designs. It has been shown that increasing the usable yield strength of steel decreases the margin of safety against fatigue although only in the shortest of spans, where vehicular loads dominate behavior. In these cases, the ‘fatigue check’ fails and additional steel would be required.

4.5.7.1 Slabs

Slabs, being shallower and having a proportionally greater LL/DL ratio may be considered to be more fatigue sensitive than the generic conditions described above. However, AASHTO LRFD 9.5.3 excludes concrete decks from being investigated for fatigue. AASHTO justifies this exclusion based on results reported by de V Batchelor et al. (1978). The effectively lower stresses in slab reinforcement are counterintuitive if one considers a slab as a one-way beam resisting flexure. However, it has been shown that slabs resist applied loads primarily through internal arch action (AASHTO 9.7.1) and that the nominal steel required is primarily to resist

local flexural effects (punching) and to provide confinement such that the arching action may be developed (Fang 1985 and Holowka et al. 1980).

Table 4.1 Fatigue stress ranges (f_r) corresponding to a fatigue life of 2 million cycles.

Bar Size	No. tests	f_y (ksi)	f_{min}	f_r (ksi)	reference
#8	157	40	0.10 f_y	38	Pfister, J.F. and Hognestad, E. 1964
		60		34	
		75		39	
		40	0.30 f_y	33	
		60		31	
		75		32	
		40	0.10 f_y	32	
		75		35	
		40	0.30 f_y	28	
		75		30	
#5	19	40	0.25 f_y	27	Lash, SD. 1969
		60		31	
		75		38	
#8	72	40	0.10 f_y	30	MacGregor, J.G., et al. 1971
		60		30	
		75		30	
		40	0.40 f_y	25	
		60		25	
		75		25	
#5	not reported	40	0.10 f_y	32	
		60		33	
		75		36	
#10	not reported	40	0.10 f_y	31	Wascheidt, H. 1965
		60		29	
		75		30	
		49	0.17 f_y	28	
		53	0.16 f_y	28	
		64	0.13 f_y	28	
		88	0.10 f_y	31	
		50		30	
		57		30	
70	31.5				
#3, #4 & #5	n.r.	120	0	45	DeJong 2005
#5	1	120	0.10 f_y	32	present study

Table 4.2 Fatigue limit predictions

N	500,000	1,000,000	2,000,000	10,000,000	20,000,000	100,000,000
S	35 ksi	30 ksi	28 ksi	23 ksi	22 ksi	18 ksi

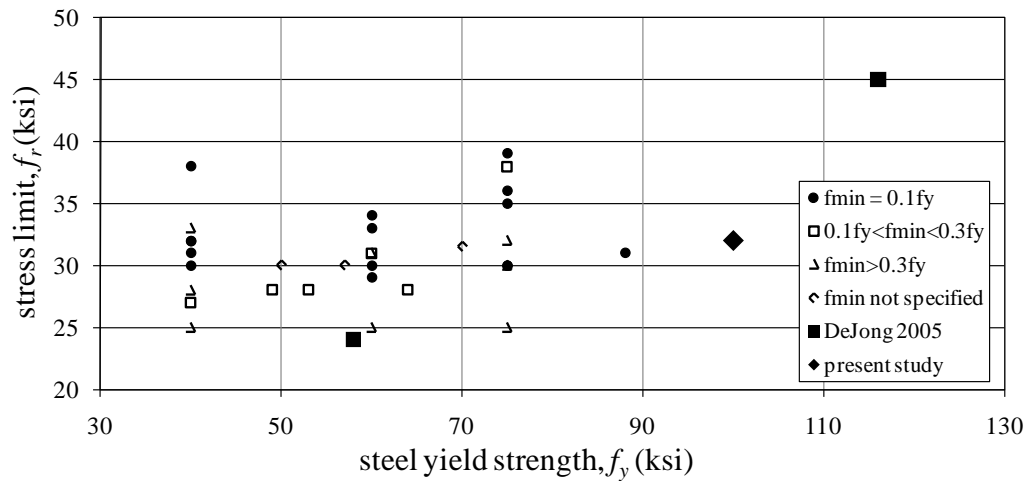


Figure 4.1 Observed 2 million cycle stress limits as a function of minimum stress level, f_{min} .



(a) Fatigue specimen test 1, before loading



(b) Fatigue specimen test 1 at 2 million cycles

Figure 4.2 Fatigue specimen test 1.

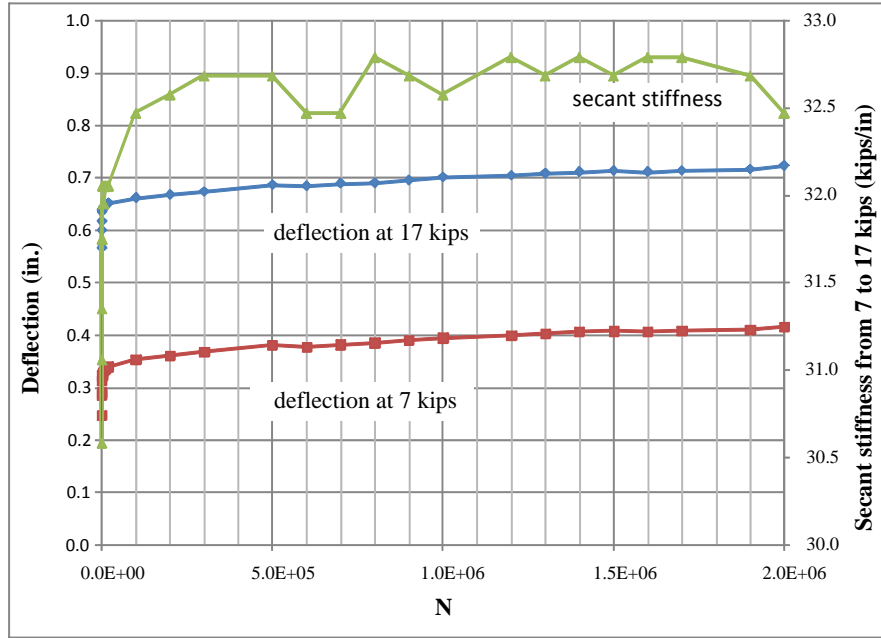


Figure 4.3 Cumulative damage curves for Fatigue test 1.

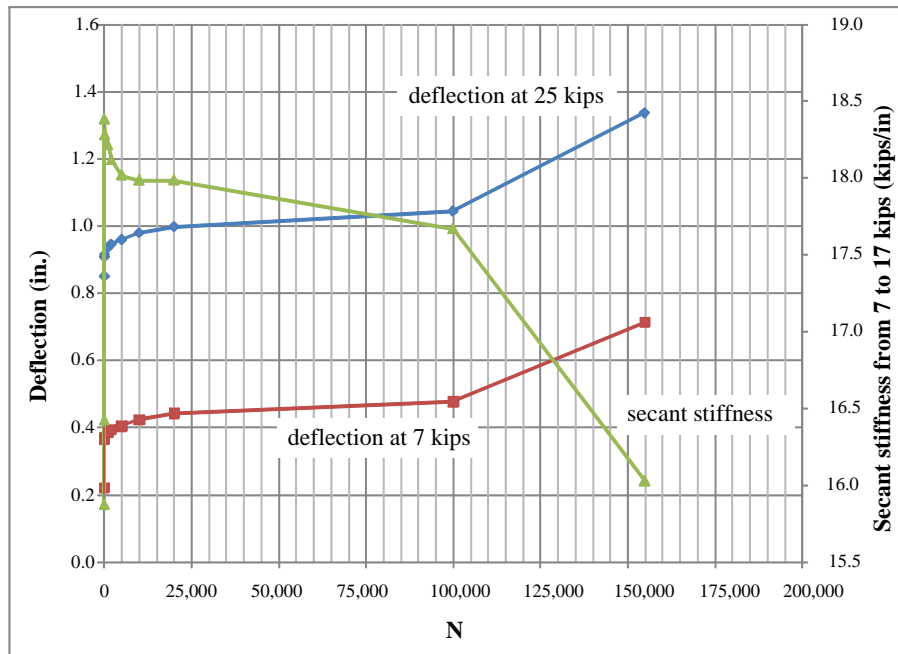
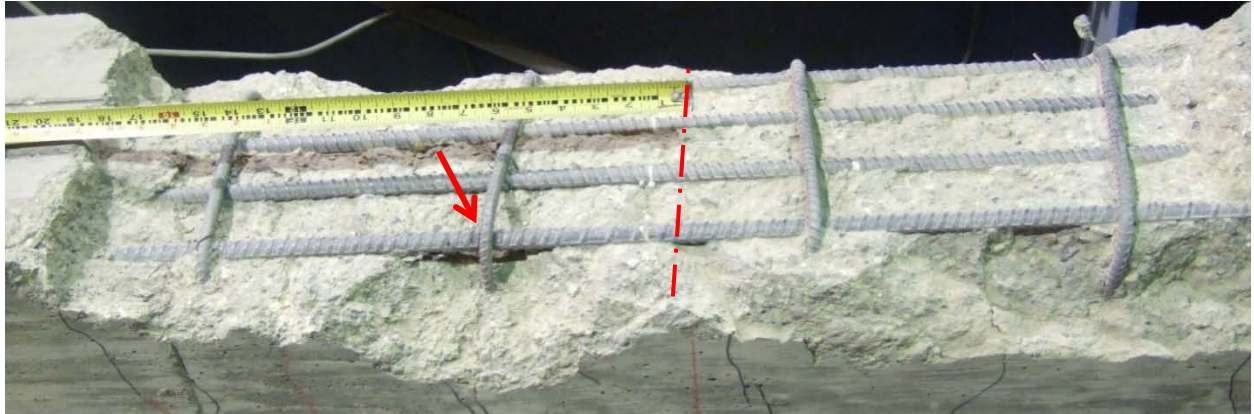


Figure 4.4 Cumulative damage curves for Fatigue test 2.

(fatigue failure occurred prior to obtaining the final data point)



(a) location of bar fracture (beam is inverted, cover has been removed).

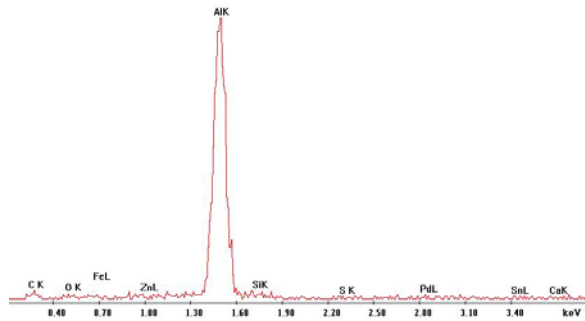
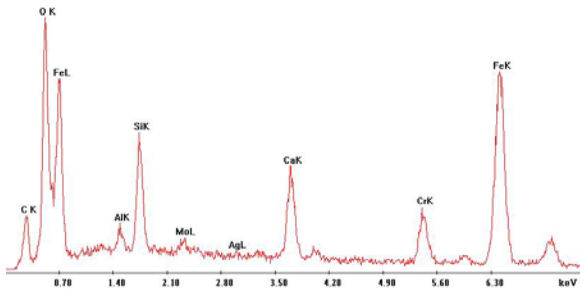
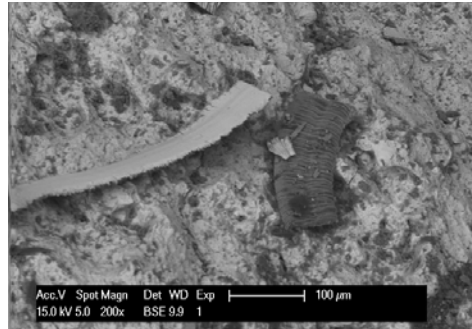
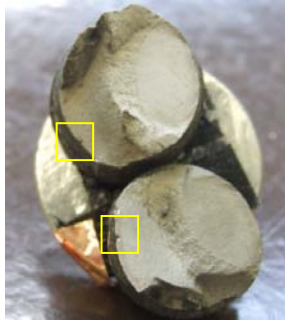


(b) fatigue fracture of bar 1.



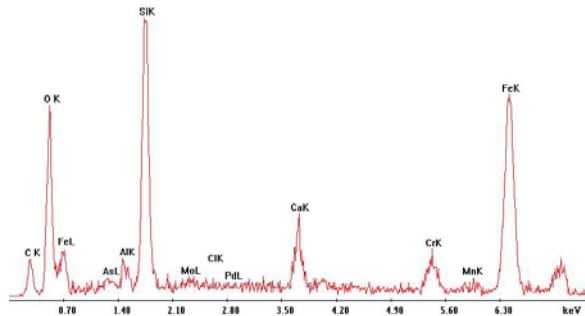
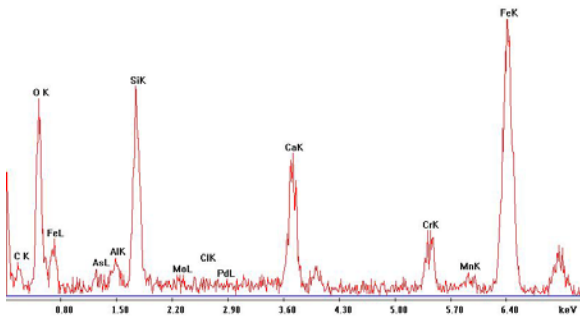
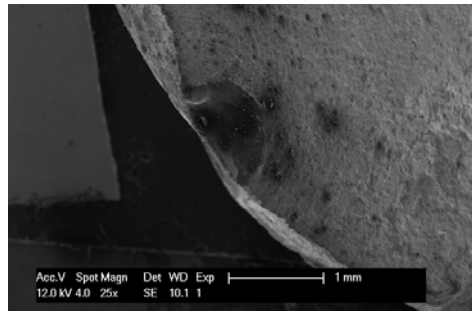
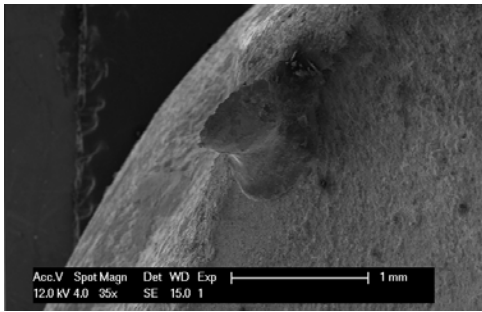
(c) fracture surface.

Figure 4.5 Fatigue failure of single bar in Fatigue Test 2.



(a) fracture and backscatter spectrum of MMFX steel (boxes indicate region of images c and d)

(b) Aluminum inclusion (darker inclusion right of center; long thin piece is steel)



(c) 'male' side of Silicon inclusion

(d) 'female' side of Silicon inclusion

Figure 4.6 SEM images of failure surface.

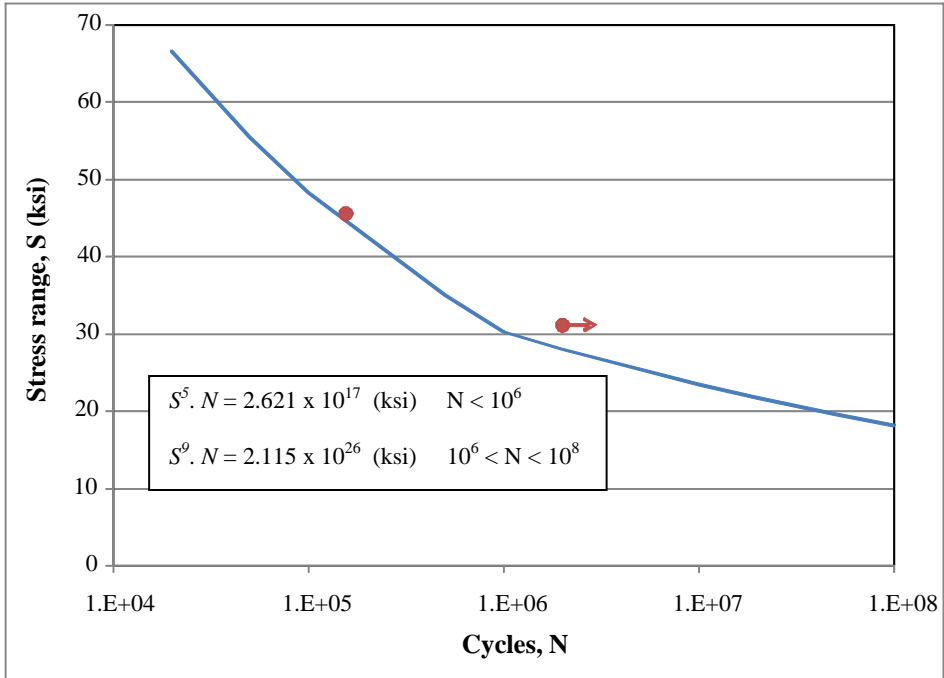


Figure 4.7 Predicted and experimental S-N data.

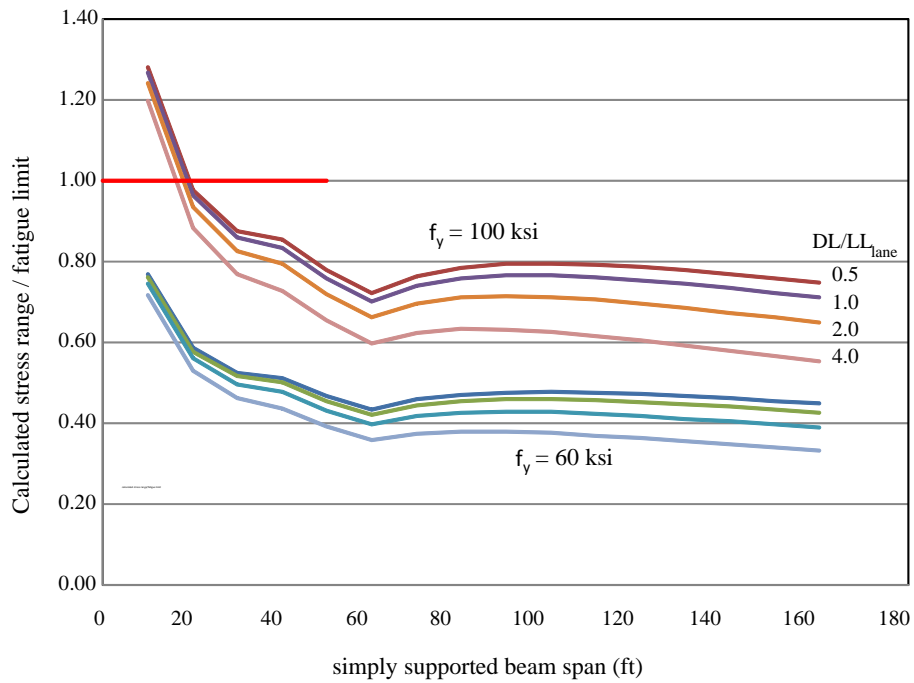


Figure 4.8 Fatigue stress as proportion of AASHTO 5.5.3.2 fatigue limit

5.0 SERVICEABILITY: DEFLECTION AND CRACK CONTROL

A reinforced concrete member is typically designed based on strength requirements applying appropriate load and material resistance factors. This approach is referred to as ultimate limit states design and is the foundation of ACI and AASHTO's load and resistance factor design (LRFD) approaches. Deflection and crack control are important performance criteria that need to be checked to ensure the structure remains serviceable under the specified loading conditions. In an LRFD design approach, these checks follow the strength design.

5.1 DEFLECTION CONTROL FOR SERVICEABILITY OF REINFORCED CONCRETE

In design code specifications, deflections in a concrete structure are controlled by either limiting the span to depth ratio of the member, resulting in a minimum member thickness (which, if respected usually mitigates the need to make complex deflection check calculations) or ensuring that calculated deflection values do not exceed specified limits that are often based on maximum deflection to span ratios. Minimum member thickness values in building codes (ACI 318-08) are calibrated for 'standard' cases and are therefore applicable only for members not supporting or attached to partitions or other construction likely to be damaged by large deflections and do not apply when the partitions are susceptible to cracking (Scanlon and Choi 1999). However, it has

been recommended that deflection values always be calculated and the code-prescribed minimum thickness values only be used for preliminary selection of member size (although in practice this is rarely the case). Since the calculation of deflection is onerous, most software packages used for design of reinforced concrete structures include the calculation of deflections; most use an effective moment of inertia to compute deflection (Scanlon et al. 2001). It is noted that minimum member and slab thickness values in bridge codes (AASHTO 2007) are based on serviceability requirements intended to ensure durability (including sufficient depth to permit a sacrificial wearing surface), to control vibration (stiff and massive structural system) and to mitigate fatigue issues in the reinforcing steel (ensuring the transient stress in the steel is low). The latter is accomplished by requiring slab details that promote the development of arching action.

The following discussions are limited to flexural deformations. For members having a shear span less than four (i.e.: disturbed regions), the effects of shear distortion need to be added to the calculated deformations. Shear deformations are beyond the scope of the present work.

5.1.1 Deflection of reinforced concrete members

Deflection of a member is calculated by double integration of the curvature along the span length. For an elastic member, the curvature, φ , may be calculated as $\varphi = M/EI$, where EI is the flexural stiffness of the cross section of the member. The deflection of a member, therefore, is a function of the span length, support or end conditions, the type of loading and the flexural stiffness. In general, the deflection of an elastic member can be expressed as:

$$\Delta = k \frac{ML^2}{EI} \quad (5.1)$$

Where,

k = a factor depending on the degree of fixity of the supports;

M = the applied moment (kips-in);

L = clear span length (ft);

E = elastic modulus (ksi);

I = moment of inertia of the section (in⁴).

Based on the flexural behavior of a reinforced concrete member, the tension side of the neutral axis may be uncracked, partially cracked, or fully cracked, depending on the loads, load history and material strengths. The modulus of concrete, E_c , is assumed to be unaffected by loading; therefore, in order to apply an elastic analysis, three different values of I must be considered depending on the section condition. When the section is uncracked, the value of I is equal to I_g , the gross section moment of inertia. When fully cracked, $I = I_{cr}$, the cracked moment of inertia which is determined from equilibrium considering ultimate stress conditions. North American design codes (including ACI 318-08 and AASHTO 2007) use an effective moment of inertia, I_e , that was originally proposed by Branson (1963, 1977) to calculate beam deflections when the beam section is partially cracked; i.e. when the beam behavior falls between that of I_g and I_{cr} .

5.1.2 Evaluation of effective moment of inertia

5.1.2.1 Branson's equation

Branson (1963) utilized a number of experimental curvatures and deflections to obtain an empirical relationship for the effective moment of inertia of a cracked concrete section, I_e . Branson's equation incorporates the effects of steel reinforcing ratio, cracking on deflections of simple and continuous reinforced concrete beams. This approach includes the effects of moment redistribution due to cracking in computing deflections of statically indeterminate beams. Based on experimental results, Branson developed the following equation for computing the effective moment of inertia of cracked reinforced concrete beams and one-way slabs.

$$I_e = I_{cr} + (I_g - I_{cr}) \left(\frac{M_{cr}}{M_a} \right)^m \leq I_g \quad (5.2)$$

Where

M_a = is the applied moment at which deflections are calculated ($M_a > M_{cr}$);

m = an empirically derived exponent; Branson reports $m = 3$ to account for average properties along a span;

M_{cr} = cracking moment of the member given as:

$$M_{cr} = f_{cr} y / I_g \quad (5.3)$$

Where

f_{cr} = the cracking stress of concrete usually expressed as a scalar multiple of $\sqrt{f'_c}$; and

y = the distance from the uncracked neutral axis to the extreme tension face of the member.

Equation 5.2 is widely known as Branson's equation. It is noted that the value of I_e calculated using Equation 5.2 is only slightly smaller than I_g in cases where M_a is only marginally larger than M_{cr} . This case generally occurs in members having a low reinforcement ratio, typically $\rho < 0.006$. For such members the calculated I_e is very sensitive to changes of M_{cr} (Gilbert 1999). Therefore, Equation 5.2 may overestimate the effective moment of inertia for lightly reinforced members when flexure members have an I_g/I_{cr} ratio greater than 3 (Scanlon et al. 2001, Bischoff 2005 and Gilbert 2006). Bischoff (2005) reports that Branson's equation underestimates short-term deflection for concrete members when the reinforcing ratio is less than approximately 1% for beams having an I_g/I_{cr} ratio greater than 3. Nonetheless, Branson's approach was quite innovative at the time; his expression for I_e represents a gradual transition from the uncracked flexural stiffness, EI_g , to the fully cracked stiffness, EI_{cr} , as loading on the member increases beyond the cracking point.

There have been several attempts by different investigators to modify Branson's equation aiming to improve the accuracy of the predicted deflections; these are briefly discussed below. With the exception of Rangan (1982), none of these modifications has been adopted by building codes; Branson's equation remains the standard calculation for the effective moment of inertia of a cracked section.

Grossman (1981)

Grossman (1981) carried out a parametric study computing the effective moment of inertia using Branson's equation for various beams and one-way slabs having different material and sectional properties. Based on the results, Grossman developed the following equation for calculating I_e , which eliminates the requirement of computing I_{cr} .

$$\frac{I_e}{I_g} = \left(\frac{M_{cr}}{M_a}\right)^2 \leq 1.0 \quad \text{if} \quad \frac{M_a}{M_{cr}} \leq 1.6, \quad \text{and} \quad (5.4)$$

$$\frac{I_e}{I_g} = 0.1 \left(\frac{M_a}{M_{cr}}\right) k^* \leq 1.0 \quad \text{if} \quad \frac{M_a}{M_{cr}} > 1.6$$

with a lower bound of $I_e/I_g = 0.35k^*$

k^* in Equation 5.4 provides adjustments for section shape, material properties and strength of the section, and is determined as follows.

$$k^* = \left(\frac{d/h}{0.9}\right) \left[\frac{\sqrt{2330/w_c}}{0.4 + (1.4M_a/M_u)(f_y/690)} \right] \quad (5.5)$$

where

w_c = unit weight of concrete (kg/m^3)

f_y = yield strength of steel (MPa).

Rangan (1982)

Rangan (1982) computed the effective moment of inertia, I_e , using Branson's equation, for a number of simply supported rectangular beams and one way slabs under service load. The mid span moment M_a in Branson's equation was replaced by the service moment M_s , which was calculated as the moment when the steel stress is equal to the yield stress, f_y . Based on these results, the following equation was proposed.

$$\text{If } n\rho > 0.045, \quad \frac{I_e}{bd^3} = 0.1599\sqrt{n\rho} \quad (5.6)$$

$$\text{If } n\rho \leq 0.045, \quad \frac{I_e}{bd^3} = 0.0019/n\rho$$

Where

$n = E_s/E_c$ modular ratio.

This approach was used by Standard Association of Australia (AS 3600, 2001) in the development of the equation to calculate the span-to-effective depth ratio for controlling deflections of beams and one-way slabs.

Al Zaid et al. (1991)

Branson's equation was developed using the results of test beams subjected to uniformly distributed loads. Based on test results, Al Zaid et al. (1991) suggested that the value of I_e calculated using Branson's equation (5.2) may be increased by 20% for beams subjected to central point loads. It is noted, however, that few such members exist in practice.

Al Shaik and Al Zaid (1993)

Results of experiments carried out by Al Shaik and Al Zaid (1993) indicate that the value of m in Branson's equation decreases with increased tensile reinforcement ratio ρ . It was proposed to calculate the value of m (Equation 5.2) using the following equation.

$$m = 3 - 0.8\rho \tag{5.7}$$

Fikry and Thomas (1998)

An improvement to Branson's equation was proposed by Fikry and Thomas (1998) as shown in Equation 5.8:

$$I_e = I_{cre} + (I_g - I_{cre})e^{\Phi} \quad (5.8)$$

where,

$$\Phi = -\left(\frac{M_a}{M_{cr}}\right)\left(\frac{L_{cr}}{L}\right)\rho \quad (5.9)$$

$$I_{cre} = (\alpha + \beta n\rho)\frac{1}{12}bd^3 \quad (5.10)$$

in which L_{cr} for a beam is defined as

$$L_{cr} = L\left(1 - \frac{M_{cr}}{M_a}2a/L\right), \text{ a is the length of the shear span,}$$

ρ = the reinforcement ratio

α and β = constants depending on the value of $n\rho$.

5.1.2.2 Tension stiffening

Cracking significantly affects the behavior of reinforced concrete structures. Once cracked, the reinforcement is assumed to carry all of the tensile force at the cracks; however, concrete continues to carry tensile load between the cracks through bond between the reinforcing bar and the concrete. This phenomenon is called tension stiffening. The tension stiffening effect in a cracked reinforced concrete member decreases with an increase of loading (Piyasena 2002); i.e.: after cracking, the load carried by the concrete gradually decreases as the applied load (moment) continues to increase. The ability of concrete to carry tension between cracks increases member stiffness thereby affecting deformation and crack widths.

Tension stiffening also plays an important role in nonlinear analysis of reinforced concrete. The degree of tension stiffening is directly related to the area, modulus and bond characteristics of the reinforcement, and crack spacing. Other parameters affecting tension stiffening include the distribution of reinforcement, bar diameter, tensile strength of concrete and concrete cover (Piyasena 2002). The area of concrete around the bars contributes to the tension stiffening effect. Tension stiffening increases with a decrease in reinforcement ratio. Concrete strength can influence the tension stiffening behavior in two different ways. Firstly, high strength concrete requires higher loads to crack the section. Secondly, better bond between concrete and reinforcement allows stresses to be transferred more effectively between the bar and concrete making the average stress contribution of concrete proportionally greater. It is further observed that bond degradation occurs near cracks at an early stage and that this degradation migrates away from the crack with increasing load (Sooriyaarachchi et al 2005).

The tension stiffening factor is zero when there is no bond between reinforcement and concrete. In concrete reinforced with conventional steel bars (A615 steel bars), tension stiffening falls to zero once the steel yields, since member capacity is limited to the yield force of the reinforcement at the crack locations (Assuming elastic-perfectly plastic behavior).

5.1.2.3 Bischoff's equation

Bischoff and Paixao (2004) and Bischoff (2005 and 2007) used the concept of tension stiffening to determine the effective moment of inertia of concrete sections. They modeled the concrete contribution to reinforced beam behavior with a tension stiffening factor $\chi_{ts} = \Delta\phi / \Delta\phi_{max}$ that decreases with increasing load once the member has cracked (Figure 5.1). The maximum tension stiffening curvature at first cracking is given by:

$$\Delta\phi_{max} = M_{cr} (1 - I_{cr}/I_g) / EI_{cr} \quad (5.11)$$

The change in curvature relative to the cracked member response is called the tension stiffening curvature $\Delta\phi = \chi_{ts}\Delta\phi_{max}$ and is used to define a rational expression for the effective moment of inertia I_e . Figure 5.1a shows the definition of effective stiffness, EI_e (given as $E_c I_e$ in the figure) and Figure 5.1b shows values used to derive this stiffness. The equation is provided for the effective moment of inertia.

$$I_e = \frac{M_a}{E_c \phi_a} = \frac{M_a}{E_c (M_a / E_c I_{cr} - \Delta\phi)} = \frac{I_{cr}}{1 - \chi_{ts} \eta (M_{cr} / M_a)} \leq I_g \quad (5.12)$$

Where

$$\eta = 1 - I_{cr} / I_g ;$$

ϕ_a is the curvature at M_a .

Approximating the tension stiffening factor χ_{ts} as being equal to M_{cr}/M_a gives:

$$I_e = \frac{I_{cr}}{1 - \eta (M_{cr} / M_a)^2} \leq I_g \quad (5.13)$$

This approximation assumes that the tension stiffening curvature varies inversely with bar stress at the crack locations. That is, $\chi_{ts} \approx f_{b,cr}/f_b$, where $f_{b,cr}$ is the stress in the bar at first cracking and f_b is the stress in the bar at a crack at M_a . This approximation is justified by results reported by Nemirovsky (1949), Rao and Subrahmanyam (1973) and Rostasy et al. (1976). Equation 5.13 has come to be referred to as Bischoff's equation.

5.1.2.4 Evaluation of Branson and Bischoff equations

The effective moments of inertia, given by Branson's (Equation 5.2) and Bischoff's (5.13) equations are shown in Figure 5.2 as a function of the ratio M_a/M_{cr} for a simply supported beam. The values are calculated for beams having reinforcing ratios of $\rho = 0.2, 0.5, 1$ and 2% and all plots are normalized by I_g .

As required, for values of maximum moment M_a less than the cracking moment M_{cr} , both equations give $I_e = I_g$. As expected, with increasing values of M_a , I_e approaches I_{cr} . For all cases, $I_e \approx I_{cr}$ for values of $M_a/M_{cr} > 3$. Typical values of M_a/M_{cr} at service load range from about 1 to 4 for a beam reinforced with ASTM A615 and about 1 to 6 for a beam reinforced with ASTM A1035 (Bischoff 2007). The significant difference between the equations is for values of $M_a/M_{cr} < 3$ in beams having $\rho < 0.01$. In these cases, Branson's equation overestimates the value of I_e . Another 'quirk' of Branson's equation is that I_e/I_g does not trend to zero as ρ trends to zero as it logically must for an unreinforced concrete beam. Bischoff's equation does yield $I_e/I_g = 0$ at $\rho = 0$.

The concept of tension stiffening for determining the effective moment of inertia can be also seen in Branson's equation. The value of $m = 3$ in Branson's equation accounts for both tension stiffening and the variation of member stiffness along the beam length. Bischoff described tension stiffening as the major factor affecting overall stiffness and corresponding deformation of a reinforced concrete member. Bischoff's expression provides more accurate predictions of deflections than Branson's equation in cases having a steel reinforcement ratio less than approximately 1%, corresponding to an I_g/I_{cr} ratio greater than 3 (Bischoff 2005). Bischoff's expression has also been shown to accurately account for cases having reinforcement with a relatively low modulus such as FRP (Bischoff 2005). Bischoff's expression is more

phenomenological in the sense that it considers a decreasing trend for tension stiffening with increasing strain after cracking. Finally, Bischoff's equation is based on fundamental mechanics and does not rely upon empirical calibration as does Branson's; thus, Bischoff's equation is thought to be more versatile in accounting for a wider range of material properties.

5.1.3 Deflection in concrete members reinforced with high strength steel bars

A reinforced concrete member is typically designed based on strength at ultimate loads and is checked for deflection and crack control at service loads. Although the controls are conservative, based on limiting stresses in the structure at service loads, the adoption of higher strength materials has led to an increase in serviceability problems. The material strength of reinforcement and concrete, bond characteristics, size of a member, and amount of reinforcement are all factors affecting the development of cracks and member deflections. Concrete members reinforced with high strength steel bars have different behavior, particularly at the resulting higher service loads, compared to concrete members reinforced with conventional steel bars. Using a higher strength reinforcing material with higher elastic service stresses may allow engineers to design members with a lower amount of reinforcement. This approach affects the flexural stiffness, EI_e , of a cracked reinforced concrete member and results in different deflection and cracking behaviors.

5.1.3.1 Analytical study of deflection

A fundamental issue in using A1035 or any other high strength reinforcing steel is that the stress at service load (f_s ; assumed to be on the order of $0.6f_y$) is expected to be greater than with conventional 60 Grade steel. Consequently, the service load reinforcing strains (i.e.: $\epsilon_s = f_s/E$) are

greater. This larger strain affects deflection and crack widths at service loads. In the following sections, discussion focuses on the behavior at loads corresponding to longitudinal reinforcing bar stresses of 36, 60 and 72 ksi, representing service load levels (i.e.: $0.6f_y$) for steel having $f_y = 60, 100$ and 120 ksi, respectively. At these service load stresses, the use of $E = 29,000$ ksi for all steel grades is acceptable (see Section 2.1.2) although experimentally determined R-O curves have been used in all cases to calculate stress from measured steel strains. The use the R-O curves in the analyses permit higher stresses to be considered where E shows some softening behavior.

The results of six flexural beam specimens (F1 through F6) tested at the University of Cincinnati as part of the NCHRP 12-77 study (Shahrooz et al. 2010) are used as a basis for comparison. These beams were all reinforced with A1035 longitudinal reinforcing bars. Details of the 16 in. deep by 12 in. wide beam sections are given in Table 5.1. All beams were tested in symmetric four-point flexure over a simple of span of 20 ft having a constant moment region of 3 ft.

5.1.3.2 Deflections of flexural members

Table 5.2 summarizes the midspan deflections of all flexural beam specimens (F1 through F6) corresponding to longitudinal bar stresses of 36, 60 and 72 ksi. The experimentally measured deflections include the actual beam deflection but also test set-up compliance but do not include deflection due to self weight. Also shown in Table 5.2, the deflections are calculated using both the Branson (Equation 5.2) and Bischoff (Equation 5.13) formulations for effective moment of inertia (I_e). In calculating the applied moment (M_a in Equation 5.2 and 5.13), the self weight of the beam is taken into account; thus, for thus the effective moment of inertia is based on the appropriate cracked section for the load level considered:

$$M_a = \frac{Pa}{2} + \frac{wL^2}{8} \quad (5.14)$$

where:

P = total applied load in four point bending (sum of two point loads);

w = self weight of beam, taken as 16.7 lb/in. in all cases;

L = length of simple span, 240 in. in all cases;

a = length of shear span, 102 in. in all cases.

In the formulations of effective moment of inertia (Equations 5.2 and 5.13), the moment to cause cracking is calculated as 80% of the moment corresponding to modulus of rupture (AASHTO §5.4.2.6):

$$M_{cr} = 0.8 \left(\frac{0.24 \sqrt{f'_c} I_g}{y_t} \right) \quad (\text{ksi}) \quad (5.15)$$

where:

I_g = moment of inertia of gross concrete section.

y_t = neutral axis of gross concrete section, nominally 8 in.

The use of the reduced value of M_{cr} accounts for cases where the applied moment (M_a) is only slightly less than the unrestrained M_{cr} (based on $0.24\sqrt{f'_c}$) since factors such as shrinkage and temperature may still cause a section to crack over time (Scanlon and Bischoff 2008).

In the calculation of deflection, the self weight is neglected since this component of the deflection is also not included in the experimentally determined deflections, against which comparisons are made. For the beams considered, the deflection associated with beam self weight is approximately 19%, 11% and 9% of the deflections corresponding to applied load at bar stress levels of 36, 60 and 72 ksi, respectively. The midspan deflections associated with the applied four point bending are calculated as:

$$\Delta = \frac{PL^3}{48E_cI_e} \left(3 \left(\frac{a}{L} \right) - 4 \left(\frac{a}{L} \right)^3 \right) \quad (5.16)$$

The Branson and Bischoff formulations yield very similar results for the specimens tested. The correlation between the formulations is not as good for the lower reinforcing ratio of 0.007 (beam F3). This observation is consistent with the observation that Branson's equation underestimates short-term deflection for concrete members when the reinforcing ratio is less than approximately 0.01 (Bischoff 2005). While both equations are suitable for calculating deflections, the Bischoff approach is based on fundamental mechanics and may therefore be applied for any type of elastic reinforcing material. The Branson formulation is empirical and calibrated for mild steel.

5.2 CRACK CONTROL IN REINFORCED CONCRETE MEMBERS

Crack development and control of cracks are among the most important considerations in the design of reinforced concrete structures. Cracks in reinforced concrete cannot be expected to be

eliminated and therefore must be controlled to ensure durability of the structure. For bridges and buildings, the primary concern with cracking is that it permits water (and salts) to reach the reinforcing steel resulting in corrosion. In containment type structures (tanks, pipes, pressure vessels), cracking also leads to leaking although this issue is beyond the scope of the present study. The basic concepts of cracking in reinforced concrete beams using conventional steel bars are fairly well understood and parameters affecting crack size and distribution are generally accepted. However, the problem of crack formation and development is a complex one involving a great many parameters and hence some of the conclusions regarding the significance of these parameters remain questionable, particularly when applied to non-conventional materials. With the allowed use of high-strength reinforcing bars and higher permissible steel stresses, a great deal of renewed research and study on cracking is warranted. A survey of available literature follows; the objectives of this literature survey are:

- To develop an understanding of the factors affecting the formation of cracking, the development of the crack pattern, and the size (width or opening dimension) of the cracks.
- To investigate critical crack widths and crack spacing as affected by high-strength steel bars and/or high bar stresses.
- To evaluate current approaches to controlling cracks and their relative effectiveness, and to evaluate these in the context of high-strength reinforcing steel.
- To provide a survey of aesthetic concerns associated with cracking to help guide the determination of “allowable crack widths”.

This study is concerned primarily with cracks caused by flexural and tensile stresses, but temperature, shrinkage, shear, and torsion can also lead to cracking.

5.2.1 Crack formation

Crack formation refers to the incidence of any narrow, irregular opening of indefinite dimensions resulting from shrinkage, flexural or direct tension stresses, or internal expansion resulting from the products of corrosion or deleterious aggregates. The incidence of flexural and direct tension cracking that occurs at various stages is defined in relation to the stresses in the reinforcement at the cracked section (Reis et al. 1965). Since steel has a constant modulus (at service load levels) regardless of grade, this approach is possibly better described with respect to steel strain, rather than stress. Nonetheless, the following description of load-induced cracking in a tension zone is based on stress as reported by Reis et al.:

1. The first stage of cracking is concerned with those cracks produced by shrinkage, corrosive effects, and low flexural loads in which the measured steel stress is well below 14 ksi ($\epsilon_s \approx 0.0005$). Cracks of this type are referred to as primary cracks.
2. The second stage of cracking is concerned with those cracks which result from the difference in inextensibility between the concrete and steel, and the bonding forces that exist between the two. Cracks formed by this mechanism are referred to as secondary cracks. Secondary crack formation is usually studied by examining the portion of the beam between two successive primary cracks or by analyzing the model of an axially loaded reinforced concrete prism in tension (as is done in this study). The steel stresses during the second stage of cracking are usually greater than 14 ksi ($\epsilon_s > 0.0005$). There is considerable disagreement

among the theories of secondary cracking concerning the significance of the variables involved, especially the nature of the bond stress distribution along the reinforcement between two successive primary cracks.

3. The third stage of cracking, also referred to as the equilibrium stage, occurs when no further secondary cracks can be formed, and existing cracks continue to widen. The steel stress is usually greater than 30 ksi ($\epsilon_s > 0.001$) at this stage of cracking.

Although the initiation of primary cracks are important, the main concern of this research is with the distribution of second and third stage cracks which occur at higher steel stresses.

5.2.2 Crack control

Crack control is provided by proportioning/detailing structural elements so that the computed crack width is less than some prescribed value. The prescribed value may be related to the need for water-tightness, anticipated durability or exposure concerns, or be based on aesthetics. Having established an allowable crack width, it is necessary to incorporate methods of control which will ensure that cracking will not exceed the allowable limit. Effective methods of crack control involve measures which will give a favorable distribution of cracks. Good crack distribution is usually characterized by a larger number of fine cracks rather than a small number of wide cracks. The establishment of a good criterion for crack control is derived from a study of the various equations relating crack width and spacing. The full utilization of high-strength reinforcement in the design of reinforced concrete members will, in most cases, involve the development of larger cracks under service loads because of the higher allowable stresses. It is

possible, therefore, that the permissible tensile stress in the reinforcement may be limited by allowable crack widths.

5.2.3 Early investigations of flexural and axial tension cracking

5.2.3.1 Flexural members

Since the early investigations of the effects of reinforcement on the strain capacity of concrete, there have been extensive studies on cracking in reinforced concrete flexural members. Considère (1906) was the first to establish that the crack spacing in beams increased with the diameter of the longitudinal reinforcement. This finding was confirmed by the tests of Graf (1921) who also showed that crack width decreased with an increase in roughness of the reinforcement (improved bond characteristics), and that crack width was approximately proportional to crack spacing. Graf concluded from a review of previous tests on reinforced concrete beams that crack development can be limited to numerous fine cracks by proper arrangement of the reinforcement.

In 1933, Westergaard (1933) developed a method, based on elasticity theory, for calculating the stresses, deformations, crack widths, and curvature in the vicinity of an individual crack. The equations suggest the relative advantage of the utilization of smaller reinforcing bars.

Thomas (1936) presented equations for average crack spacing and width which were in good agreement with available test data. His equations are identical to those resulting from an assumed parabolic bond stress distribution. It was suggested that these equations could be adapted to flexural members by defining an equivalent reinforcing percentage. Thomas noted that the relationship between steel stress and crack width was not entirely linear (Figure 5.3) and that crack width decreased with an increase in steel percentage. The non-linear relationship of

crack width and steel stress was due to the low tensile strength of the reinforcement. The use of higher strength steel bars in concrete will lead to an equivalent flexural capacity with a smaller area of reinforcing steel. Therefore, the development of a crack pattern and crack spacing would be different. However, the question remains as to whether or not the crack spacing continues to decrease while the stress on the reinforcement increases. In other words, it is still unknown whether a flexural member with high strength reinforcing will exhibit more cracks at its service load (typically taken as a steel stress, $f_s = 0.6f_y$) or exhibit larger crack widths. Based on Figure 5.3, since using high-strength steel bars will decrease the amount of steel in a concrete section, it may be hypothesized that there will be an increase in crack widths at higher service load levels.

Theoretical and experimental results by Romualdi and Batson (1963) further support the crack control advantages of distributing the reinforcement so that, for a given reinforcement ratio, the reinforcement would be as closely spaced as possible. It was found that the tensile cracking strength of concrete increased in proportion to the inverse square root of the reinforcement spacing.

Mathey and Watstein (1960) performed a series of flexural beam tests to determine the effect of the magnitude of steel stresses and nature of the stress-strain characteristics of different bar types on various cracking deformations. They obtained relationships between the computed steel stresses and the beam deflections, width and spacing of cracks, and strains in the steel and concrete.

Hognestad (1961) performed flexural tests to determine the significance of certain design factors that could be used to control cracking. The test results confirmed the hypothesis of Rehm (1957) that crack width is not proportional to crack spacing.

Kaar and Mattock (1963) conducted tests on flexural members reinforced with steel having yield strengths of 50 ksi and 60 ksi (high-strength for the time) deformed bars with the purpose of establishing design criteria for crack control. An analysis of the data resulted in a simple empirical equation indicating that crack width is essentially proportional to steel stress and, for a given steel stress, proportional to the area of concrete surrounding each bar. The empirical relationship for crack width, w , was found to be:

$$w = 0.115 \sqrt[4]{A} f_s \times 10^{-3} \quad (5.17)$$

Where

$A = A_e/n$, is the area of concrete in tension surrounding each bar

n = number of bars in concrete area effectively subjected to uniform tension, A_e

f_s = tensile stress in the reinforcement at a crack; the equation applies for $f_s < 70$ ksi.

5.2.3.2 Tension cracking

When a reinforced concrete member is loaded gradually in pure tension, cracking of the concrete will take place in one or more places along the length of the member when the tensile stress in the concrete exceeds the tensile strength of the concrete. After cracking, the tensile stress in the concrete adjacent to the crack is relieved because of the slip that takes place between the concrete and reinforcement. Tensile stress in the concrete between cracks is present because of the bond between the reinforcement and concrete. The distribution and magnitude of the bond stress along the reinforcement will determine the distribution of the concrete stress between cracks along the length of the member (see Figure 5.4a). As tension loading is increased, cracking will continue to take place until the stress in the concrete does not exceed the concrete

tensile strength because of excessive slip and reduction of distance between cracks. Essentially, the distance between cracks becomes sufficiently small that the stress to cause concrete cracking can no longer be developed by the reinforcing present. When this condition is reached, the crack spacing reaches its minimum, but the crack widths will continue to increase as the tensile stress in the reinforcement increases (third stage cracking as described by Reis et al. 1965). Assuming this behavior to be valid and that second stage cracking is fully developed by 30 ksi (Reis et al.), it may be hypothesized that crack patterns in members having high strength reinforcing steel will not vary from those having conventional steel. Thus, only crack width and not crack spacing will be affected by utilizing the higher steel strength.

The cracking behavior of reinforced concrete members in axial tension is similar to that of flexural members, except that the maximum crack width is larger than that predicted by the expressions for flexural members (Broms 1965a,b). The lack of strain gradient and restraint imposed by the compression zone of flexural members is probably the reason for the larger tensile crack width. Data are limited, but it appears that the maximum tensile crack width can be expressed in a form similar to that used for flexural crack width (ACI 224R-01, 2001):

$$w = 0.10 f_s \sqrt[3]{d_c A_s} \times 10^{-3} \quad (5.18)$$

Where

d_c = Minimum concrete cover to centroid of steel at the tensile face.

$A_s = A_e/n$, is the effective area of concrete in surrounding each bar

A_e = the area of concrete having the same centroid as the n reinforcing bars

A more complicated procedure for predicting crack width in tension members has been developed that incorporates both slip and bond stress (Yang and Chen 1988).

5.2.4 Methods of effective crack control

The final crack pattern in a member is determined at the end of the second stage of cracking (Reis et al. 1965). Therefore, the methods used of controlling the spacing and width of secondary cracks are most important to the overall performance of a member. Based on the early studies reported above, the following are the main factors involved in the control of the final crack pattern: a) reinforcement stress, b) the bond characteristics of reinforcement, c) the distribution of reinforcement over the effective concrete area subject to tension, d) the diameter of reinforcement, e) the percentage of reinforcement, f) the concrete cover over the reinforcement, and g) the material properties of the concrete.

5.2.4.1 Reinforcement stress

Steel stress is proportional to the maximum crack width. To optimize reinforcing bar utilization, stresses under service conditions should exceed $0.50f_y$ and are typically assumed to be about $0.60f_y$ to $0.66f_y$ (ACI 318 assumptions at different times). When high-strength reinforcing bars having yield strengths higher than 60 ksi are used, the optimal stress utilization exceeds 30 ksi. This stress is the value used by Reis et al. (1965) to establish that the crack pattern of a member. At stresses higher than this threshold, no further cracking is expected, and only crack widths increase as the stress is increased.

5.2.4.2 Bond characteristics

Crack spacing and width are decreased by increasing the bond strength between the reinforcement and concrete. Bond is affected by the mechanical deformation (ribs) on the bars. There is no reason to assume any difference in bond strength between high strength and conventional bars having the same deformation or rib patterns. Although the bar deformation patterns are the same for conventional A615 and high strength A1035 reinforcing steel, some researchers have reported improved bond performance with A1035 (Sumpter 2007 and Zeno 2009). This apparent improvement is believed to result from the deformations in A1035 steel being more pronounced due to the rolling requirements of this tougher grade of steel.

5.2.4.3 Distribution of reinforcement

Probably the most important method of controlling cracks from the design viewpoint is the distribution of the reinforcement over the tension zone. Kaar and Mattock (1963) concluded that the best crack control is obtained when the reinforcing bars are well distributed over the effective concrete area subject to tension. The effective distribution of the reinforcement provides the maximum utilization of the concrete in the tension zone by enabling it to sustain as much of the tension load as is possible for a given number bars and steel percentage. The maximum crack width can be decreased by minimizing the area of concrete surrounding each bar (Reis et al. 1965). These observations lead to the rule of thumb that “a greater number of smaller diameter bars are preferred to a small number of larger bars.”

5.2.4.4 Diameter of reinforcement

The maximum crack width that occurs in a member with a specified effective area of concrete in tension and steel reinforcing ratio ($\rho = A_s/A_c$) can be decreased by decreasing the diameter of the

reinforcing bars. This is because small bars have a larger surface area-to-volume ratio and thus have proportionally greater surface area through which the steel stresses are transferred to the concrete. The use of a large number of reinforcing bars of small diameter allows the tensile stress in the concrete to approach a more uniform distribution. Limitation on the use of small diameter bars, however, include economic and fabrication considerations.

5.2.4.5 Reinforcing ratio

If the bar diameter and effective concrete area in tension are kept constant, an increase in the percentage of reinforcement will decrease the spacing and width of cracks. Of course, as the steel ratio is increased, it should be properly distributed over the tension zone as discussed in the previous sections. The reinforcement ratio ($\rho = A_s/A_c$) is not as important as the effective reinforcement ratio of the tension zone ($\rho_e = A_s/A_e$) with respect to crack control.

5.2.4.6 Concrete cover

The maximum crack width is generally smallest at the reinforcement and increases with distance through the concrete surrounding the reinforcement. Therefore, increasing the concrete cover will cause an increase in the maximum crack width that occurs at the exterior surface of the member although the crack behavior at the reinforcing bar remains unchanged. Clark (1956) found that crack width at the face of a beam increases linearly with the distance between the steel centroid and tensile face. Hognestad (1961) found that the crack width at the level of the steel on the beam sides increases somewhat with side cover. Increased cover, on the other hand, can serve to resist splitting types of failures and the associated longitudinal cracking. Section curvature also amplifies crack width.

5.2.4.7 Material properties of concrete

The material properties of concrete do not strongly influence the maximum crack width that is likely to occur. This disconnection is apparently due to the fact that the other parameters affecting crack widths are related in such a way that the strength properties of the concrete are cancelled. It is difficult to state whether it is more advantageous to use a concrete with a high strain capacity or a higher tensile strength. Each of these material properties theoretically affects crack width by its influence on the effective concrete area in tension, bond characteristics, position of the neutral axis, and modular ratio. Shrinkage and creep characteristics may be more important, especially affecting crack initiation (Reis et al. 1965).

5.2.5 Code provisions and expressions for cracking and crack control

Gergely and Lutz (1968) made an extensive statistical evaluation of data from previous investigations. They examined a large number of equations and variables and reached the following conclusions regarding the factors affecting the crack width:

- a) The steel stress is the most important variable.
- b) The cover thickness is an important variable but is not the only consideration.
- c) The bar diameter is not a major variable.
- d) The size of the side crack width is reduced by the proximity of the compression zone in flexural members.
- e) The bottom crack width increases with the strain gradient through the depth of the section (i.e.: thinner sections exhibit proportionally greater crack widths).

- f) The major variables are the effective area of concrete in tension, A_e , the number of bars n , the side or bottom cover, t_s or t_b , and the steel stress, f_s .

Gergely and Lutz proposed two equations that best fit all the experimental data to predict the most probable maximum crack width in reinforced concrete flexural members: For the most probable maximum crack width in a constant moment region at the level of the reinforcement:

$$w_s = 0.091 \times 10^{-3} \frac{\sqrt[3]{t_s A}}{1 + \frac{t_s}{h_1}} (f_s - 5) \quad (5.19a)$$

Which is conventionally simplified:

$$w_s = 0.076 \times 10^{-3} \frac{\sqrt[3]{t_s A}}{1 + \frac{2}{3} \frac{t_s}{h_1}} f_s \quad (5.19b)$$

For the most probable maximum crack width in a constant moment region on the bottom (or tension) face of the beam:

$$w_b = 0.091 \times 10^{-3} \sqrt[3]{t_b A} (f_s - 5) \quad (5.20a)$$

Which is conventionally simplified:

$$w_b = 0.076 \times 10^{-3} \sqrt[3]{t_b A R} f_s \quad (5.20b)$$

Where

$A_s = A_e/n$, is the effective area of concrete surrounding each bar (in²);

A_e = the area of concrete having the same centroid as the n reinforcing bar (in²);

f_s = steel stress calculated by elastic cracked section analysis (ksi);

$R = h_2/h_1$ (also known as β);

t_b = bottom cover measured from the center of lowest bar (in);

t_s = side cover measured from the center of outer bar (also known as d_c) (in);

$h_1 = (1-k)d$;

$h_2 = h-kd$;

d = effective depth of beam;

h = overall depth of beam;

k = distance from neutral axis to compression face divided by effective depth of beam

5.2.5.1 ACI 318

In pre-1999 ACI code applications, the Gergely-Lutz equation (5.20) was recast so that the crack width was implicit rather than explicit:

$$z = f_s^3 \sqrt{d_c A} \quad (5.21)$$

Where z was an acceptance parameter having units of force/length. Acceptance values were specified for interior and exterior exposures. These corresponded to implied crack widths of 0.022 in and 0.018 in., respectively.

The traditional ‘z-factor’ or Gergely-Lutz (1968) approach of *directly* assessing cracking behavior of concrete beams was dropped by ACI 318 (2005) in 1999 in favor of a simplified version of the alternative approach proposed by Frosch (1999) which prescribed spacing limits for longitudinal reinforcing steel thereby *indirectly* controlling crack width. The empirically-tuned z-factor approach was considered inadequate to address cases having very large concrete cover (ACI 224 2001). Additionally, research showed no conclusive evidence linking reinforcement corrosion with crack width (Beeby 1983). Despite the latter assertion, the simplified version of the Frosch approach adopted by ACI implicitly assumes a maximum crack width of 0.018 in. which was also the value assumed for exterior exposure conditions when applying the ACI z-factor approach prior to 1999. Frosch (2001) calculates crack widths, w_c , as the product of reinforcing strain, $\varepsilon_s = f_s/E_s$, and crack spacing, S_c :

$$w_c = \varepsilon_s S_c \quad (5.22)$$

To determine the crack width at the beam surface, it is necessary to account for the strain gradient. Assuming that plane sections remain plane, the strain gradient is illustrated in Figure 5.5. The crack width computed at the level of the reinforcing steel (Equation 5.22) can be multiplied by an amplification factor (β) that accounts for the strain gradient. The factor, β , is computed as follows:

$$\beta = \frac{\varepsilon_2}{\varepsilon_1} = \frac{h-c}{d-c} \quad (5.23)$$

Based on the work of Broms (1965a, b), the crack spacing depends primarily on the maximum concrete cover. Specifically, the minimum theoretical crack spacing will be equal to the distance from the point at which the crack spacing is considered to the center of the reinforcing bar located closest to that point, d_c . In addition, the maximum spacing is equal to twice this distance, $2d_c$ (Frosch 2001). As illustrated in Figure 5.6 the critical distance for the maximum crack spacing can occur at two locations and the crack spacing, S_c , can be calculated as follows:

$$S_c = \psi_s d^* \quad (5.24)$$

where:

d^* = controlling cover distance (shown in Figure 5.6)

ψ_s = crack spacing factor taken as 1.0, 1.5 and 2.0 for minimum, average and maximum crack spacing, respectively.

Based on the physical model, Frosch developed the following simple equation to predict crack widths that could be used regardless of the actual concrete cover:

$$w_c = 2 \frac{f_s}{E_s} \beta \sqrt{d_c^2 + \left(\frac{s}{2}\right)^2} \quad (5.25)$$

Acknowledging that crack spacing and crack width are functions of the bar spacing, Frosch proposed that crack control could also be achieved by limiting the longitudinal reinforcement spacing based on acceptable crack width limits. This rationale led to a

rearrangement of Equation 5.25 to solve for the maximum permissible bar spacing, s (Figure 5.6) as:

$$s = 2\sqrt{\left(\frac{w_c E_s}{2f_s \beta}\right)^2 - d_c^2} \quad (5.26)$$

Where cracked-elastic conditions are assumed

ACI Committee 318 made some modifications to this equation and adopted a new crack control equation to evaluate the maximum longitudinal bar spacing, s , for the 1999 code as follows:

$$s = \frac{540}{f_s} - 2.5c_c \leq \frac{432}{f_s} \quad (5.27)$$

Where

c_c = clear concrete cover for reinforcement nearest the tension face (in.);

f_s = stress in the steel which ACI 318 permits to be taken as $0.60f_y$.

This simplified equation of the cracking model is based on the following assumptions:

$\beta = 1 + 0.08d_c$;

$w_c = 0.016$ in. limiting crack width (in.);

$d_c = c_c + 0.5$ in., (i.e., #8 average bar size.)

Due to the recalibration of ACI load factors in 2002, the assumed service load stress, f_s , was increased from $0.60f_y$ to $0.67f_y$, effectively changing the *de facto* assumed crack width: $w_c =$

$0.016(0.67/0.60) = 0.018$. The value of $w_c = 0.018$ is the assumed crack width limit for exterior exposure in the pre-1999 ACI 318 codes that used the Gergely-Lutz equation. The relaxed interior crack width limit is neglected in post-1999 ACI 318 codes.

Equation 5.27 is simply an alternate (and simpler) representation of Equation 5.26. Crack control through either Equation is said to be “indirect” because the maximum bar spacing is indirectly constrained by a limiting crack width, w_c . Notice that Equation 5.27 uses the subscript “s” to refer to steel reinforcement. In those cases where there is only one bar nearest to the extreme tension face, the maximum bar spacing is defined as the width of the extreme tension face. In members with multiple layers of tension reinforcement, Equation 5.27 is defined based on the assumption that only the bottom layer affects crack widths.

5.2.5.2 AASHTO LRFD

AASHTO Equation 5.7.3.4-1 (AASHTO 2007) takes the same form as the ACI equation (Equation 5.27):

$$s \leq \frac{700\gamma_d}{\beta_s f_{ss}} - 2d_c \quad (5.28)$$

Where:

f_{ss} = service level stress in the steel reinforcement (ksi);

$$\beta = 1 + \frac{d_c}{0.7(h - d_c)};$$

d_c = distance from tension face to centroid of nearest reinforcing bar, in.;

For Class 1 exposure (moderate exposure), the equation is calibrated, through $\gamma_d = 1$, for a crack width of 0.017 in.; for Class 2 exposure (severe exposure), $\gamma_d = 0.75$. The *de facto* crack width is $\gamma_d(0.017)$.

5.2.5.3 Permissible crack widths

Crack widths are conventionally correlated with durability: associating a permissible crack width with a particular exposure. The premise is that crack widths are related to the ability of water to migrate to the reinforcing steel thereby driving corrosion. As described above, typical interior exposure is permitted crack widths of 0.022 and exterior exposures are permitted 0.018. These values are legacies of the work of Gergely and Lutz (1968). This approach has been perpetuated elsewhere. For instance when GFRP bars are used to reinforce concrete elements, the Canadian Highway Bridge Design Code (CSA 2006) permits increased allowable crack widths of 0.020 to 0.028 in. based on the corrosion resistance of GFRP. Significantly, Beeby (1983) showed no conclusive evidence linking reinforcement corrosion with crack width while Poursaei et al. (2010) show that a crack as small as 0.004 in. acts as a free surface with respect to water ingress.

ACI Committee 224 (2001) suggests that crack widths exceeding 0.0016 in. may be unacceptable from the standpoint of aesthetics. Similarly, Halvorsen (1987) states that a case can be made that crack widths ranging from 0.006 to 0.012 in. could be considered unacceptable for aesthetic reasons as they are visible to the naked eye, hence, generating a sense of insecurity or structural failure.

5.2.6 Crack control in concrete members reinforced with high strength steel bars

Early studies showed that an increase in crack width is due to an increase in steel stress and, to a lesser extent, to an increase in the curvature of the member. Thomas (1936) pointed out that an increase in the curvature at a constant steel stress tends to distribute the cracking rather than widen individual cracks. An increase in the steel stress affects the difference in the elongation between the reinforcing steel and concrete and causes additional slip to occur. This slip is the main cause of the increase in crack size. Slip occurs in the vicinity of a crack and extends to a point where the differential strain is zero. At that point the bond stress and resistance to slip reach maximum values and decrease toward the mid-section between cracks (Figure 5.4). The overall values of bond force decrease with an increase in load. This decrease can be attributed to a) the effects of the increase of transverse contraction of the reinforcing bar (i.e.: Poisson effect) and b) the disintegration of the concrete at the concrete-steel interface (Odman 1962). Therefore, the crack width increases while the crack spacing remains constant. If the load is increased further, the slip between concrete and reinforcement continues to increase. Due to the comparatively low values of concrete extensibility, the increase in crack width can be considered essentially equal to the increase in the steel strain. Indeed, the use of crack widths to estimate steel strain was found to be remarkably predictive in the fatigue tests reported in Chapter 4 (see 4.5.4). Three aspects of cracking behavior will be addressed as described in the following sections.

5.2.6.1 Crack widths

In view of the improved corrosion resistance of high-strength reinforcement meeting ASTM A1035 specifications, it is possible that the crack width criterion can be relaxed to allow larger

spacing of high-strength reinforcing bars without adversely affecting the deflection limit state, which is affected by spacing between cracks and crack widths.

5.2.6.2 Crack spacing

The use of high-strength reinforcement will reduce the total area of steel required for flexural resistance. The smaller amount of steel will increase stresses at the service limit state (f_s) and shift the neutral axis upward in the section. As a result, the maximum permissible spacing of bars is reduced for a given limiting crack width (Equation 5.28).

Destefano et al. (2003) compared the value of the maximum bar spacing for a range of service load stresses for a number of models and code equations. Figure 5.7 shows the bar spacing versus the allowable bar stress for a given concrete cover. Based on Figure 5.7, one can conclude that increasing the allowable bar stress, results in a gradual decrease of maximum bar spacing. Based on Frosch's (2001) physical model, the crack spacing has a direct relation with maximum bar spacing (Equation 5.26). Thus, increasing the stress and strain in reinforcement bars in a flexural beam should result in the same crack pattern as produced using 60 ksi steel bars although larger crack widths are expected at the service load stress level.

In addition, a simple parametric study can show that ASTM A1035 bars need to be spaced more closely than ASTM A615 bars in order to meet crack width requirements for AASHTO (2007). Considering Equation (5.26) for different bar sizes, and assuming $d_c = 1.5''$ and $f_y = 60$ ksi for A615 and 100 ksi for A1035 bars, the required bar spacings given in Table 5.3 are obtained. Clearly, A1035 bars need to be spaced more closely than A615 bars although the required spacings are not apparently practical.

Two options may be used to increase the spacing of ASTM A1035 bars: 1) accept wider crack widths, and/or 2) reduce the cover. In order to achieve the same spacing as ASTM A615

bars, the crack width for ASTM A1035 bars needs to be increased by the ratio of their yield stresses: f_{yA1035}/f_{yA615} , essentially a factor of 2. For the cases shown in Table 5.3, the acceptable crack widths for ASTM A1035 will have to be 0.035 in. and 0.027 in. for Class 1 and Class 2 exposure, respectively, to result in the same spacing for A1035 as for A615 with present limits. It is unclear whether better corrosion resistance of ASTM A1035 bars justifies these larger crack widths. It is also noted that one school of thought (Beeby 1983) discounts the effects of crack width on corrosion behavior in any event, potentially justifying an increase in allowable crack widths. However, aesthetics also affect acceptable crack widths (ACI 224 2001). In cases where aesthetics are seen to govern crack width limits, no increase in crack width would be permitted. The second option of reducing the cover (d_c) does not have a significant impact on crack spacing and is ill-advised for other performance-related reasons.

A study by Mast et al. (2008) indicates that the measured crack width in beams reinforced with A1035 bars under service loading conditions is only slightly larger than the acceptable crack widths for beams reinforced with conventional A615 steel. Considering that some high-strength steel also exhibits reduced corrosion rates under severe environmental conditions, the slightly increased crack widths may be justified provided it is not objectionable from the aesthetics point of view (Mast et al. 2008).

5.2.6.3 Effect of repeated load

In many cases, particularly with bridges, the effects of repeated loading may have a greater practical importance than the absolute maximum load for judging the risk of corrosion of the reinforcement. Repeated loading causes existing cracks to widen through progressive slip between the reinforcement and concrete. At the same time, existing cracks also propagate further towards the compression side of the member. Theoretical relationships between the increase in

crack width and the number of loading cycles have not been developed for high strength reinforced concrete members.

5.2.6.4 Analytical study of crack characterization

In the case of using conventional steel bars in flexural members, it has been shown that during the second stage of cracking, for steel stresses usually greater than 14 ksi, the presence of existing primary cracks affects the formation of secondary cracks under increasing moment. Away from a primary crack, stresses are transferred by bond from the reinforcement to the concrete. If enough force is transferred from the steel to the concrete, the strains that are developed may exceed the strain capacity or the tensile strength of the concrete at a certain section and another crack will form perpendicular to the reinforcement. Theoretically the section at which secondary crack formation occurs is midway between existing cracks. This mechanism continues until the tensile forces developed through bond transfer are insufficient to produce additional cracks. To compare and demonstrate the crack behavior of members reinforced with conventional steel bars and members reinforced with high-strength steel bars, a relatively complex material modeling in a simple direct tension model can be used.

5.2.6.5 Direct tension model to investigate the crack development

In general, the absolute displacements of the steel u_s , and of the concrete u_c between adjacent cracks in a concrete member are different. Due to this relative displacement (often referred to as 'slip'), $s = u_s - u_c$, bond stresses (technically, interfacial shear stresses) are generated between the concrete and the reinforcing steel. The magnitude of these bond stresses depends on the surface condition and deformation pattern (ribs) of the reinforcing steel, the concrete strength, f_c , concrete quality, and the degree of slip itself. Between adjacent cracks, a part of the tension force

in the reinforcing steel acting at the crack is transferred into the concrete by bond. This transfer takes place over a length of bar referred to as the ‘transmission length’, L . This is the mechanism associated with the so-called ‘tension stiffening effect’.

The local decrease of the relative displacement along the transmission length, L , is characterized by the strain difference (CEB-FIP 1990):

$$\frac{ds}{dx} = \varepsilon_s - \varepsilon_c \quad (5.29)$$

Based on the CEB-FIP Model code (1990), for monotonic loading the bond stress between concrete and reinforcing bar can be calculated as a function of the relative displacement, s , according to Equation 5.30:

$$\tau(x) = \tau_{max} \left[\frac{s(x)}{s_1} \right]^n \quad (5.30)$$

where

$s_1 = 0.024$ in. for unconfined concrete and 0.039 in. for confined concrete,

τ_{max} = the maximum bond stress capacity; for good bond conditions: $\tau_{max} = 2.0\sqrt{f'_c}$.

Depending on the selection of the coefficient n ($0 \leq n \leq 1$) in Equation 5.30 all usual forms of bond stress-slip relationships can be modeled. Setting $n = 0$ models bond characteristics with a constant stress while $n = 1$ provides a linear relationship (CEB-FIP 1990). In addition, the bond stress along the transmission length decreases the stress in the reinforcement and increases the stress in the concrete proportionately. This relationship is shown schematically in Figure 5.8.

As shown in the Figure 5.8, in a reinforced concrete member subjected to tension (or the tension zone in a flexural member), the reinforcement at both loading ends (which may be interpreted as crack locations) sustains the total external force with the stress f_{so} . At an arbitrary location between cracks, however, the tensile stress in the reinforcement is smaller than f_{so} ; this difference is transferred to the concrete by bond along the transmission length, L_1 . From force equilibrium, therefore, the following relationship is valid at an arbitrary location.

$$T_1 = A_s f_{so} = T_s + T_c = A_s f_s(x) + A_c f_c(x) \quad (5.31)$$

If one assumes the stress and strain in both reinforcement and concrete to have a linear relationship then Equation 5.31 can be rewritten as follows:

$$T_1 = A_s f_{so} = A_s E_s \varepsilon_s(x) + A_c E_c \varepsilon_c(x) \quad 0 \leq x \leq L/2 \quad (5.32)$$

If the length L is adequate to develop the full bond stress, at a distance L_1 the reinforcement and concrete have the same strain ($\varepsilon_s = \varepsilon_c = \varepsilon_2$); that is there is a region experiencing no relative displacement (slip) between the concrete and steel (Figure 5.8a). In this ‘no slip’ region, the applied tension force is distributed in proportion to the stiffness of the effective concrete and reinforcement and the bond stress is equal to zero (Equation 5.30). The total applied load in the no slip region is:

$$T_1 = f_{so} A_s = (E_c A_c + E_s A_s) \varepsilon_2(x) \quad L_1 \leq x \leq L/2 \quad (5.33)$$

To obtain the value of L_l and ε_2 , an additional relationship is required. Considering equilibrium on either side of a crack, as shown in Figure 5.10, requires:

$$T_s = T_1 - \int_0^x \tau(x)p dx \quad (5.34)$$

Where

T_s = the force in the bar,

$\tau(x)$ = the bond stress distribution along the length of the bar and

p = the bar circumference, assumed constant along the bar length.

Therefore, at L_l :

$$T_s(L_1) = \varepsilon_2 E_s A_s = f_{so} A_s - \int_0^{L_1} \tau(x)p dx \quad (5.35)$$

The relative bond stress relationship along the length of the bar is also required. The derived mechanics-based relationships show that bond stress is a function of relative bar slip, slip is a function of bar force, and bar force is a function of bond stress. As a result, even relatively simple bond stress-slip models require an iterative solution that needs to be evaluated using approximate methods. To simplify this process, a simple triangular form for the bond stress distribution along the length L_1 is assumed (Figure 5.8, dashed lines). This form requires two assumptions: firstly, a value for the maximum bond stress; in this study, the CEB-FIP value for good bond conditions, $\tau_{max} = 2.0\sqrt{f'_c}$, is adopted. Secondly, the distance over which τ_{max} is developed is required; in this study, CEB-FIP recommendation of 5 bar diameters ($5d_b$) is

adopted as shown in Figure 5.8. The formation of bond stress along the length of a bar changes while the tension force increases. Figure 5.9 illustrates the development of bond stress along the length of the bar. Based on these simplifications, values of L_1 and ε_2 can be found by solving Equations 5.33 and 5.35.

In order to determine the crack development in a member, the total force transmitted from the reinforcement to the concrete is calculated:

$$T_c = \int_0^{L_1} p\tau(x) dx \quad (5.36)$$

Where

$$T_c = f_c A_c = E_c \varepsilon_2 A_c$$

p = the circumference of the reinforcement.

If L_1 provides adequate length to produce the cumulative tension stress transferred to the concrete section, f_c , and this stress is greater than ultimate tension capacity of concrete f_{cr} , then cracks will form. At the same stress level, additional cracks will continue to develop until the length between two cracks is not adequate to transfer sufficient tension to the concrete to develop a new crack.

While the tension load (T_l) increases beyond that which caused the first series of cracks, the relative strain in the reinforcement at the loaded ends and cracks will increase. According to Figure 5.11, the arbitrary location where strain in the reinforcement is equal to the strain in the concrete (Point B) occurs at a distance $L_2 > L_1$. In this case, the bond stress along the length of the reinforcement corresponding to the tension force will be in a new form in which α decreases (in

Figure 5.11, $\alpha_2 < \alpha_1$). The cumulative bond stress increases while α decreases. This transfers more force to concrete section and may or may not cause additional cracks between the first cracks. The process continues until the transferred tension stress is too small in the concrete section to exceed f_{cr} (please refer to the detail calculation of this investigation in Appendix).

Parametric study

To investigate the effect of using higher-strength reinforcing steel on the cracking behavior, the approach described above is adopted in a parametric study shown schematically in Figure 5.12. The study considers a single tension bar (#4, #6, #8 and #10 bars were considered) in a concrete prism subject to tension. The length of the prism, $L = 200$ in., is taken to be sufficiently long that multiple cracks will develop over its length.

The size of the reinforcing bar (d_b) and the reinforcement ratio (ρ) are both factors which affect crack development and are varied in this study. Figure 5.12 represents a simple concrete member reinforced with only one bar. The reinforcement ratio is varied by changing the area of concrete that may be effectively engaged by the bar. CEB-FIP Code (1978) reported that the maximum region of concrete affected by a bar in tension is approximately a square area centered on the bar having a dimension $15d_b$. Thus the minimum tension reinforcing ratio is $\rho_{\min} = 0.0035$. This value is reflected in both the AASHTO (2007) and ACI (2008) codes.

Crack Spacing

The results from this study are shown in Table 5.4. In every case, a 200 in. long square concrete prism (Figure 5.12) is assumed having an area $A_c = A_s/\rho$. External tension load is applied to the reinforcing bar up to the bar's ultimate capacity. For each bar size considered (#4, #6, #8, and

#10), the stress-strain relationship used for the bar is the appropriate experimentally determined Ramberg-Osgood (R-O) relationship (Equation 2.1) having parameters provided in Table 2.3. Since no #10 bars were tested, the R-O curves for #8 bars were also applied to the #10 bars. Although the R-O relationships for high strength steel are used, these are valid for conventional bars through yield since the modulus (E_s) in the R-O relationships is constant to values of stress beyond 60 ksi. Thus the reported data for stress levels below $f_s = 60$ ksi are valid for both conventional (A615) and high strength (A1035) reinforcing bars. To consider conventional 60 ksi steel in this exercise, simply truncate all data where f_s exceeds 60 ksi.

In Table 5.4, the values of bar stress, f_s , at which the initial cracks develop, are shown. As described above, depending on the value of L_1 subsequent cracking may also develop between these cracks (second and third series). Based on the geometry of the specimen and bar size, there is a specific tension load at which the last series of cracks in the specimen forms. Further increase of the tension load would not result in additional cracks forming but would increase the existing crack widths. Bar stresses causing the last series of cracks to form are shown in Figure 5.13. As shown in this figure, the results for different bar sizes are the same and only depend on the reinforcement ratio. In Table 5.4, the resulting crack spacing for each series is also given. Based on the approach taken, all cracks will develop at the same stress and have the same spacing reflecting the average values for the concrete and steel considered. Clearly, this observation does not reflect the material variation encountered in the 'real world' but the assessment of average values is deemed to be appropriate. Relationships between average and maximum values are discussed briefly below.

Based on this approach, it is shown that crack development and spacing are affected by bar size and the effective concrete area surrounding the reinforcement. As the reinforcing ratio

falls, the behavior becomes dominated by a small number of large cracks (Table 5.4). Whereas at typical reinforcing ratios (0.01 and 0.015), cracking occurs in a progressive manner and is better distributed. This should result in some variation in crack width along the member. As the reinforcing ratio becomes larger, cracking remains distributed but crack widths may be expected to be more uniform since cracking stresses vary very little. In all cases, for reinforcing ratio $\rho = 0.01$ and higher, all cracks form at bar stresses below 70 ksi. Consequently, in a concrete section having a reinforcing ratio $\rho = 0.01$ or higher, regardless of steel grade, the crack width and crack spacing are the same. Using higher strength bars allow higher stresses to develop in the steel but additional cracks are only likely to form at lower reinforcing ratios.

Crack Width

Average crack widths resulting from this analysis, w_{avg} , can be determined using the slip-strain relationship shown in Equation 5.29.

$$w_{avg} = 2 \int_0^{S/2} (\varepsilon_s - \varepsilon_c) dx \quad (5.37)$$

Where,

S = Minimum Crack spacing (From Table 5.4)

The value obtained by this method represents the average crack width along the entire 200 in. specimen length. Figure 5.14 illustrates the average crack widths calculated for the range of reinforcing ratios and bar sizes considered. Figure 5.14 clearly shows the stress at which the cracks are expected to form and the progression of crack opening as the bar stress increases.

Based on Figure 5.14d for $\rho \leq 0.02$, it can be concluded that through reinforcing bar stresses of 72 ksi, average crack widths (it is only possible to consider average crack widths in an analytical context) remain below 0.017 in. for all but the largest bars considered (#10). The results were relatively insensitive to changes in reinforcing ratio.

5.2.6.6 Observed crack widths

Extensive crack width data were collected from the flexural test specimens F1 to F6 from University of Cincinnati (see Table 5.1). To assess the effects of using higher strength steel, the crack widths corresponding to various stresses in the reinforcing steel were determined and are plotted in Figure 5.15. Figure 5.15a provides the average crack width measured from all cracks in the constant moment region. Figure 5.15b provides the maximum crack width measured in this region. The ratio of maximum to average measured crack widths for all specimens at all stress levels is 1.8, consistent with available guidance for this ratio which tends to range between 1.5 and 2.0. In all cases, the ratio of maximum to average crack width falls with increasing bar stress. At approximately 36 ksi, this ratio is 1.7, falling to 1.6 at 60 ksi and 1.5 at 72 ksi.

The data shown in Figure 5.15 clearly show that at rational service load levels ($f_s < 72$ ksi), average crack widths are all below the present AASHTO *de facto* limit of 0.017 in.. Indeed, with the exception of beam F2, maximum crack widths also fall below this threshold through bar stresses of 72 ksi. Crack width is largely unaffected by the reinforcing ratio within the range considered. It is noted that all 12 in. wide beams had four bars (#5 or #6) in the lowermost layer; thus, crack control reinforcing would be considered excellent for these beams.

Considering the measured crack widths in this experimental study, it appears that the existing equations are inherently conservative. This conservativeness allows present

specifications to be extended to the anticipated higher service level stresses associated with the use of high strength reinforcing steel.

Table 5.1 Details of flexural beam specimens F1-F6 (Shahrooz et al. 2010).

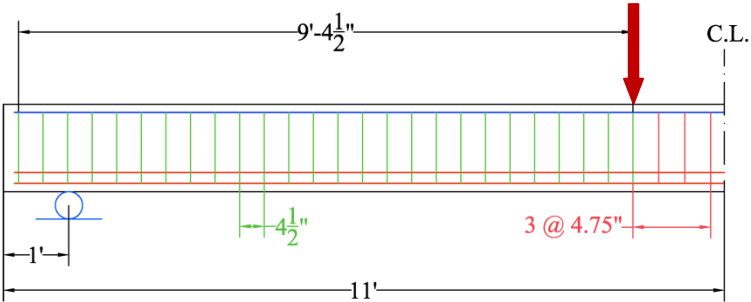
		F1	F2	F3	F4	F5	F6
A1035 longitudinal steel	lower layer	4 #5	4 #6	4 #5	4 #5	4 #6	4 #5
	second layer	2 #5	2 #6	n.a.	4 #5	4 #6	2 #5
$\rho = A_s/bd$		0.012	0.016	0.007	0.016	0.023	0.012
f_v (0.2% offset) (ksi)		130.2	121.8	130.2	129.2	134.4	129.2
R-O parameters	A	0.0145	0.0203	0.0145	0.0145	0.0130	0.0145
	B	186	198	186	186	184	186
	C	2.5	2.4	2.5	2.5	2.5	2.5
f'_c (ksi)		12.9	12.9	12.9	16.5	16.3	16.9
Specimen cross sections							
Specimen elevation							

Table 5.2 Comparison of experimental and calculated deflections at service load levels.

Beam and bar stress	$\rho = A_s/bd$	M_{max}	Deflection				
			Experimental	Branson		Bischoff	
		(kipin)		(in.)	calculated (in.)	calc/exp	calculated (in.)
F1 @ 36 ksi	0.012	899.1	0.582	0.372	0.639	0.365	0.627
F1 @ 60 ksi	0.012	1319.8	1.145	0.600	0.524	0.590	0.515
F1 @ 72 ksi	0.012	1554.4	1.400	0.723	0.517	0.713	0.509
F2 @ 36 ksi	0.016	1041.7	0.527	0.318	0.604	0.312	0.592
F2 @ 60 ksi	0.016	1730.2	1.145	0.567	0.496	0.561	0.490
F2 @ 72 ksi	0.016	2087.2	1.450	0.695	0.479	0.689	0.476
F3 @ 36 ksi	0.007	648.5	0.527	0.270	0.513	0.288	0.547
F3 @ 60 ksi	0.007	903.5	0.855	0.479	0.560	0.483	0.565
F3 @ 72 ksi	0.007	1102.4	1.182	0.633	0.536	0.629	0.533
F4 @ 36 ksi	0.016	896.5	0.625	0.286	0.458	0.280	0.448
F4 @ 60 ksi	0.016	1406.5	1.146	0.501	0.437	0.492	0.429
F4 @ 72 ksi	0.016	1651.3	1.354	0.601	0.444	0.592	0.437
F5 @ 36 ksi	0.023	1315.4	0.688	0.330	0.480	0.326	0.474
F5 @ 60 ksi	0.023	2098.2	1.271	0.551	0.434	0.547	0.431
F5 @ 72 ksi	0.023	2519.0	1.583	0.669	0.423	0.666	0.421
F6 @ 36 ksi	0.012	569.2	0.458	0.156	0.341	0.166	0.363
F6 @ 60 ksi	0.012	1012.9	0.938	0.429	0.458	0.424	0.453
F6 @ 72 ksi	0.012	1242.4	1.229	0.561	0.456	0.552	0.449

Table 5.3 Required AASHTO bar spacing, s (in)

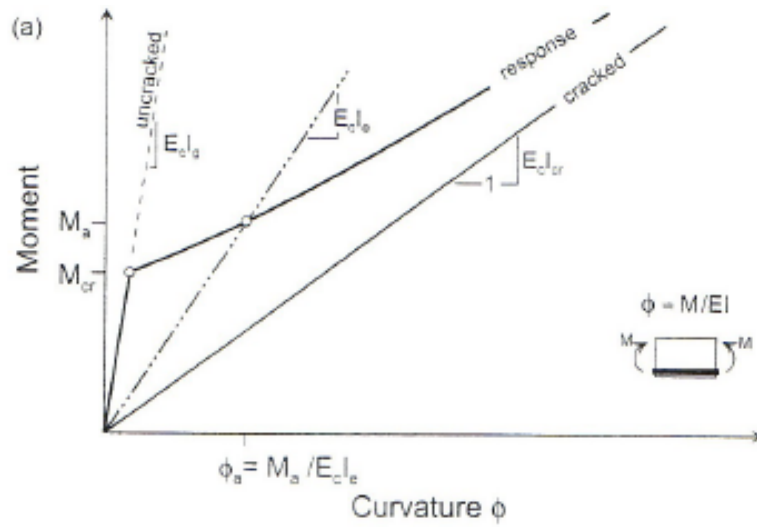
Target w_c (in.)	Exposure Class	Bar Type	f_y (ksi)	f_s (ksi)	Bar Size								
					#3	#4	#5	#6	#7	#8	#9	#10	#11
0.017	Class 1	A615	60	36	10.8	10.7	10.6	10.5	10.4	10.3	10.1	10.0	9.9
0.01275	Class 2	A615	60	36	7.6	7.5	7.3	7.2	7.1	6.9	6.8	6.6	6.5
0.017	Class 1	A1035	100	60	5.5	5.3	5.2	5.0	4.8	4.7	4.5	4.3	4.0
0.01275	Class 2	A1035	100	60	2.9	2.7	2.4	2.1*	1.7*	1.2*	----	----	----

* Spacing smaller than permitted based on other requirements

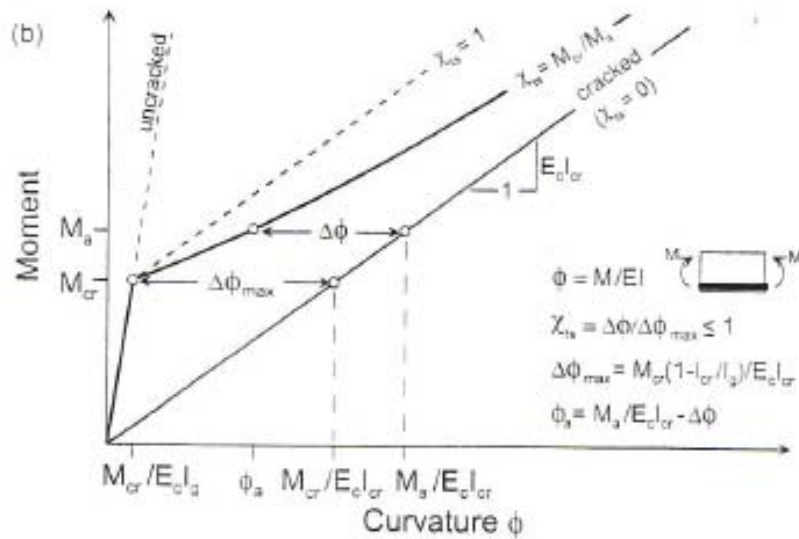
Table 5.4 Direct tension analysis results.

Bar size	ρ	Initial Crack series		Second Crack series		Third Crack series	
		f_s	S	f_s	S	f_s	S
#4	0.02	30	6.25	33	3.125	no additional cracks	
	0.015	38	6.25	42	3.125	no additional cracks	
	0.01	56	12.5	68	6.25	no additional cracks	
	0.0075	73	12.5	89	6.25	no additional cracks	
	0.005	107	25	134	12.5	no additional cracks	
	0.0035	150	25	no additional cracks			
#6	0.02	30	6.25	no additional cracks			
	0.015	38	12.5	45	6.25	no additional cracks	
	0.01	56	12.5	64	6.25	no additional cracks	
	0.0075	73	25	90	12.5	no additional cracks	
	0.005	106	25	132	12.5	no additional cracks	
	0.0035	149	50	no additional cracks			
#8	0.02	30	12.5	33	6.25	no additional cracks	
	0.015	38	12.5	42	6.25	no additional cracks	
	0.01	55	25	67	12.5	no additional cracks	
	0.0075	72	25	89	12.5	no additional cracks	
	0.005	106	50	133	25	no additional cracks	
	0.0035	149	50	no additional cracks			
#10	0.02	30	12.5	33	6.25	no additional cracks	
	0.015	38	12.5	42	6.25	no additional cracks	
	0.01	55	25	67	12.5	no additional cracks	
	0.0075	72	25	82	25	85	12.5
	0.005	106	50	134	25	no additional cracks	
	0.0035	149	100	no additional cracks			

Note: f_s is the stress level at the crack appearance and S is the crack spacing



a) Flexural member response based on effective moment of inertia I_e



b) Flexural member response incorporating tension stiffening

Figure 5.1 Tension stiffening (Bischoff 2007)

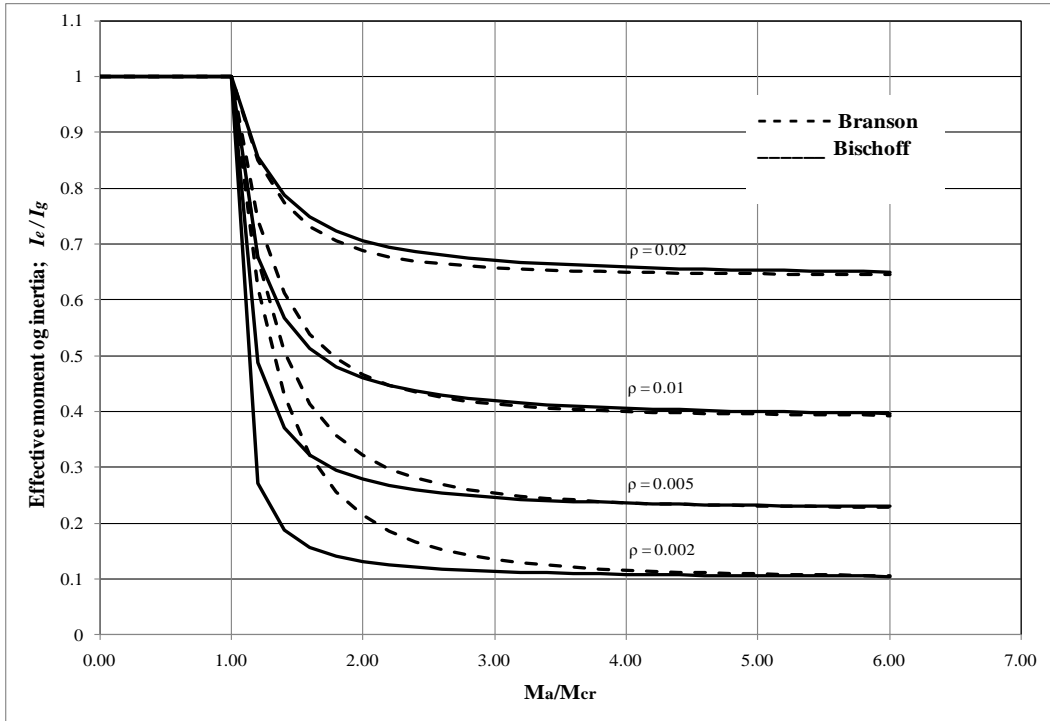


Figure 5.2 Branson's and Bischoff's equations as a function of M_a/M_{cr}

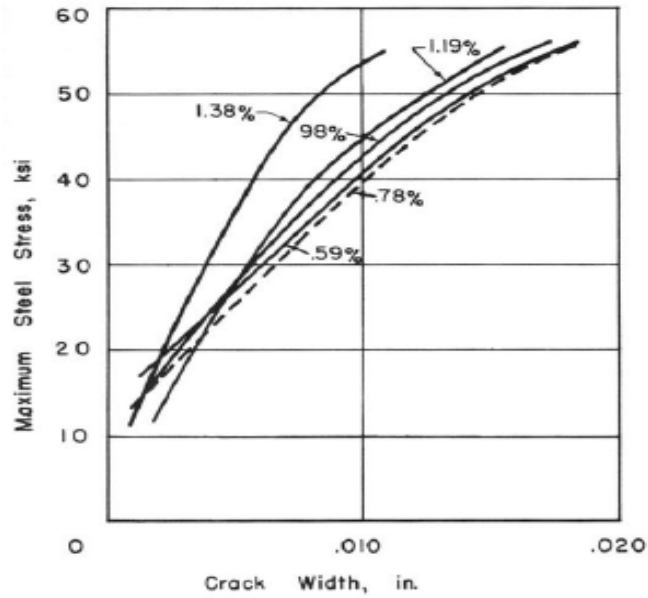
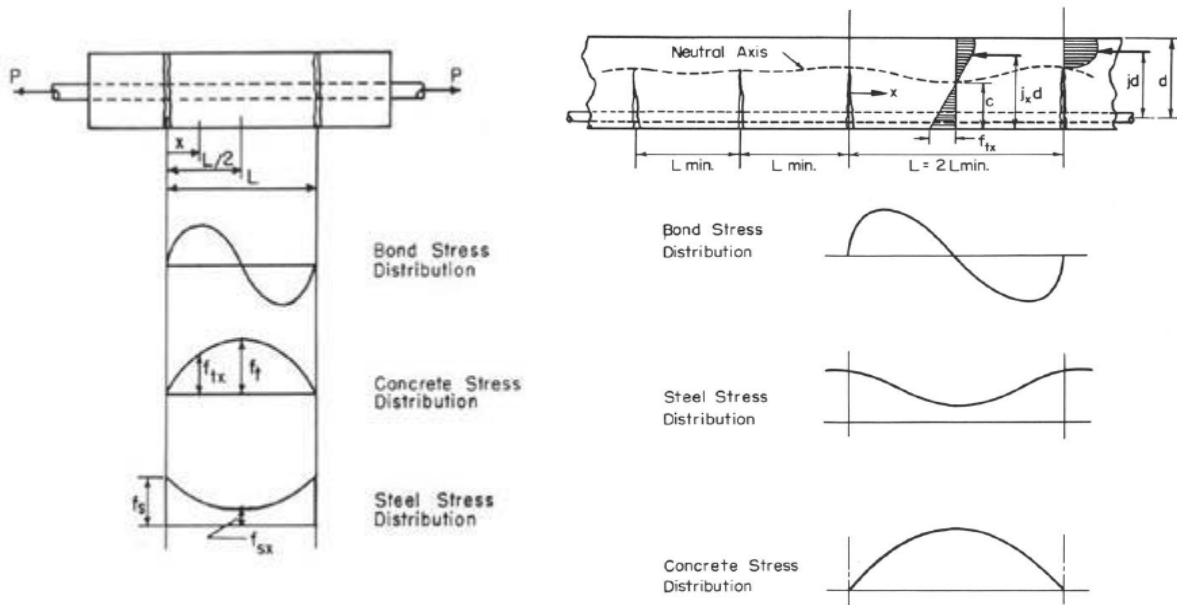


Figure 5.3 Steel stress versus crack width (Thomas 1936)



a) an axial tension member

b) stress distribution in a cracked beam

Figure 5.4 Stress distribution and configuration in a concrete member between two cracks (Reis et al 1965).

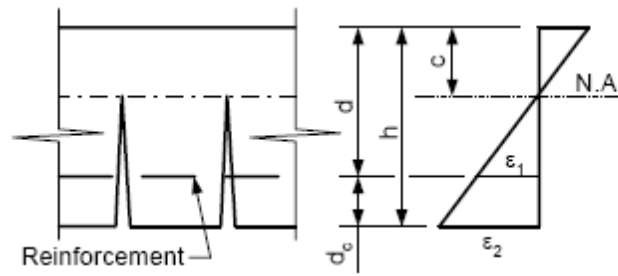


Figure 5.5 Strain profile

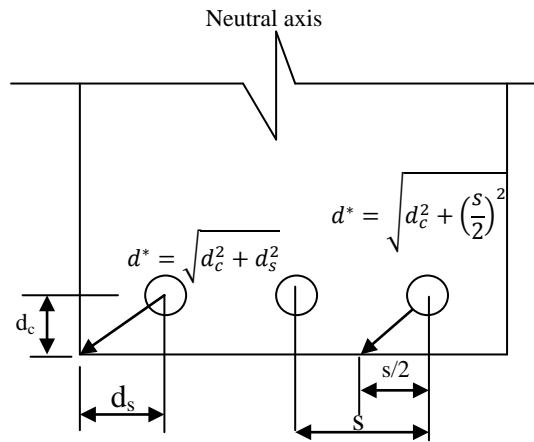


Figure 5.6 Dimensions used in crack control equations.

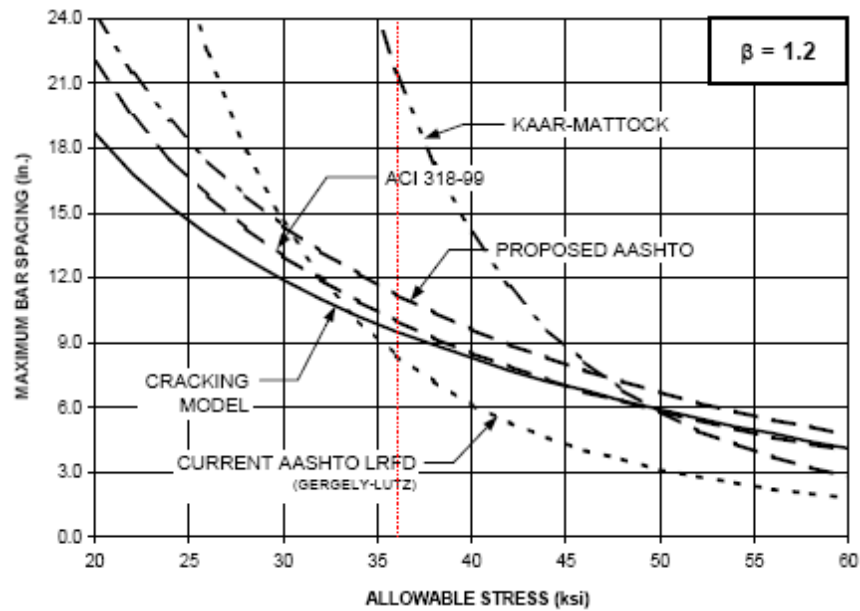
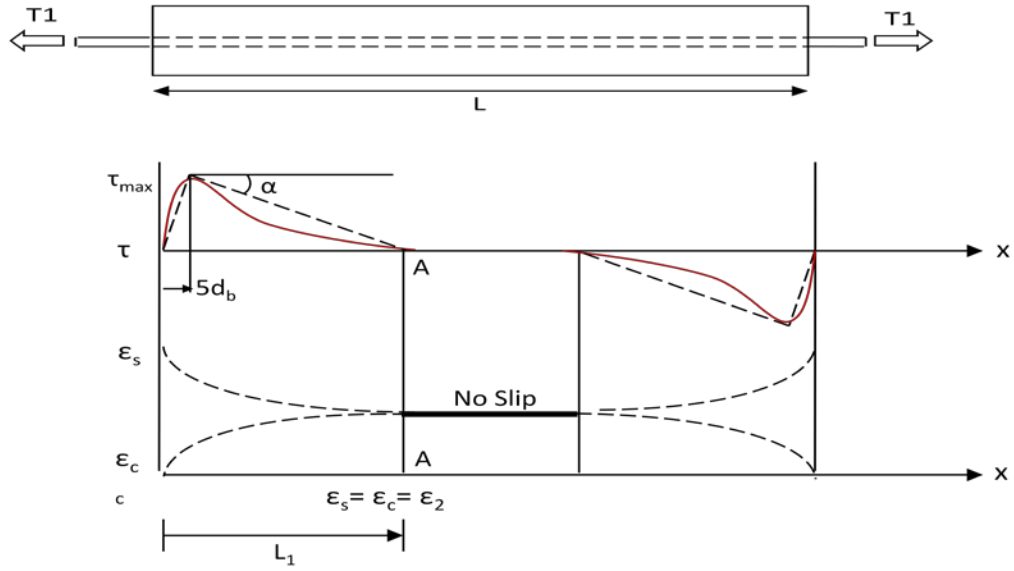
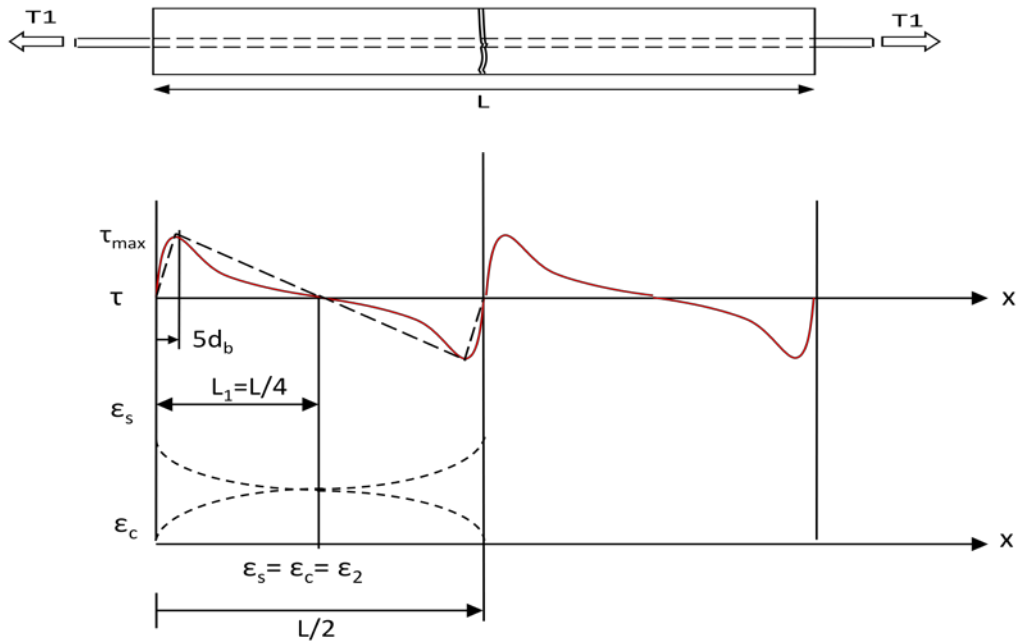


Figure 5.7 Allowable Stress vs. Bar Spacing; assumes 2 in. concrete cover and #8 bar (Destefano et al. 2003).



a) Bond stress and resulting steel and concrete strain distribution before cracking.



b) No additional cracks have been developed after the first series of cracks at the tension load (T_1).

Figure 5.8 Crack development in direct tension test.

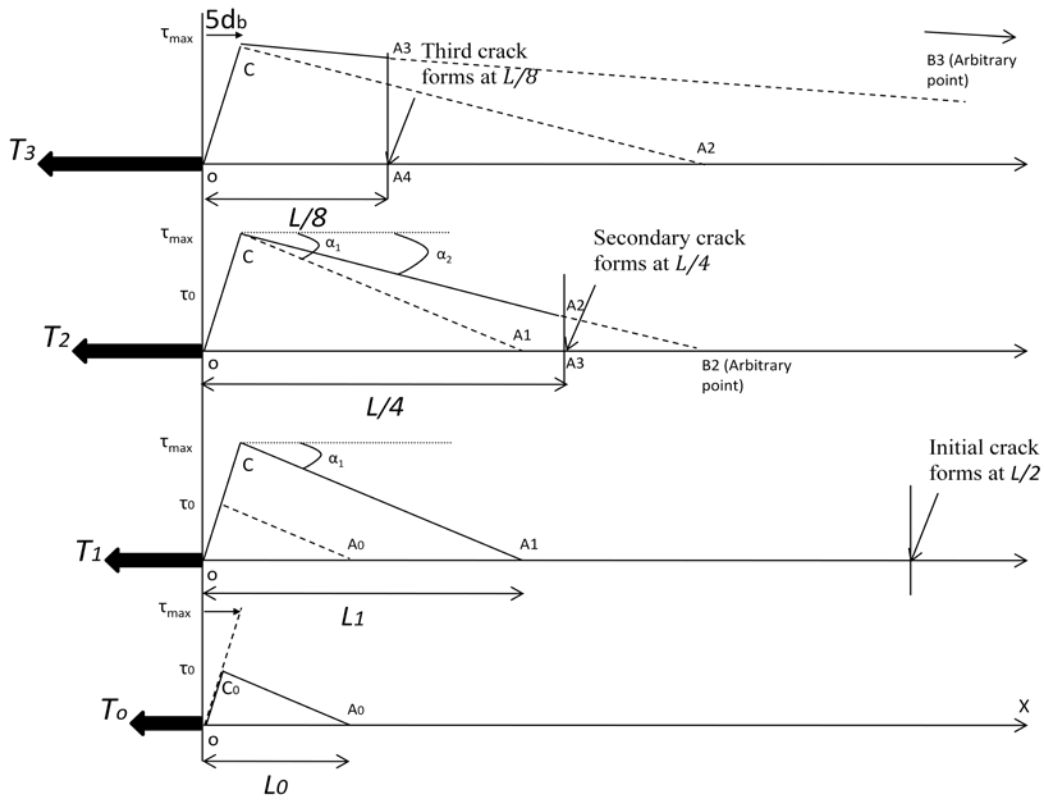


Figure 5.9 The adopted model of bond stress distribution.

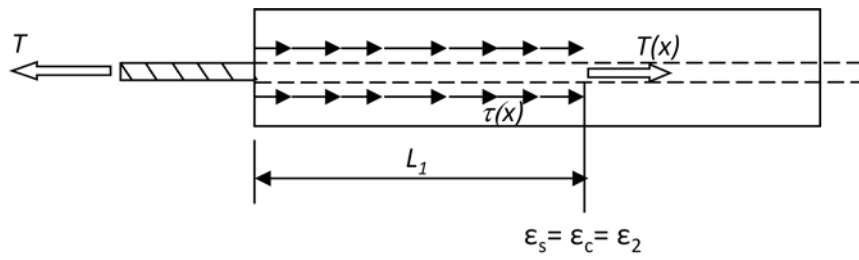


Figure 5.10 Free body diagram of reinforcing steel in segment to one side of crack.

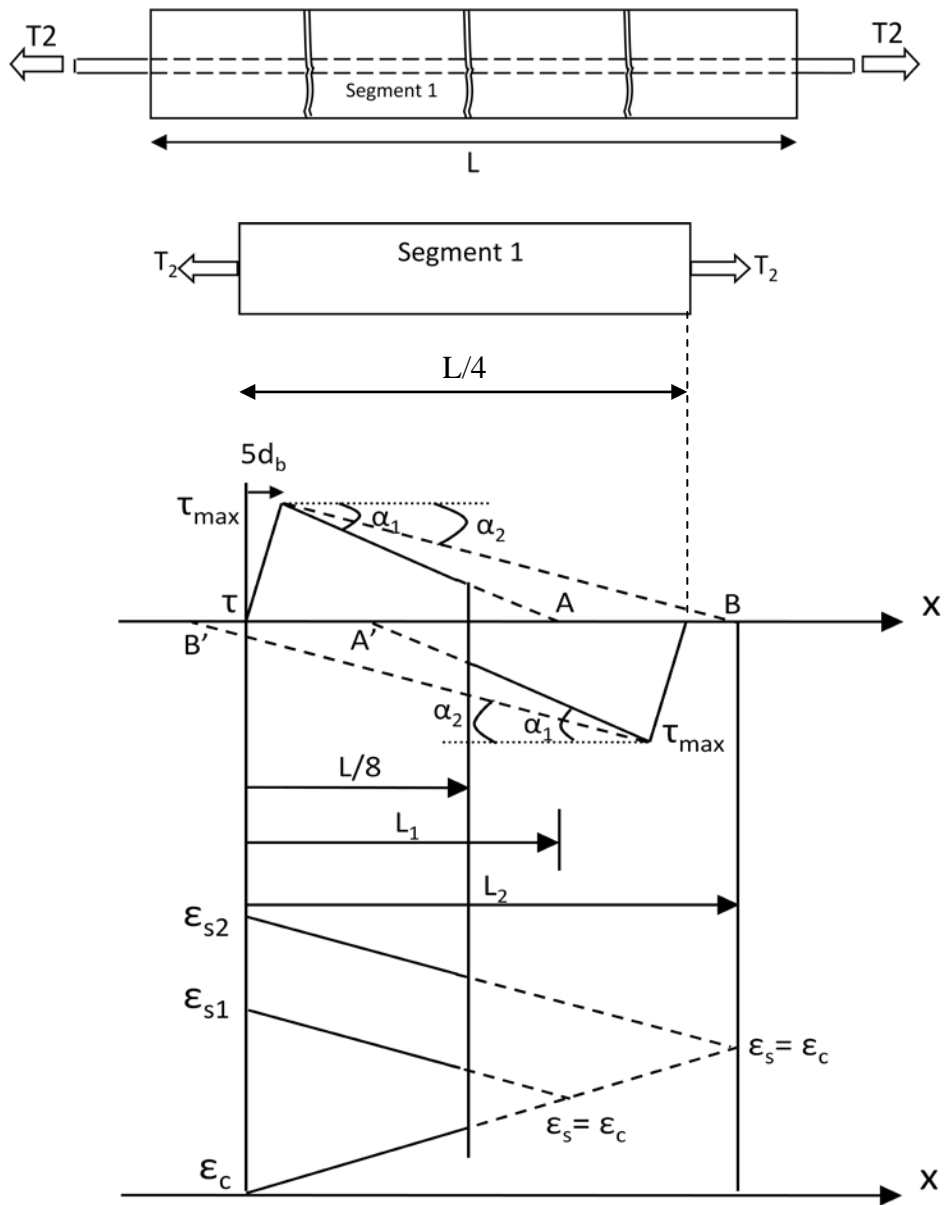


Figure 5.11 Bond stress and resulting steel and concrete strain distribution between adjacent cracks in a reinforced concrete member.

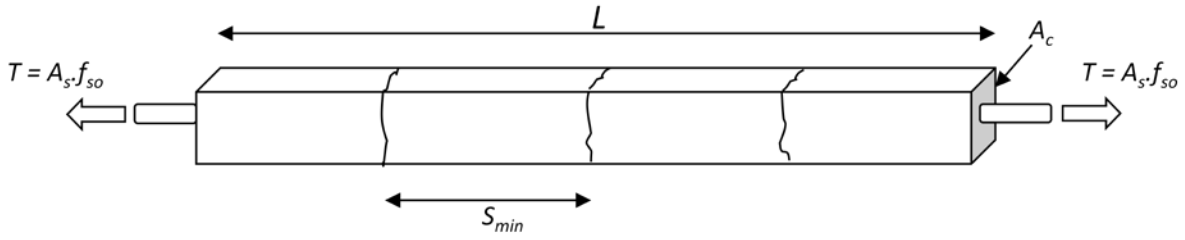


Figure 5.12 Direct tension test in the parametric study.

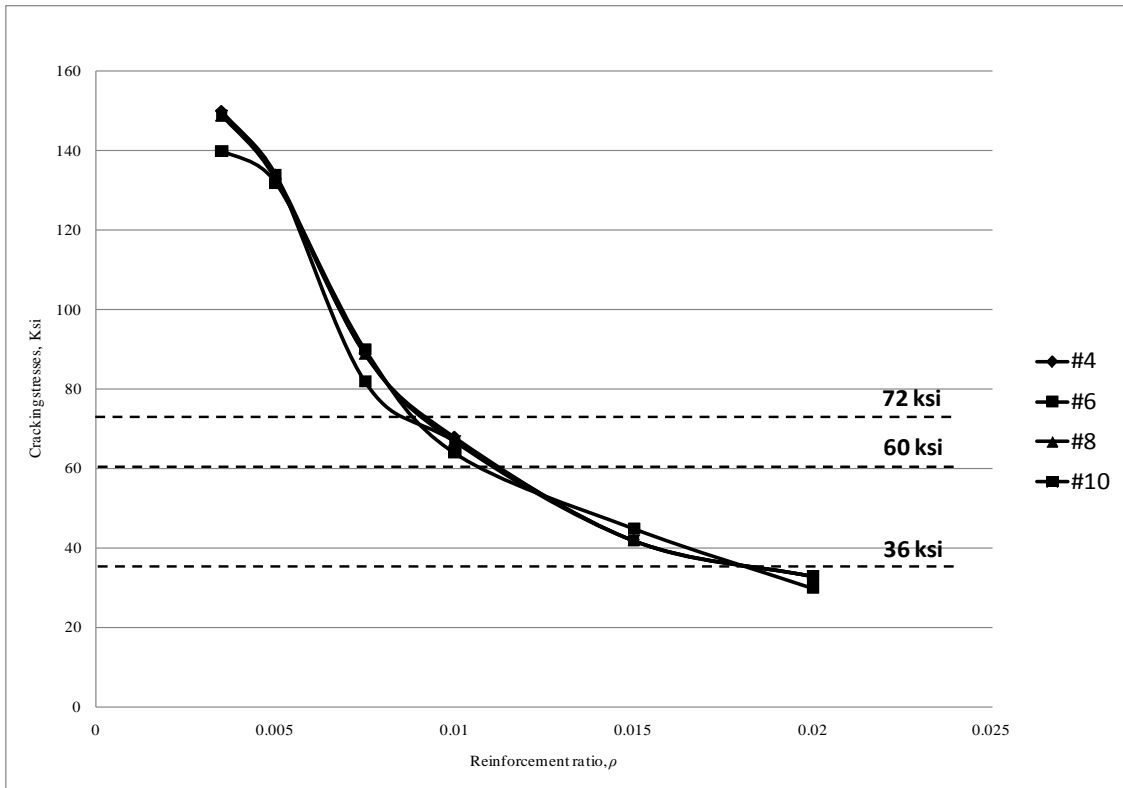
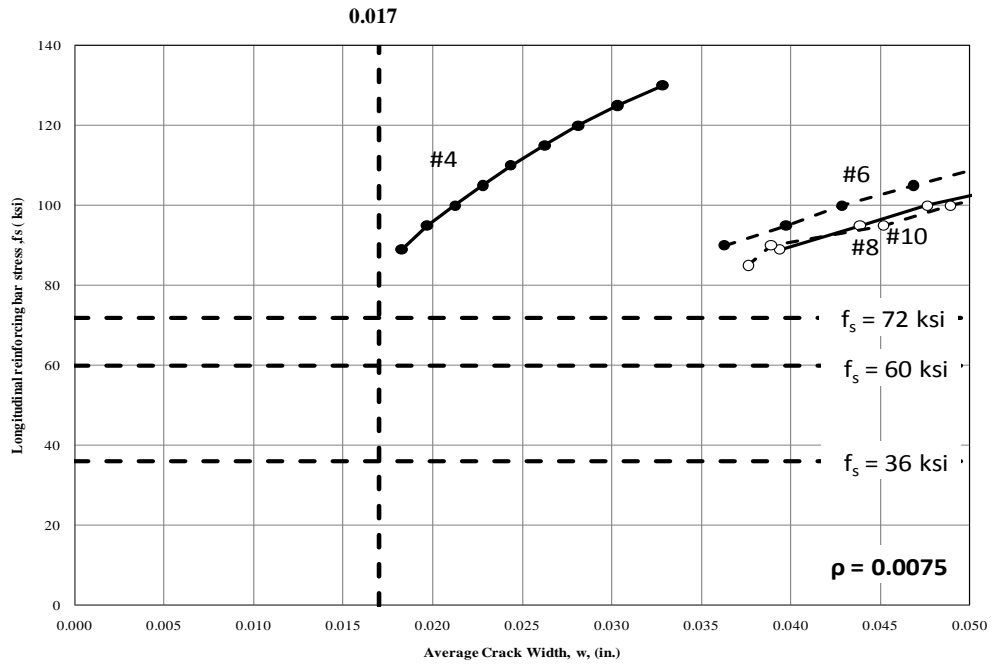
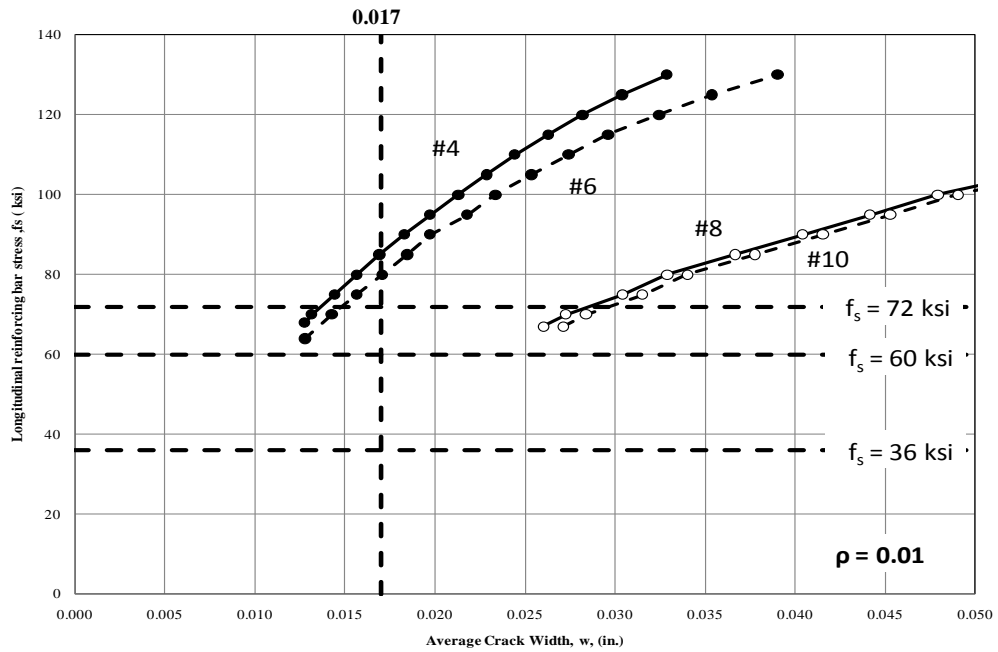


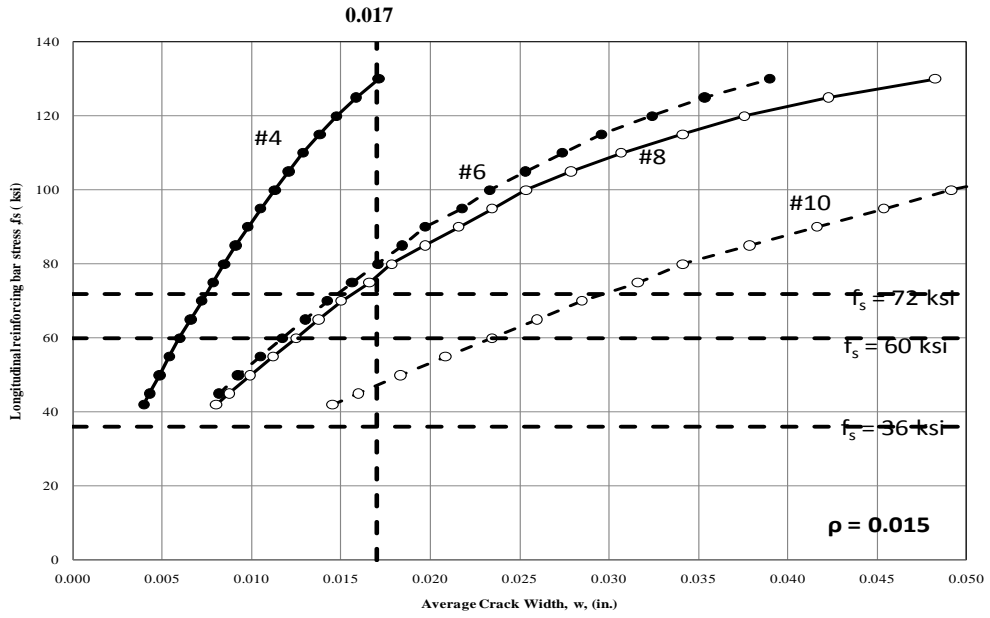
Figure 5.13 Corresponding bar stresses causing the last crack formation. (Based on Table 5.4)



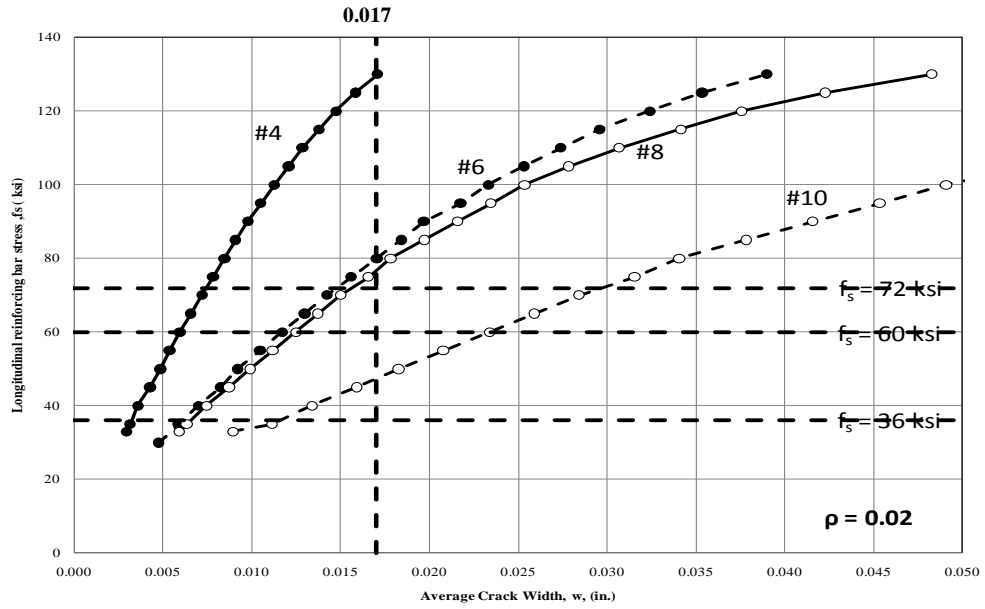
a) Predicted crack widths from parametric study. $\rho = 0.0075$



b) Predicted crack widths from parametric study. $\rho = 0.01$

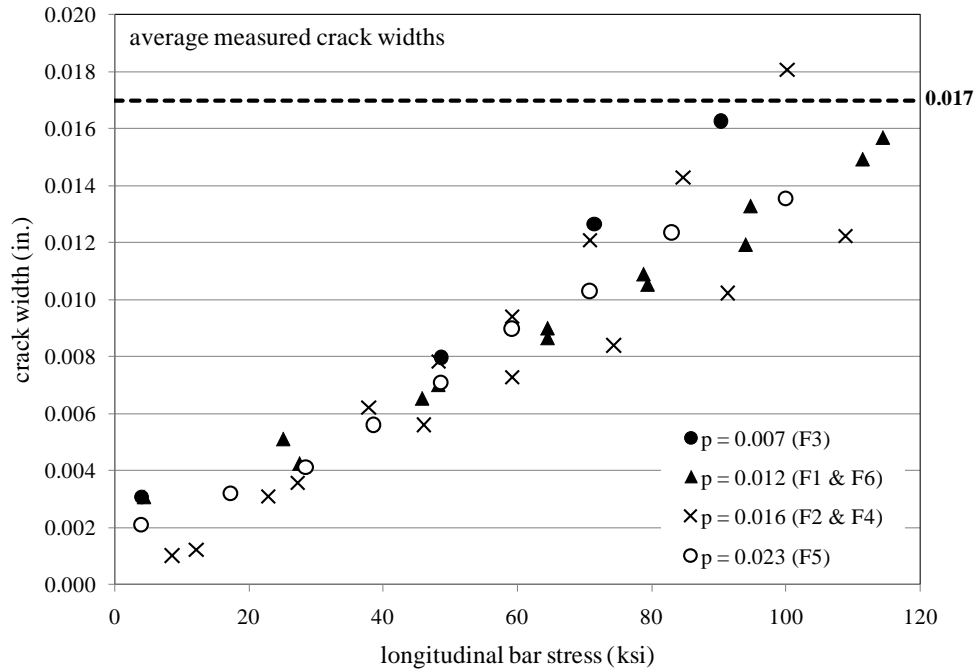


c) Predicted crack widths from parametric study. $\rho = 0.015$

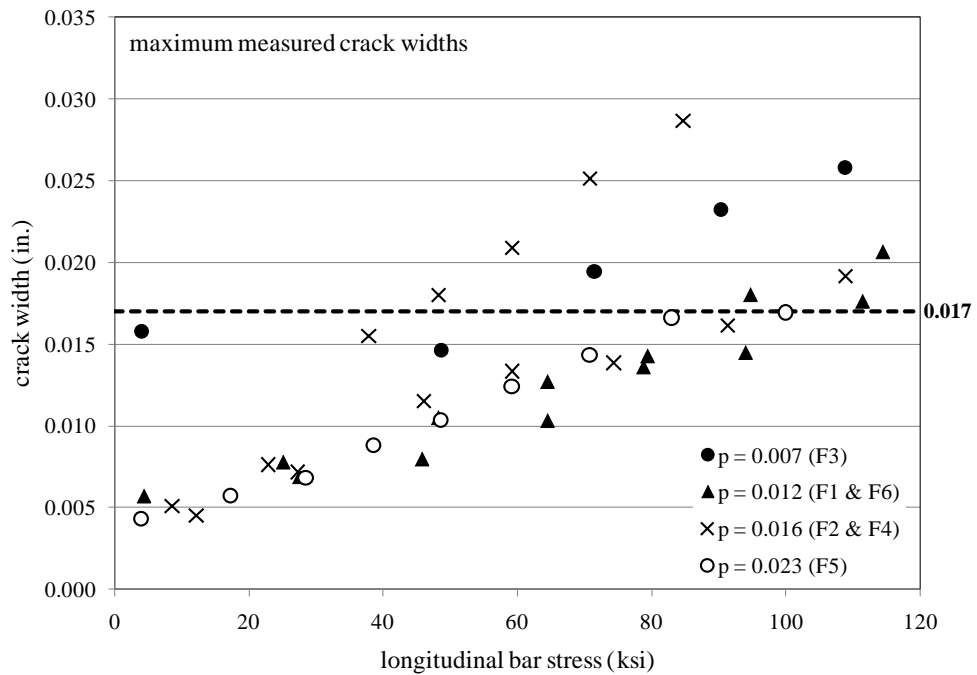


d) Predicted crack widths from parametric study. $\rho = 0.02$

Figure 5.14 The extension of crack opening vs. reinforcing bar stresses.



(a) average crack widths



(b) maximum crack widths

Figure 5.15 Measured crack widths with longitudinal reinforcing bar stress for flexural beams.

6.0 CONCLUSIONS, RECOMMENDATIONS AND FUTURE RESEARCH

6.1 CONCLUSIONS AND RECOMMENDATIONS

This research is based on a portion of National Cooperative Highway Research Program (NCHRP) Project 12-77 *Structural Concrete Design with High-Strength Steel Reinforcement*. With the integration of innovative materials into the nation's infrastructure, the validity of using such materials must be considered. This study considers the use of high-strength steel reinforcing bars as an alternative to conventional ASTM A615 Grade 60 reinforcing bars in concrete structures.

Recent revisions to §9.2 of the *AASHTO Construction Specifications* and to *AASHTO MP 18 Standard Specification for Uncoated, Corrosion-Resistant, Deformed and Plain Alloy, Billet-Steel Bars for Concrete Reinforcement and Dowels* permit the specification of ASTM A1035 reinforcing steel. A1035 reinforcing bars are low carbon, chromium steel bars characterized by a high tensile strength (100 or 120 ksi determined using the 0.2% offset method) and a stress-strain relationship having no yield plateau. Because of their high chromium content, A1035 bars are reported to have superior corrosion resistance when compared to conventional reinforcing steel grades. For this reason, designers have specified A1035 as a direct, one-to-one, replacement for conventional reinforcing steel as an alternative to stainless steel or epoxy-coated bars. The *Specifications*, however, limit the yield strength of reinforcing steel to 75 ksi for most

applications. Therefore, although A1035 steel is being specified for its corrosion resistance, its higher yield strength cannot be utilized.

A number of grades of steel reinforcement with yield strengths exceeding 80 ksi are commercially available in the United States. If allowed, using steel with this higher capacity could provide various benefits to the concrete construction industry by reducing member cross sections and reinforcement quantities, leading to savings in material, shipping, and placement costs. Reducing reinforcement quantities would also prevent congestion problems leading to better quality of construction. Finally, coupling high-strength steel reinforcement with high-performance concrete should result in a much more efficient use of both materials.

This report provides an evaluation of existing *AASHTO LRFD Design Specifications* relevant to the use of high-strength reinforcing steel with respect to issues associated with bond and development of hooked anchorages, fatigue, and serviceability considerations.

6.1.1 Anchorage of high-strength steel reinforcing bars having standard hooks in concrete

The applicability of current *Specification* requirements for hooked bar development lengths was confirmed through a series of eighteen pull-out tests. ‘Proof test’ hooked-bar pull-out specimens, having development lengths that were shorter than those required by present *Specifications* equations (with all appropriate reduction factors applied) were tested. The bars ruptured outside of the anchorage region with very little slip, which clearly indicates the efficacy of the hooked bar development requirements in *Specifications*. The study clearly demonstrates that the present *AASHTO* and *ACI* requirements for hooked anchorage tension development may be extended to develop bar stresses of at least 125 ksi for concrete strengths up to 10 ksi.

In using higher strength steel, greater bar strain and slip will occur prior to development of the bar. The associated displacement of the bar lugs drives a longitudinal splitting failure beyond that where yield of conventional bars would occur; thus, confining reinforcement is critical in developing higher strength bars. The results of this study and previous work clearly indicate that confining reinforcement should always be used when developing, splicing or anchoring ASTM A1035 reinforcing steel.

6.1.2 Fatigue behavior of concrete beams having high-strength reinforcement

The two large-scale tests conducted as part of this study and a review of available published data demonstrate that presently accepted values for the fatigue or ‘endurance’ limit for reinforcing steel are applicable and likely conservative, when applied to higher strength bars.

The fatigue behavior of ferrous metals is largely unaffected by the yield strength of the material itself; thus, the current *Specifications* baseline endurance limit of 24 ksi is unchanged. The impact of applying the current *Specifications* equation to higher-strength reinforcing steel is that f_{min} may be increased by taking advantage of the higher strength steel. As a result, the fatigue limit is irrationally reduced. It is therefore proposed to normalize f_{min} by the yield stress, f_y . Thus, the following equation is recommended.

$$f_f \leq 24 - 20(f_{min}/f_y) \quad (\text{ksi units})$$

Additionally, it is shown that fatigue considerations will rarely affect the design of typical reinforced concrete members having $f_y \leq 100$ ksi.

6.1.3 Serviceability consideration of concrete members reinforced with high strength steel bars

A fundamental issue in using A1035 or any other high-strength reinforcing steel is that the stress at service load (f_s ; assumed to be on the order of $0.6f_y$) is expected to be greater than when conventional 60 Grade steel is used. Consequently, the service-load reinforcing strains (i.e., $\epsilon_s = f_s/E$) are greater than those for conventional Grade 60 steel. The large strains affect deflection and crack widths at service loads.

Based on the results of flexural tests conducted as part of a related study (Table 5.1), deflections and crack widths at service load levels were evaluated. Both metrics of serviceability were found to be within presently accepted limits, and were predictable using current *Specifications* provisions. A limitation on service-level stresses of $f_s \leq 60$ ksi is recommended; this is consistent with recommendation that $f_y \leq 100$ ksi.

6.1.3.1 Parametric study of deflection

A parametric evaluation of Branson's empirical method (currently used in the *Specifications*) and Bischoff's mechanics-based approach to estimating cracked section deflections was conducted. Both methods are based on calculations of an effective moment of inertia, I_e of a cracked concrete section. A significant difference between Branson's and Bischoff's equation is noted for because with $M_d/M_{cr} < 3$ and $\rho < 0.01$. In these cases, Branson's equation overestimates the value of I_e . Another 'quirk' of Branson's equation is that I_e/I_g does not trend to zero as ρ approaches to zero as it logically must for an unreinforced concrete beam. Bischoff's equation does yield $I_e/I_g = 0$ at $\rho = 0$.

Based on the flexural test results considered, the Branson and Bischoff formulations produce very similar results for the specimens considered. The correlation between the formulations is not as good for the cases with lower reinforcing ratio of 0.007. This trend is consistent with the observation that Branson's equation underestimates short-term deflection for concrete members when the reinforcing ratio is less than approximately 0.01. While both equations are suitable for calculating deflections, the Bischoff approach is based on fundamental mechanics and may therefore be applied for any type of elastic reinforcing material. The Branson formulation is empirical and calibrated for mild steel.

6.1.3.2 Crack control

Based on a parametric study on crack widths, it is shown that crack development and spacing are affected by bar size and the effective concrete area surrounding the reinforcement. As the reinforcing ratio falls, the behavior becomes dominated by a small number of large cracks. Whereas for typical reinforcing ratios (0.01 and 0.015), cracking occurs in a more progressive manner and is better distributed, and hence some variation in crack width along the member should be expected. As the reinforcing ratio becomes larger, cracking remains distributed but crack widths may be expected to be more uniform since cracking stresses vary very little. In all cases considered, for reinforcing ratios $\rho = 0.01$ and higher, cracks form at bar stresses below 70 ksi. Consequently, in a concrete section with reinforcing ratio $\rho = 0.01$ or higher, regardless of reinforcing grade, the crack width and crack spacing will be similar.

Based on this study, it can be concluded that through reinforcing bar stresses of 72 ksi, average crack widths remain below 0.017 in. for cases having $\rho < 0.02$ and for all but the largest bars considered (#10). The results were relatively insensitive to changes in reinforcing ratio. These results were confirmed by comparison to available experimental data.

The ratio of maximum to average crack width was observed to be slightly less than that commonly associated with Grade 60 steel. Additionally, this ratio decreased at higher stress levels.

6.2 FUTURE RESEARCH

The following topics associated with the adoption of high-strength reinforcing steel and steel grades having no discernable yield plateau are recommended for future studies.

6.2.1 Bond characteristics

This research has been based on the embedment of hooked beam or girder longitudinal reinforcing bars into a column joint region where often insufficient length is available to develop a straight bar. Additionally, this study evaluated smaller bar size tests intended to represent the anchorage of stirrups in girder sections or the anchorage of primary reinforcing in cantilever slabs.

This series of tests was effectively a proof study of present AASHTO development requirements. In the conduct of this study and related work (Zeno 2009), some differences in the bond characteristics of A1035 reinforcing steel were hypothesized from experimental observations. Further detailed study of straight bar development length of A1035 bars is required. Such study should include a range of bar sizes over a range of development lengths and confinement conditions in order to develop splitting, pullout and bar yield failures. Additionally,

the physical characteristics of the bar deformations should be assessed to determine if this factor contributes to the apparent different bond characteristics of A1035 bars.

6.2.2 Fatigue characteristics

Limited available data indicate that the fatigue limit of higher-strength, and particularly micro-composite alloy steel, may be markedly improved over that of conventional black steel. A study to establish reliable S-N relationships for different grades of reinforcing steel is recommended. Such a study must consider full-section bars (not coupons), include a range of bar sizes and be modeled on programs used to establish existing code-prescribed S-N relationships (such as Helgason et al. 1969 or Tilly and Moss 1982).

6.2.3 Serviceability consideration

Some studies have examined serviceability of concrete beams reinforced with high strength steel bars. Unfortunately, the reported data on crack opening and crack width are very limited. Therefore, for future experimental researches, better monitoring and reporting of crack data are highly recommended.

APPENDIX

AN ANALYTICAL APPROACH TO CALCULATE THE CRACK FORMATION IN A REINFORCED CONCRETE PRISM

According to the assumptions made for the geometry of bond stress distribution (figure 5.9), the unknown parameters can be determined. The step by step calculation of crack formation is as follows:

Step 1: Applying tension load T_0 on the end side of the bar (please refer to Figures 5.9 and 5.12);

Equation below is valid for any section between one ends to L_0 ;

$$T_0 = A_s f_{s0} = A_s E_s \varepsilon_s(x) + \text{Cumulative bond stress (Perimeter of the bar} \times \text{area of } OC_0A_0)$$

for $0 \leq x \leq L_0$;

ε_s and ε_c at L_0 at distance L_0 are equal (ε_2) and can be determined by solving equations 5.33 and 5.35.

Step 2: Check the value f_c ;

$$T_c = f_c A_c = \text{Cumulative bond stress (maximum bond stress is less than } 2.0\sqrt{f'_c} \text{)}$$

If L_0 is smaller than the half of the specimen's length but $f_c < f'_c$ then no crack forms. In the next step the tension load increases.

Step 3: Increasing tension load $T_1 > T_0$ (please refer to Figure 5.9);

$$T_1 = A_s f_{s1} = A_s E_s \varepsilon_s(x) + \text{Cumulative bond stress (Perimeter of bar} \times \text{area of } OCA_1)$$

for $0 \leq x \leq L_1$;

Again, ε_s and ε_c at point A_1 are equal (ε_2) and can be determined by solving equations 5.33 and 5.35.

Step 4: Check the value f_c ;

$$T_c = f_c A_c = \text{Cumulative bond stress (maximum bond stress is equal to } 2.0\sqrt{f'_c} \text{)}$$

If L_1 is smaller than the half of specimen's length and the transferred tension stress exceeds the ultimate tension stress in the concrete ($f_c > f'_c$) then crack will form in the middle of the specimen. If crack forms then the length of specimen would be considered as $L/2$, otherwise the length of specimen remains the same (If a crack took place in the first step then the length would be the distance between two adjacent cracks which is half the original length). In the next step the tension load increases.

Step 5: Increasing tension load $T_2 > T_1$ (According to figure 5.9, α decreases from α_1 to α_2)

$$T_2 = A_s f_{s2} = A_s E_s \varepsilon_s(x) + \text{Cumulative bond stress (Perimeter of bar} \times \text{area of } OCA_2A_3)$$

for $0 \leq x \leq L_2$;

Again, ε_s and ε_c at arbitrary point B_2 are equal (ε_2) and can be determined by solving equations 5.33 and 5.35.

Step 6: Check the value f_c ;

$$T_c = f_c A_c = \text{Cumulative bond stress (maximum bond stress is equal to } 2.0\sqrt{f'_c} \text{)}$$

Since point B_2 is located at a distance greater than $L/4$, therefore the cumulative bond stress should be calculated from the left side (point O) to one fourth of specimen's length ($L/4$). If the transferred tension stress in the concrete section exceeds the ultimate tension capacity of concrete ($f_c > f'_c$) then another crack will form at one fourth of the length L from one end. If

crack forms then the length of specimen would be considered as $L/4$, otherwise the length of specimen remains the same. In the next step the tension load increases.

Step 7: Increasing tension load $T_3 > T_2$ (α decreases from α_2 to α_3)

$$T_2 = A_s f_{s2} = A_s E_s \varepsilon_s(x) + \text{Cumulative bond stress (Perimeter of bar} \times \text{area of } OCA_3A_4)$$

$$\text{for } 0 \leq x \leq L_3;$$

Again, ε_s and ε_c at arbitrary point B_3 are equal and can be determined by solving equations 5.33 and 5.35.

Step 8: Check the value f_c ;

$$T_c = f_c A_c = \text{Cumulative bond stress (maximum bond stress is equal to } 2.0\sqrt{f'_c} \text{)}$$

Same as previous step, since the location of B_3 , where ε_s and ε_c are equal, is out of range therefore the cumulative bond stress should be considered from the left side to $L/8$. If the transferred stress in the concrete section at distance $L/8$ exceeds the ultimate tension stress in the concrete, $f_c > f'_c$, then again another crack will form at the distance $L/8$ from left end of the bar. If crack forms then the length of specimen would be considered as $L/8$, otherwise the length of specimen remains the same.

The process continues until the length of the segment becomes too small. Consequently the cumulative tension stress transferred to the concrete section is not adequate enough to exceed the ultimate tension stress capacity of the concrete section. Therefore at this point, no matter how much the tension force increases, no additional crack forms in the specimen.

REFERENCES

- AASHTO, 2007. *AASHTO LRFD Bridge Design Specifications*, 4th Edition, 2008 and 2009 Interim, American Association of State Highway and Transportation Officials, Washington, DC.
- Abrams, D.A., 1913. *Tests of Bond between Concrete and Steel*. Engineering Experiment Station, University of Illinois Bulletin No. 71, Urbana, Illinois, December.
- ACI Committee 224, 2001. *ACI 224R-01 Control of Cracking in Concrete Structures*, American Concrete Institute, Farmington Hills, MI, 46 pp.
- ACI Committee 318, 2008. *ACI 318-08 Building Code Requirements for Reinforced Concrete and Commentary*, American Concrete Institute, Farmington Hills, Michigan, 436 p.
- ACI Committee 408, 2003. *ACI 408R-03 Bond and Development of Straight Reinforcing in Tension*, Farmington Hills MI, 49 pp.
- Ahlborn, M. Theresa and DenHartigh, C. Timothy, 2003, *Comparative Bond Study of Stainless and High-Chromium Reinforcing Bars in Concrete* Transportation Research Record, Vol. 1845, P 88-95.
- Al-Shaikh, A. H. and Al-Zaid, R. Z. 1993, *Effect of Reinforcement Ratio on the Effective Moment of Inertia of Reinforced Concrete Beams*, ACI Structural Journal, Vol. 90, No. 2, pp. 144-149.
- Al-Zaid, R. Z., Al-Shaikh, A. H. and Abu-Hussein, M. M., 1991, *Effect of loading Type on the Effective Moment of Inertia of Reinforced Concrete Beams*, ACI Structural Journal, Vol. 88, No. 2, pp. 184-190.
- ASTM A1035/A1035M-07. *Standard Specification for Deformed and Plain, Low-Carbon, Chromium, Steel Bars for Concrete Reinforcement*. Conshohocken, PA: ASTM International, 2007.
- ASTM A615/A615M-06. *Standard Specification for Deformed and Plain Carbon-Steel for Concrete Reinforcement*. Conshohocken, PA: ASTM International, 2006.

- ASTM A706/A706M-08 Standard Specification for Low-Alloy Steel Deformed and Plain Bars for Concrete Reinforcement, Conshohocken, PA: ASTM International, 2008.
- ASTM E8-04 Standard Test Methods for Tension Testing of Metallic Materials.
- Barker, R.M., Puckett, J.A., 1997. *Design of Highway Bridges – Based on AASHTO LRFD Bridge Design Specifications*, Wiley-Interscience, New York, N.Y., 1169 pp.
- Bannister, J. L., 1969, *The Behavior of Reinforcing Bars under Fluctuating Stress*. Concrete V. 3, No. 10, pp. 405-409.
- Beeby, A. W., 1983, Cracking Cover at Corrosion of Reinforcement, *Concrete International*, Vol. 5, No. 2, pp. 35-40.
- Bischoff P. H. 2007, *Rational Model for Calculating Deflection of Reinforced Concrete Beams and Slabs*, Can. J. Civil Engineering. 34, pp. 992-1002.
- Bischoff P. H. and Paixao R., 2004, *Tension Stiffening and Cracking of Concrete Reinforced with Glass Fiber Reinforced Polymer (GFRP) bars*; Can. J. Civil Engineering 31, pp 579-588.
- Bischoff P. H., 2005, *Reevaluation of Deflection Prediction for Concrete Beams Reinforced with Steel and Fiber Reinforced Polymer Bars*, Journal of Structural Engineering, ASCE; May 2005 pp. 752-767
- Bond of Reinforcement in Concrete—State of the Art Report. Task Group Bond Models, Fédération Internationale du Béton, Lausanne, Switzerland, 2000.
- Branson, D . E ., 1963, *Instantaneous and Time- Dependent Deflections of Simple and Continuous Reinforced Concrete Beams*, Research Report No. 7, Alabama Highway Department, Montgomery, Aug. 1963, 94 pp.
- Branson, D. E., 1977, *Deformation of Concrete Structures*, McGraw-Hill, New York.
- Broms, B. B., 1965a, *Technique for Investigation of Internal Cracks in Reinforced Concrete Members*, ACI JOURNAL, *Proceedings* V. 62, No. 1, Jan. 1965, pp. 35-44.
- Broms, B. B., 1965b, *Crack Width and Crack Spacing in Reinforced Concrete Members*, ACI JOURNAL, *Proceedings* V. 62, No. 10, Oct. 1965, pp. 1237-1256.
- Burton, K. T. and Hognestad, E., 1967, *Fatigue Tests on Reinforcing Bars-Tack Welding of Stirrups*. ACI J. 64, pp. 244-252.
- CEB-FIP Model Code 1990, Comité Euro-International du Béton, June 1991.
- CEB-FIP, Model Code for Concrete Structures 1978, CEB-FIP International recommendations, 3rd ed., Comité Euro-International du Béton, Paris, 348 pp.

- Ciancone, G. G., Michael, A. P. and Hamilton III H. R.; 2008, *Behavior of Standard Hook Anchorage with Corrosion Resistant Reinforcement*, Department of Civil and Coastal Engineering University of Florida, Technical Report, FDOT No. BD 545-40, June.
- Considère, A., 1906, *Reinforced Concrete*, 2nd edition. , pp. 110-118
- Corley, W.G., Hanson, J.M. and Helgason, T., 1978. *Design of Reinforced Concrete for Fatigue*, Journal of the Structural Division, Proceedings of the American Society of Civil Engineers, Vol. 14, No. ST6, pp. 921-932.
- CSA. 2004. *Design of Concrete Structures*. Standard A23.3-04, Canadian Standards Association (CSA), Toronto, Ont.
- CSA. S6-2006. *Canadian Highway Bridge Design Code*. 10th Edition. Canadian Standards Association / National Standard of Canada. Nov-2006.
- Darwin, D.; Tholen, M. L.; Idun, E. K., 1996b, *Development Length Criteria for Conventional and High Relative Rib Area Reinforcing Bars*, ACI Structural Journal, V. 93, No. 3, May-June, pp. 347-359.
- Darwin, D.; Tholen, M. L.; Idun, E. K.; and Zuo, J., 1996a, *Splice Length of High Relative Rib Area Reinforcing Bars*, ACI Structural Journal, V. 93, No. 1, Jan.-Feb., pp. 95-107.
- DeJong, S.J., and MacDougall, C., 2006. *Fatigue Behaviour of MMFX Corrosion-Resistant Reinforcing Steel*, Proceedings of the 7th International Conference on Short and Medium Span Bridges, Montreal, Canada.
- Destefano R., Evans J., Sun C. and Tadros M., 2003 *Flexural Crack Control in Concrete Bridge Structures*, Proceedings of 3rd International Symposium on High Performance Concrete and PCI National Bridge Conference, October.
- DeV Batchelor, B., Hewitt, B.E. and Csagoly, P.F. 1978. Investigation of the Fatigue Strength of Deck Slabs of Composite Steel/Concrete Bridges. Transportation Research Record 644.
- DeVries, R.A., 1996, *Anchorage of Headed Reinforcement in Concrete*, PhD Dissertation, The University of Texas at Austin, Austin, Texas, December.
- Elagroudy, Hossam Aly; 2003, *Bond Characteristics of Micro-Composite Multi-structural Formable Steel used in Reinforced Concrete Structures* A MD Thesis of North Carolina State University.
- El-Hacha, R., El-Agroudy, H. and Rizkalla, S., 2006, *Bond Characteristics of High-Strength Steel Reinforcement*. ACI Structural Journal, Vol. 103, No. 6, pp. 771-782.

- Fang, K.I. 1985. Behavior of Ontario-Type Bridge Decks on Steel Girders PhD dissertation, University of Texas at Austin.
- Fikry, A. M. and Thomas, C., 1998, *Development of A Model for The Effective Moment of Inertia of One-way Reinforced Concrete Elements*, ACI Structural Journal, V. 95, No. 4, pp. 444- 455.
- Frosch, R. J. , 2001, *Flexural Crack Control in Reinforced Concrete, Design and Construction Practices to Mitigate Cracking*, SP 204, American Concrete Institute, Farmington Hills, Mich., pp. 135-154.
- Frosch, R. J., 1999, *Another Look at Cracking and Crack Control in Reinforced Concrete*, ACI Structural Journal, V. 96, No. 3, May-June, pp. 437-442.
- Frost, N. E., Marsh, K. J. and Pook, L. P., 1974, *Metal Fatigue*, pp. 54-57. Clarendon Press, Oxford.
- Gergely, P., and Lutz, L. A., 1968. *Maximum Crack Width in Reinforced Concrete Flexural Members*, ACI SP20: *Causes, Mechanism, and Control of Cracking in Concrete*, American Concrete Institute, pp.87–117.
- Gilbert, R. I., 1999, *Flexural Crack Control for Concrete Beams and Slabs: An evaluation of design Procedures*, Proceedings of the 16th Australasian Conference on the Mechanics of Structures and Materials, Sydney, Australia, pp. 175 – 180.
- Gilbert, R. I., 2006, Discussion to *Re-evaluation of deflection prediction for concrete beams reinforced with steel and FRP bars*, by Peter H. Bischoff. Journal of Structural Engineering, ASCE, 132(8): pp. 1328 1330.
- Goto, Yukimasa, 1971, *Cracks Formed in Concrete Around Deformed Tension Bars*, Journal of the American Concrete Institute, Proceedings Vol. 68, No. 4, pg. 244-251, Detroit, Michigan, April.
- Graf, O., 1921, *Crack Development*, (Translation), Handbuch fur Eisenbetonbau (3rdEdition, Vol. 1), 1921. pp. 104-115
- Grossman, J. S., 1981, *Simplified Computations for Effective Moment of Inertia I_e and Minimum Thickness to Avoid Deflection Computations*, Proceedings, ACI Journal, Vol. 78, No. 6, pp. 423-439.
- Halvorsen, G. T., 1987, *Code Requirements for Crack Control*, SP-104: Concrete and Concrete Construction, American Concrete Institute, Farmington Hills, MI, pp. 275-322.
- Hamad, Bilal. S.; Jirsa, J. O.; and D'Abreu N. I. 1993, *Anchorage Strength of Epoxy-Coated Hooked Bars*, ACI Structural Journal, V.90, No. 2, March-April, pp. 210-217.”

- Harries, K. and Aidoo, J., 2005, *Deterioration of FRP-to-Concrete Bond Under Fatigue Loading, Proceedings of International Symposium on Bond Behaviour of FRP in Structures (BBFS 2005)*, December 2005.
- Harries, K.A., Shahrooz, B.M., Soltani, A., Miller, R., Russell, H.G. 2010 (accepted) *Bond and Anchorage of High Strength Reinforcing Steel*, Transportation Research Record.
- Helgason, T., Hanson, J. M., Somes, N. F., Corley, G. and Hognestad, E., 1969, *Fatigue Strength of High-Yield Reinforcing Bars*. NCHRP. Report No. 169. Transportation Research Board, Washington.
- Helgason, T., Hanson, J.M., Somes, N.F., Corley, W.G. and Hognestad, E. 1976. *Fatigue Strength of High-Yield Reinforcing Bars*. NCHRP Report 164, Transportation Research Board, Washington DC.
- Hognestad, E., 1961, *High Strength Bars as Concrete Reinforcement, Part 1, Introduction to a Series of Experimental Reports*, Journal of PCA Research and Development Laboratories, PCA Development Department Bulletin D52, Vol. 3, No. 3, Sept.
- Holowka, M., Dorton, R.A., and Csagoly, P.F. 1980. Punching Shear Strength of Restrained Circular Slabs. Ontario Ministry of Transportation.
- Jirsa, J. O.; Lutz, L. A.; and Gergely, P., 1979, *Rationale for Suggested Development, Splice, and Standard Hook Provisions for Deformed Bars in Tension*, Concrete International, V. 1, No. 7, July, pp. 47-61.
- Kaar, P. H., and Mattock, A. H., 1963, *HighStrength Bars as Concrete Reinforcement, Part 4, Control of Cracking*, Journal of the PCA Research and Development Laboratories, Vol. 5, No. 1 Jan. , pp.15-38
- Lepage, A., H. Tavallali, S. Pujol, and J. Rautenberg. 2008 *Towards Earthquake-Resistant Concrete Structures with Ultra High-Strength Steel Reinforcement* 14th World Conference on Earthquake Engineering. Beijing: International Association for Earthquake Engineering.
- Lutz, LeRoy A., 1966, *The Mechanics of Bond and Slip of Deformed Reinforcing Bars in Concrete*. Department of Structural Engineering, Cornell University, Report No. 324, Ithaca, New York, August.
- MacGregor and Wight 2005, [*Reinforced Concrete: Mechanics and Design*](#), 4th Edition. Prentice Hall, New Jersey.
- MacGregor, J.G., Jhamb, I.C. and Nuttall, N., 1971. *Fatigue Strength of Hot-Rolled Reinforcing Bars*, ACI Journal Proceedings, American Concrete Institute, Vol. 68, No. 3, pp. 169-179.

- Mains, R.M., 1951, *Measurement of the Distribution of Tensile and Bond Stresses Along Reinforcing Bars*, Journal of the American Concrete Institute, Proceedings Vol. 48, No. 3, pp. 225-252, Detroit, Michigan, November 1951.
- Mallet, O., 1991. *Fatigue of Reinforced Concrete*, HMSO, London.
- Marques, J.L.G. and Jirsa, J.O., 1975, A study of Hooked Bar Anchorages in Beam-Column Joints, *ACI Journal*, Vol. 72, No. 5. pp 198-209.
- Mast, R. F., M. Dawood, S. M. Rizkalla, and P. Zia., 2008, *Flexural Strength Design of Concrete Beams Reinforced with High-Strength Steel Bars*. ACI Structural Journal 105, no. 4, pp. 570-577.
- Mast, R.F., 2006. Personal Correspondence.
- Mathey, R. G., and Watstein, D., 1960, *Effect of Tensile Properties of Reinforcement on the Flexural Characteristics of Beams*, Journal of the American Concrete Institute, Proceedings Vol. 56 June, pp. 1253-1273
- Mattock, AH & Hawkins, NM, 1972, *Shear Transfer In Reinforced Concrete*. Prestressed Concrete Institute, Vol 17, pp. 55-75.
- Minor, J., and Jirsa, J.O., 1975, *Behavior of Bent Bar Anchorages*, Journal of the American Concrete Institute, Proceedings Vol. 72, No. 4, pp. 141-149, Detroit, Michigan, April.
- Moss, D. S., 1980. *Axial Fatigue of High Yield Reinforcing Bars in Air*, Transport and Road Research Laboratory Report SR622.
- Moss, D. S., 1982, *Bending Fatigue of High-Yield Reinforcing Bars in Concrete*. TRRL Supplementary Rep. 748, Transport and Road Research Laboratory, Crowthorne, U.K.
- Nawy, EG, 1968, *Crack Control in Reinforced Concrete Structures,*” Journal of the American Concrete Institute, Proc. Vol. 65, Farmington Hills, MI, October 1968, pp. 825-838
- NCHRP 12-77 2009. *Interim and Monthly Project Reports*.
- Nemirovsky, J.M. 1949. *Rigidity of Flexural Loaded Reinforced Concrete Members and Opening of Cracks*. Central Research Institute for Building Design (TsNIPS), Research Results for Conventional and Prestressed Reinforced Concrete Construction, Collected Papers, Stroiisdat, State Publication for Construction Literature, Moscow, Russia. [In Russian]
- Neville, A.M., 1975, *Properties of Concrete* 2nd edition, Pitman.

- Odman, S. T. A., 1962, *Stresses in Axially Reinforced Concrete Prisms Subjected to Tension and Exposed to Drying*, Stockholm: Swedish Cement and Concrete Research Institute at the Royal Institute of Technology, NR34.
- Orangun, C. O., Jirsa, J. O. and Breen, J. E., 1977. *A Reevaluation of Test Data on Development Length and Splices*, Journal of the American Concrete Institute, Vol. 74 No. 3, pp. 114-122.
- Pinc, R. L., Watkins, M. D., Jirsa, J. O., 1977, *Strength of Hooked Bar Anchorages in Beam-Column Joints*, Civil Engineering Structures Research Laboratory – Report No. 33, The University of Texas at Austin.
- Piyasena R., 2002, *Crack Spacing, Crack Width and Tension Stiffening Effect in Reinforced Concrete Beams and One-Way Slabs*, PhD Dissertation , Griffith University.
- Poursaei, A., Geiker, M.R., Hansen, K.K., Peled, A. and Weiss, W.J., 2010. X-ray Absorption Measurements of Fluid Ingress in Cracked Concrete Under Load, presentation made at ACI Spring Convention, March 22, 2010, Chicago.
- Ramirez, J.A. and Russell, B.W., 2008, *Transfer, Development, and Splice Length for Strand/Reinforcement in High-Strength Concrete*, NCHRP Report 603.
- Rangan, B. V., 1982, *Control of Beam Deflections by Allowable Span-Depth Ratios*, ACI Journal, Proceedings, Vol. 79, No. 5, pp. 372-377.
- Rao, P.S., and Subrahmanyam, B.V. 1973. *Trisegmental Moment-Curvature Relations for Reinforced Concrete Members*. ACI Journal, 70(5): pp. 346-351.
- Rehm, G., 1957, *The Fundamental Law of Bond*, RILEM-Symposium on Bond and Crack Formation in Reinforced Concrete, Stockholm, Vol. II, pp. 491-498.
- Reis, E. E. Jr., Mozer, J. D. , Bianchini, A. C. and Kesler, C. E., 1964, *Causes and Control of Cracking in Concrete Reinforced with High Strength Steel Bars -- A Review of Research*, T. & A. M. Report No. 261, University of Illinois.
- Romualdi, J. P., and Batson, G. B., 1963, *The Behavior of Reinforced Concrete Beams with Closely Spaced Reinforcement*, Journal of the American Concrete Institute, Proceedings Vol. 60, pp. 775-789.
- Rostasy, F.S., Koch, R., and Leonhardt, F. 1976. *Zur Mindestbewehrung für Zwang von Aussenwänden aus Stahlleichtbeton (Minimum Resistant Reinforcement for Exterior Walls of Light Weight Concrete)*. Deutscher Ausschuss für Stahlbeton, Vol. 267. pp. 1-83 [In German].
- Scanlon, A. and Choi, B., 1999, *Evaluation of ACI 318 Minimum Thickness Requirements for One-Way Slabs*, ACI Structural Journal, Vol. 96, No. 4, pp. 616-622.

- Scanlon, A., Cagley Orsak, D.R., and Buettner, D.R. 2001, *ACI Code Requirements for Deflection Control in Concrete Structures*. Edited by E.G. Nawy and A. Scanlon. American Concrete Institute, Farmington Hills, Mich. SP-203, pp. 1-14.
- Seliem, H.M., Hosny, A., Rizkalla, S., Zia, P., Briggs, M., Miller, S., Darwin, D., Browning, J., Glass, G.M., Hoyt, K., Donnelly, K. and Jirsa, J.O., 2009, *Bond Characteristics of ASTM A1035 Steel Reinforcing Bars*, ACI Structural Journal, Vol. 106, No. 4, pp. 530-539.
- Shahrooz M. B., Harries A. K., Miller A. R., Russell G. H., 2010 *Structural Concrete Design with High-Strength Steel Reinforcement*, Final Report, NCHRP ; Project Number 12-77.
- Snowden, L. C., 1971, *The Static and Fatigue Performance of Concrete Beams with High Strength Deformed Bars*. Building Research Station, Current Paper CP 7/71.
- Sooriyaarachchi H, Pilakoutas K, Byars EA, 2005, *Tension Stiffening Behaviour of GRP-Reinforced Concrete*. In 7th International Symposium for Fibre-Reinforced Polymer (FRP) Reinforcement for Concrete Structures "C FRPRCS7, Kansas City, November, pp. 975-989. ISBN 0-87031-189-1.
- Standards Association of Australia , 2001. SAA Concrete Structures Code – AS 3600. Sydney, NSW.
- Sumpter, M. S. "Behavior of High Performance Steel as Shear Reinforcement for Concrete Beams." ACI Structural Journal 106, no. 2 (2007): 171-177.
- Thomas, F. G., 1936, *Cracking in Reinforced Concrete*, The Structural Engineer, Vol.14, No. 7 July, pp. 298-320.
- Tilly, G. P., and Moss, D. S. 1982. *Long Endurance Fatigue of Steel Reinforcement*. Proc., ABSE Coll., Lausanne, Switzerland.
- Vijay, P.V., GangaRao, H.V.S. and Prachasaree, W. 2002. *Bending Behavior of Concrete Beams Reinforced with MMFX Steel Bars*, West Virginia University July 2002.
- Ward, Elizabeth L; 2008, *Analytical Evaluation of Structural Concrete Members with High-Strength Steel Reinforcement*; A MD Thesis of University of Cincinnati.
- Wascheidt, H., 1965. *On the Fatigue Strength of Embedded Concrete Reinforcing Steel (Zur Frage der Dauerschwingfestigkeit von Betonstählen im einbetonierten Zustand)*, Doctoral Thesis, Technical University of Aachen, Germany [in German].
- Westergaard, H. M., 1933, *Stresses at a Crack, Size of the Crack, and the Bending of Re-inforced Concrete*, Journal of the American Concrete Institute, Proceedings Vol.30, Nov. 1933, pp. 93-102.

Yang, S., and Chen, J., 1988, *Bond Slip and Crack Width Calculations of Tension Members*, ACI Structural Journal, V. 85, No. 4, July-Aug., pp. 414-422.

Zeno, G. 2009, *Use of High-Strength Steel Reinforcement In Shear Friction Applications*, MSCE thesis, University of Pittsburgh, 2009.

Zuo, J.; and Darwin D., 2000, *Splice Length of Conventional and High Relative Rib Area Reinforcing Bars in Normal and High Strength Concrete*, ACI Structural Journal, V. 97, No. 4, Jul.-Aug., pp. 630-641.